


2016

POWER MAXIMIZATION FOR PYROELECTRIC, PIEZOELECTRIC, AND HYBRID ENERGY HARVESTING

Murtadha A. Shaheen
almalikima@vcu.edu

Follow this and additional works at: <http://scholarscompass.vcu.edu/etd>

 Part of the [Acoustics, Dynamics, and Controls Commons](#), [Ceramic Materials Commons](#), [Electro-Mechanical Systems Commons](#), [Energy Systems Commons](#), and the [Polymer and Organic Materials Commons](#)

© The Author

Downloaded from

<http://scholarscompass.vcu.edu/etd/4462>

This Dissertation is brought to you for free and open access by the Graduate School at VCU Scholars Compass. It has been accepted for inclusion in Theses and Dissertations by an authorized administrator of VCU Scholars Compass. For more information, please contact libcompass@vcu.edu.

POWER MAXIMIZATION FOR PYROELECTRIC, PIEZOELECTRIC, AND HYBRID ENERGY HARVESTING

A dissertation submitted in partial fulfillment of the requirements for the degree of
Doctor of Philosophy at Virginia Commonwealth University

By

Murtadha A. Shaheen

Master of Science in Electrical Engineering, Basrah University, Basrah, Iraq, 2004

Bachelor of Science in Electrical Engineering, Basrah University, Basrah, Iraq, 2000

Director: Karla Mossi, Ph.D.
Associate Professor, Department of Mechanical and Nuclear Engineering
School of Engineering

Virginia Commonwealth University
Richmond, Virginia
August, 2016

Acknowledgement

I would like to thank some people who have helped tremendously during this process, for all of whom I am deeply grateful. My loving parents, my wife Nahwa, and my kids, Narjis, Mohammed Baqir, Sumana, and Rayhana have been there to celebrate my establishments and to encourage me emotionally during difficult times.

My advisor Dr. K. Mossi has made this big accomplishment possible with her generous and scientific support. Her guide has made me have the confidence to establish future research on my own.

I would like to thank my committee members: Dr. Gary M. Atkinson, Dr. Ümit Özgür, Dr. Atulsimha Jayasimha, and Dr. John Speich for their insightful comments, and time. Particularly, I would like to thank Dr. Özgür for his valuable suggestions. In addition, I have to thank express gratitude to the MNE administration office for their help in ordering the required materials and equipment.

I would also like to thank Dr. Brian Hinderliter for his advice. I thank my graduate and undergraduate colleagues who worked in smart materials for their help.

Table of Contents

List of Tables	vi
List of Figures	vi
List of Symbols	x
Abstract	xiii
1. Introduction	1
1.1 Pyroelectricity.....	1
1.2 Piezoelectricity.....	9
1.3 Modeling for piezoelectric bimorph cantilever with RLC load.....	17
1.4 Hybrid Pyro-Piezoelectric energy harvesting	17
1.5 Approach	19
2. Pyroelectric energy Maximization.....	21
2.1 Introduction.....	21
2.2 Pyroelectric equivalent circuit.....	24
2.3 Pyroelectric Single Pole Low Pass Filter (PSLPF).....	27
2.4 Resistive impedance matching.....	29
2.5 Experimental setup for PVDF and PZT-5A PSLPF circuit.....	31
2.6 The PVDF single pole low pass filter circuit.....	33

2.7 The PZT-5A single pole low pass filter circuit.....	35
2.8 Effect of temperature on capacitance and resistance of a pyroelectric material.....	36
2.9 Pyroelectric energy harvesting setup.....	37
2.10 Results and discussions.....	45
3. Piezoelectric energy scavenger modeling.....	47
3.1 Introduction	47
3.2 Modeling of piezoelectric bimorph with RLC load.....	48
3.3. Experimental Set up.....	60
3.4 Results and discussions	61
3.5 Model Validation.....	62
4. Piezoelectric Operating Frequency Tuning and Bandwidth Widening	65
4.1 Introduction.....	65
4.2 Frequency Tuning Techniques.....	68
4.3 Hybrid Technique for PH frequency tuning and bandwidth widening.....	70
4.4 Experimental setup for hybrid tuning system.....	70
4.5 Results and discussion.....	73
4.6 Enhanced Piezoelectric Energy Harvesting and Hybrid Frequency Tuning.....	81
4.7 Experimental Set up of enhanced power hybrid tuning system.....	82
4.8 Results and discussion for enhanced power system.....	85

5. Hybrid Pyro-Piezo Energy Harvester.....	95
5.1 Introduction	95
5.2 Pyroelectric, piezoelectric, and hybrid energy harvesting	96
5.3 Study of heat effect on the impedance.....	96
5.4 Experimental set up for hybrid energy harvesting.....	99
5.5 Results and Discussion.....	100
5.6 Voltage doubler circuit for hybrid energy harvesting.....	105
6. Conclusions and Future work.....	109
6.1 Conclusions.....	109
6.2 Future Work.....	115
References.....	116
Appendices	129
A1.1. Effect of temperature on Dielectric constant for some piezo ceramics	130
A1.2. Effect of temperature and frequency on resistivity for piezo ceramics.....	130

List of Tables

Table 1.1 Properties of Materials: Anisotropy, Symmetry	4
Table 2.1 Piezoelectric Materials Characteristics.....	32
Table 2.2 Functional modes for the PSLPF.....	34
Table 2.3 Comparison of measured R_p , X_p , and Z_p for PSLPF, LCR meter, and IA.....	36
Table 3.1 Material properties of the piezoelectric bimorph: T226-A4-503X	61
Table 3.2 Experimental and simulated data for power of the piezoelectric generator.....	64
Table 4.1 Physical properties and dimensions of TH-7R.....	85
Table 4.2 Properties of the three different unimorphs.....	91
Table 5.1 Regular and voltage doubler hybrid energy harvesting.....	108

List of Figures

Figure 1.1 Pyroelectricity and thermal, mechanical, and electrical properties of a	2
Figure 1.2 a cantilever with a tip mass at the free end.....	13
Figure 1.3 a band-pass filter of cantilever beams and proof masses.....	14
Figure 2.1 equivalent circuit for a single pyroelectric cell.....	25
Figure 2.2 Pyroelectric single pole low pass filter PSLPF.....	28
Figure 2.3 Experimental setup of PSLPF for both PVDF and PZT-5A cells.....	32
Figure 2.4 Measured pyroelectric R_p , X_p , and Z_p for PVDF using PSLPF.....	34
Figure 2.5 Measured pyroelectric R_p , X_p , and Z_p for PZT-5A using PSLPF.....	35

Figure 2.6 Measured Z_p , R_p , X_p and C_p of PVDF for temp., changes at 100 mHz.....	38
Figure 2.7 Measured Z_p , R_p , X_p and C_p of PZT-5A for temp., changes 100 mHz.....	38
Figure 2.8 Experimental prototype for the cyclic pyroelectric energy harvester.....	39
Figure 2.9 PVDF and PZT-5A for pyro. energy harvesting with cyclic heating.....	40
Figure 2.10 Temperature, voltage, and power density changes of PVDF cell	41
Figure 2.11 Pyro. voltage and power density versus R_L for PVDF at 100 mHz.....	42
Figure 2.12 temperature, voltage, and power density of PZT-5A cell	43
Figure 2.13 Pyroelectric voltage and power density vs. R_L for PZT-5A at 100 mHz.....	44
Figure 3.1 the equivalent circuit for a piezoelectric energy harvester with R load.....	49
Figure 3.2 Equiv. circuit for the piezoelectric energy harvester with RLC load.....	51
Figure 3.3 the input base vibration acceleration.....	63
Figure 3.4 the experimental and simulated output voltages at C_{sh} equal to zero.....	63
Figure 3.5 the experimental and simulated voltages for the cases of L_{sh} and no L_{sh}	64
Figure 4.1 Cantilever with a proof mass at the free end.....	68
Figure 4.2 Band-pass filter of cantilever beams and proof masses.....	70
Figure 4.3 equivalent circuit for the developed hybrid piezoelectric tuning system.....	72
Figure 4.4 Experimental set up for the hybrid frequency tuning method.....	73
Figure 4.5 Output voltages first bimorph with resonance of 93.5 Hz.....	74
Figure 4.6 Output powers of the first bimorph with resonance of 93.5 Hz.....	74

Figure 4.7 Output voltage of the second bimorph with resonance of 99.5 Hz.....	75
Figure 4.8 Output powers of the second bimorph with resonance of 99.5 Hz.....	75
Figure 4.9 Output voltages for the third cantilever at resonance of 114 Hz.....	77
Figure 4.10 Output power for the third cantilever at resonance of 114 Hz	77
Figure 4.11 Voltages of the series piezo. system at 93.5 Hz, 99.5 Hz, and 114 Hz.....	78
Figure 4.12 Powers of the series piezo. system at 93.5 Hz, 99.5 Hz, and 114 Hz.....	78
Figure 4.13 The 12 power peaks for the series system with load resistance of 100 k Ω	79
Figure 4.14 Equivalent circuits for enhanced power hybrid energy harvester.....	83
Figure 4.15 Equivalent circuits for improved adjusting capacitor method.....	84
Figure 4.16 Powers for various R_L and C_{sh} with corresponding resonant frequencies.....	87
Figure 4.17 Power outputs using a L_{sh} of 700 mH and two different shunt capacitors.....	88
Figure 4.18 Power outputs using a shunt inductor L_{sh} of 2 H and shunt capacitors.....	88
Figure 4.19 Resonance frequencies f_r versus shunt capacitors C_{sh}	89
Figure 4.20 Experimental setup for enhanced power hybrid tuning method.....	91
Figure 4.21 AC voltages of three different unimorphs with 10 k Ω load resistance.....	92
Figure 4.22 Vibration acceleration signal with 10 k Ω load resistance.....	92
Figure 4.23 Output voltages vs. frequency for enhanced power hybrid energy harvester.....	93
Figure 4.24 Power density versus frequency for enhanced power hybrid energy harvester....	93
Figure 4.25 Voltages for three resonance frequencies of the bimorph cantilevers.....	94

Figure 5.1 the Experimental set up for the hybrid energy harvesting.....	97
Figure 5.2 Resistance and capacitance of the piezoelectric material versus temperature.....	98
Figure 5.3 Impedance of the piezoelectric material versus temperature.....	99
Figure 5.4 Piezo Voltage for T226-A4-503X at 0.21 g and 115 Hz, and R_L of 25 k Ω	102
Figure 5.5 Pyro. voltage for T226-A4-503X at 100 mHz, 0.44 deg /s, and R_L of 25 k Ω	102
Figure 5.6 Instantaneous hybrid piezo-pyroelectric voltage	102
Figure 5.7 Piezoelectric and hybrid peak power versus load impedance.....	103
Figure 5.8 Pyroelectric power versus load impedance.....	104
Figure 5.9 Hybrid Pyro- Piezo Energy Harvester Using Voltage Doubler scheme.....	104
Figure 5.10 Experimental set up for Hybrid Energy Harvester with Voltage doubler.....	106

List of Symbols

A	Capacitor area
C	Capacitance
C_p	Pyroelectric capacitance, F
C_{11}	Mechanical compliance of the piezoelectric material
R_p	Pyroelectric resistance, Ω
h_b	Thickness of beam
Z_p	Total pyroelectric impedance
T	Temperature, $^{\circ}\text{C}$
P	Power, W
f	Frequency, Hz
v	Volume, cm^3
I	Pyroelectric output current, A
I_p	Pyroelectric source current, A
D	Electrical displacement, C/m^2
d_{31}	Electromechanical coupling coefficient
E	Electric field, V/m
\dot{T}	First derivation of temperature
\dot{V}	First derivation of electric potential
A	Surface area of pyroelectric cell, cm^2
b	Thickness of pyroelectric cell, cm
p	Pyroelectric coefficient, $\text{C}/\text{m}^2\text{K}$

ε	Permittivity, F/m
J	Surface current density, A/m ²
J_d	Displacement current density, A/m ²
J_c	Conduction current density, A/m ²
L	Length of the beam
m_{eff}	Effective mass
σ	Conductivity of the material, S
ω_c	Corner frequency, Hz
ω_{low}	Lower bound frequency
ω_{up}	upper bound frequency
V_{out}	Output voltage, V
V_{in}	Input voltage, V
R_{Lopt}	Optimal load resistance, Ω
R_L	Load resistance, Ω
S_n	Number of switch, #
t	thickness
V_{dc}	DC biasing voltage, V
V_{ac}	AC voltage, V
\int	Strain
$\dot{\int}$	First derivative for strain
$\ddot{\int}$	Second derivative for strain
V	output voltage
\dot{V}	First derivative of the output voltage

k^*	effective spring constant
m	mass
m_b	mass of piezoelectric cantilever beam
b_m	damping coefficient
\ddot{b}	A constant relates vertical force to stress
D	piezoelectric strain coefficient
E	dielectric constant of the piezoelectric material
ε^*	The permittivity of the material
Y_c	Young modulus of the piezoelectric ceramic layer
t_c	Thickness of the piezoelectric material layer
R_L	Load resistance
C_p	Inherent piezoelectric capacitance
C_{sh}	The shunt capacitance
L_{sh}	The shunt inductor
\ddot{u}	Input vibration in terms of acceleration
a^*	Acceleration
$\varnothing(x)$	Moment of the beam as a function of distance x

Abstract

POWER MAXIMIZATION FOR PYROELECTRIC, PIEZOELECTRIC, AND HYBRID ENERGY HARVESTING

By Murtadha A Shaheen, Ph.D.

A dissertation submitted in partial fulfillment of the requirements for the degree of Doctor of Philosophy at Virginia Commonwealth University

Virginia Commonwealth University

Director: Karla Mossi, Ph.D.
Associate Professor, Department of Mechanical and Nuclear Engineering
School of Engineering

Research in the area of environmental energy harvesting to power small electronic components has developed in the last few years. In particular, researching materials that exhibit a piezoelectric or a pyroelectric effect have been the subject of extensive investigation for energy harvesting applications. These applications however are faced with many technical challenges to maximize power efficiently. The goal of this dissertation consists of improving the efficiency of energy harvesting using pyroelectric and piezoelectric materials in a system by the proper characterization of electrical parameters, widening operating frequency, and coupling of both effects with the appropriate parameters.

Impedance characterization and matching is very critical for power maximization in pyroelectric energy harvester. A new simple stand-alone method of characterizing the impedance of a pyroelectric cell has been demonstrated. This method utilizes a Pyroelectric single pole low pass filter technique, PSLPF. Utilizing the properties of a PSLPF, where a known input voltage

is applied and capacitance C_p and resistance R_p can be calculated at a frequency range of 1 mHz to 1 Hz. The PSLPF method presented here demonstrates that for pyroelectric materials the impedance depends on two major factors: (1) average working temperature, and (2) the heating rate. Neglecting these two factors can result in inefficient and unpredictable behavior of pyroelectric materials when used in energy harvesting applications.

Vibration energy scavengers provide the maximum power when working at resonance, which means that the harvesters are not efficient in environment vibrations with time-dependent frequencies. Design and implementation of a hybrid approach using multiple piezoelectric bimorph cantilevers is presented. This is done to achieve mechanical and electrical tuning, along with bandwidth widening. In addition, a hybrid tuning technique with an improved adjusting capacitor method was applied to this system. A small toroid inductor of 700 mH is connected in parallel to the load resistance and shunt capacitance. Results show an extended frequency range up to 12 resonance frequencies (300% improvement) along with improved power up to 197%.

Finally, a hybrid piezoelectric and pyroelectric system is designed and tested. Using a new voltage doubler circuit for rectifying and collecting pyroelectric and piezoelectric voltages individually is proposed and tested. The investigation showed that the hybrid energy is possible using the voltage doubler circuit from two independent sources for pyroelectricity and piezoelectricity due to marked differences of optimal performance. The obtained results were significantly higher than harvested energy simultaneously from the same material.

Chapter 1: Introduction

1. Background and Motivation

Energy scavenging systems are those which convert different types of ambient energy such as wind, heat, vibration, and light into useful electrical energy. The harvesting of ambient energy to power small electronic components has received incredible consideration over the last decade (Gambier P et al. 2012). Among the most important phenomena utilized in energy harvesting is pyroelectricity and piezoelectricity.

1.1 Pyroelectricity

Pyroelectricity can precisely be defined as the temperature reliance of the spontaneous polarization in an anisotropic material (S. B. Lang, 1974; M. ref; S. Bauer and S. B. Lang, 1996; S.B. Lang 2005). As an example for pyroelectric effect, consider a sample of pyroelectric material such as barium titanate as shown in Figure1.1a. The unit cells of this material have pairs of charges called dipoles and each dipole has a moment. The dipoles are crowded so that components of their moment in every unit cell combine in the path normal to the parallel flat surfaces. The moment of dipole per unit volume of the material is termed the polarization \mathbf{P}_s which is always nonzero in a pyroelectric division. \mathbf{P}_s exists when an electric field is not available. Electrons or ions nearby will be moved toward to the sample by attraction force as presented in Figure1.1a. Assume that two conductive electrodes are then connected to the surfaces and linked through a sensitive galvanometer. When the temperature of the material is not changing, then so is \mathbf{P}_s and the current flow is equal to zero. A rise in temperature results in the net dipole moment and, accordingly, \mathbf{P}_s to decrease. The quantity of bound charge then drops, and the free charges restructure to compensate for the change in bound charge producing a

pyroelectric current. If the material was cooled, the sign of current would be inverted (S.B. Lang 2005).

1.1.1 The Primary, Secondary, and Tertiary Pyroelectric Effect

There is a thermodynamically reversible interface that may arise among the mechanical, thermal, and electrical properties of a crystal as shown in the triangular diagram in Figure 1.1 b. It can be noticed from the lines joining pairs of circles that a small variation in one of the parameters causes a corresponding change in the other. There are three short bold lines connecting pairs of elastic, thermal, and electric variables. These lines define the physical characteristics of elasticity, heat capacity, and electrical permittivity, respectively. For instance, a small increase in temperature θ yields a rise in entropy S relational to the heat capacity divided by temperature. The diagram also demonstrates coupled effects, designated by lines connecting pairs of circles at different angles.

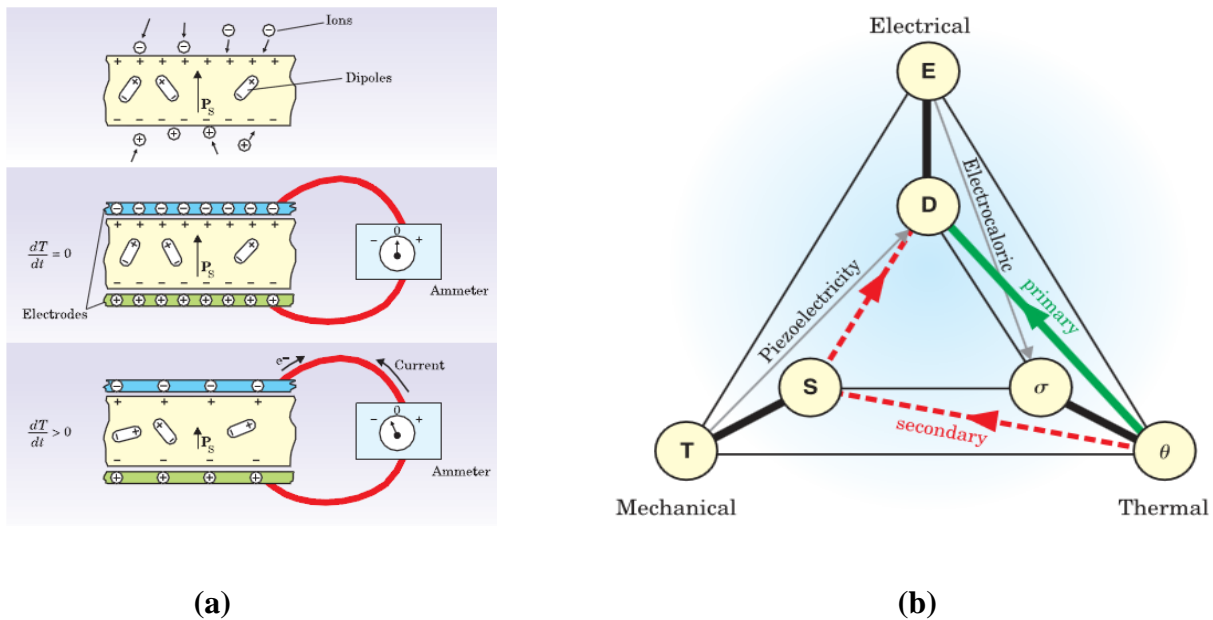


Figure 1.1 (a) Pyroelectricity (b) mechanical, thermal, and electrical properties of a crystal (Adapted from S.B. Lang 2005).

Pyroelectricity is a combined effect that relates a variation in temperature T to a variation in electrical displacement:

$$dD = p dT \quad \text{Equation 1.1}$$

Where: D is the electric displacement, p is the pyroelectric coefficient, and T is the temperature.

The pyroelectric coefficient can be defined by:

$$p = (\partial P / \partial T)_{S,E} \quad \text{Equation 1.2}$$

Where P is the spontaneous polarization, E is electric field; S is the elastic stress. S and E are the constant constraints.

The two contributions forming pyroelectric effect are represented by the colored lines in Figure 1.1 b. In the first contribution, the crystal is fastened under constant strain S_1 . A change in temperature causes a variation in electric displacement as presented by the green line, and this is called the primary pyroelectric effect. Crystal deformation causes the second contribution: Thermal expansion leads to a strain that adjusts the electric displacement via a piezoelectric process which is described by the dashed red lines and it is called the secondary pyroelectric effect. It is tremendously difficult to measure the primary effect directly.

Experimentally, the pyroelectric effect under constant stress which is called the total effect is what is usually measured. The pyroelectric effect is equal to the sum of red and green lines shown in Figure 1.1b. The primary, secondary, and total pyroelectric coefficients of several materials for comparison are shown in Table 1.1. Ferroelectrics are pyroelectric materials whose direction of polarization could be inverted by an appropriate electric field. They are also characterized by a threshold temperature called the Curie temperature T_c , above which the material is non polar pyroelectric. Below Curie Temperature T_c , ferroelectric materials are polar and can show pyroelectric effect. Ferroelectric materials are of greater interest for applications

Table 1.1 Properties of Materials: Anisotropy, Symmetry, (R. E. Newnham, 2005)

Material	Primary Coefficient	Secondary Coefficient	Total Coefficient $\mu\text{C}/\text{m}^2\cdot\text{K}$
Ferroelectrics			
Poled Ceramic			
BaTiO₃	-260	+60	-200
PbZr_{0.95}Ti_{0.05}O₃	-305.7	+37.7	-268
Crystal			
LiNbO₃	-95.8	+12.8	-83
LiTaO₃	-175	-1	-176
Pb₅Ge₃O₁₁	-110.5	+15.5	-95
Ba₂NaNb₅O₁₅	-141.7	+41.7	-100
Sr_{0.5}Ba_{0.5}Nb₂O₆	-502	-48	-550
(CH₂CF₂)_n	-14	-13	-27
Triglycine sulfate	+60	-330	-270
Nonferroelectrics			
Crystal			
CdSe	-2.94	-0.56	-3.5
CdS	-3.0	-1.0	-4.0
ZnO	-6.9	-2.5	-9.4
Tourmaline	-0.48	-3.52	-4.0
Li₂SO₄·2H₂O	+60.2	+26.1	+86.3

since generally they have larger pyroelectric coefficients than non-ferroelectrics. Tertiary pyroelectric effect is created by non-uniform heating producing non-uniform stresses that can cause polarization through a piezoelectric effect. Tertiary effect is of a little interest now. An inverse pyroelectric effect is called the electro caloric effect. In this effect, a change in an applied electric field generates a change in entropy and, accordingly, a variation in temperature. Three conditions must be satisfied to produce the pyroelectric effect in any solid material: A nonzero dipole moment must be available in the molecular structure; there must be no center symmetry in the material; and the material must have either no axis of rotational symmetry or a single axis of rotational symmetry that is not comprised in an inversion axis. Of the 32 crystal point-group symmetries, only 10 of them permit the presence of pyroelectricity (S.B. Lang 2005).

1.1.2 Maximum Pyroelectric Energy Harvesting

Pyroelectric materials are used for providing a low power and can be considered as micro or nano generators. The investigation of the feasibility of efficient heat energy scavenging utilizing this pyroelectric effect and improving the efficiency of the power conversion from heat to electricity has become important (Guyomar et al., 2008). One of the pyroelectric materials that is easily available for energy scavenging is lead zirconate titanate (PZT) (Dalola et al., 2010; Hsiao et al., 2012; Krishnan et al., 2014; Lee et al., 2012; Xie et al., 2008; Yang et al., 2012a, 2012b, 2012c, and Wilkie K, 2000, Torah R et al., 2008). Another material of interest, polyvinylidene difluoride (PVDF) polymer as a low cost and flexible pyroelectric material, has attracted interest for energy harvesting applications as shown by several researchers (Kouchachvili and Ikura, 2007; Navid et al., 2010; Navid and Pilon, 2011; Olsen et al., 1985; Yang et al., 2012b). All the research performed up to date on maximum power harvesting from pyroelectric devices indicate that material properties' optimization, external circuitry power loss minimization, and impedance

matching are three key factors on achieving efficient pyroelectric energy harvesting. Researchers have investigated generating currents from thermal variations using pyroelectric materials based on fabricated PZT and commercial PVDF films. Cuadras et al. (2006) showed that economical PZT films are useful in pyroelectric energy harvesting and the parallel association of different cells provided the opportunity to optimize the power output for a given combination of the cell internal resistance and load resistance. Currents in the order of 0.1 mA and charges in the order of 10 mC have been satisfied for a temperature gradient of 60 K (Cuadras et al., 2010). Chang and Huang (2010) have proposed a PZT and stainless steel laminate composite with an 88% pyroelectric coefficient enhancement to increase its maximum power density, efficiency, and electro thermal coupling factor by 254%. Kandilian et al. (2011) showed that maximum energy density of 100 mJ cm^{-3} per cycle between temperatures of $80 \text{ }^\circ\text{C}$ and $170 \text{ }^\circ\text{C}$ by commercial PMN-32PT capacitors subjected to the Olsen cycle. Amokrane et al. (2012) showed rectifier-generated voltages using comparators and MOSFET as diodes ranging from 0.8 to 2.5 V which is higher than those obtained with conventional rectifiers. Sebald et al. (2008) studied methods for optimizing pyroelectric energy harvesting and described the most important parameters when choosing materials and designing a device. Krishnan et al. (2014) showed they could achieve a power density of 421 mW/cm^3 with PZT-5H. Impedance matching in general is very important to maximize power delivered to the load for piezoelectric energy harvesting. For example, when the resistive load of the circuit exceeds the impedance of the piezoelectric cell, lower efficiency power generation will be achieved (Sodano et al., 2004). In a recent work, Kong et al. (2010) demonstrated an alternative method for impedance matching called resistive matching for piezoelectric energy harvesting. Since utilizing a large inductor value in order to complete the conjugate impedance matching is impractical, resistive impedance matching would be a better

solution. However, impedance matching has not been thoroughly considered in pyroelectric studies on energy harvesting. Pyroelectric experimental work depends on trial and error or statistical approaches to choose the optimum load resistance. In a recent paper, as an illustrative example, the resistance is chosen to be 1 MO and it was not optimized for maximum pyroelectric power generation (Xie et al., 2010). Erturun et al. showed the effect of various resistances, up to 10 MO, on stored energy for a temperature rate of 0.1 Hz and capacitance of 100 mF. The optimal values for heat rate, resistance, and capacitance were estimated to be 0.05 Hz, 7330 k Ω , and 100 mF, respectively (Erturun et al., 2014). In another similar work, to optimize power, the resistance used in the energy harvesting circuit was tested for a range of 1 to 12MO, and based on that; the optimal resistance was evaluated to be 8M Ω for a PZT sample (Mane et al., 2011).

Some key points that previous published work in the area of pyroelectric energy harvesting show that the electrical part of the pyroelectric cell is modeled as a capacitor, while the inherent parallel resistor has been ignored. This parameter is usually neglected because common measurement techniques only show infinite resistance, which is not accurate. Hence, if the equivalent circuit for a pyroelectric cell is incomplete, optimum impedance matching becomes impossible. Pyroelectric energy harvesters require equipment for impedance measurements at low frequencies, such as 1 Hz and lower. The most commonly available equipment to measure the impedance is an LCR precision meter, such as QuadTech 7400 with a range from 10 Hz and above, and the impedance analyzer, such as HP4194 with a range of 100 Hz to 40 MHz. Some spectroscopy equipment such as the Solartron 1296A Dielectric Interface System actually has the capability to do characterization for dielectric in the frequency range from 10 mHz to 10 MHz, but it is not a standalone unit. It needs to interface with the 1260A impedance analyzer. It

requires very long cycle times for samples due to the sub-hertz frequencies. All of these devices are costly and bulky.

The purpose of this work is to demonstrate a new simple stand-alone method of characterizing the impedance of a pyroelectric cell. This method utilizes a pyroelectric single pole low-pass filter technique (Shaheen M., et al 2016). Utilizing the properties of a pyroelectric single pole low-pass filter technique, a known input voltage is applied and using simple equations, capacitance C_p and resistance R_p at a frequency range of 1 mHz to 1 Hz can be calculated. For verification purposes, an LCR meter and an impedance analyzer were exploited at 10 and 100 Hz, respectively. Results showed that R_p values for two materials, lead zirconate titanate-5A and polyvinylidene difluoride, were within 8%, and C_p values were within 7.5%. In addition, to verify the importance of the impedance values in energy harvesting applications, output power was measured with varying impedance values. The optimal load resistances for PVDF and PZT-5A were consistent with the measured pyroelectric impedance at the particular heat range with 10.9% and 1.4%, respectively. The pyroelectric single pole low-pass filter method presented here demonstrates that for pyroelectric materials the impedance depends on two major factors: (1) average working temperature and (2) the heating rate. Neglecting these two factors can result in inefficient and unpredictable behavior of pyroelectric materials when used in energy harvesting applications.

1.2 Piezoelectricity

Piezoelectric Effect can be defined as an existence of an electrical voltage across sides of a piezoelectric cell when it is under stress and of strain when an electric field is applied. Pierre Curie and his brother Jacques explored this effect in 1880 (Pierre Curie, 1859-1906). It is assigned by the displacement of free charges such as ions, producing the electric polarization of the crystal basic structural unit. When an electric field is applied, the ions are relocated by electrostatic forces, causing mechanical deformation in the crystal. This effect occurs naturally in specific materials such as quartz crystals, but can be created in other materials, such as some ceramics containing mainly Lead, Zirconium, and Titanium cell (PZT). The poling process is used to “stimulate” the piezo properties of the mix of metals. The material is first heated to Curie temperature T_c . Then, an electric field is applied in the preferred direction, pushing the ions to align along this “poling” axis. When the ceramic material cools, the ions “recall” this polling and act accordingly.

1.2.1 Piezoelectric energy harvesting

A diversity of wireless and portable applications has been developed in the past two decades providing convenience and new capabilities. However, the batteries used to power such devices require tedious maintenance or replacement, and often results in going above the volume requirements of some applications (Kong et al., 2010). To address this issue, energy scavenging systems have been presented by researchers. Different energy sources existing in the environment, such as light, wind, heat, and vibration, can be the sources for energy harvesting. Among them, the vibration can be found almost everywhere in our daily life and, hence, have fascinated much research consideration (Tang et al., 2010). Many research works have been

proposed for piezoelectric energy scavenging from ambient vibration (Richards D 2004, Beeby, S. P et al., 2006; Anton, S. R. and Sodano, 2007; Saadon, S. et al., 2011; Kim B. et al., 2014; Zhu, D. 2010, and Ottman K 2003, Wickenheiser M. 2010, and Rastegar J 2006). Some researchers presented series of piezoelectric energy harvesting devices with low-level vibrations of common household and other home environments (Sohn W 2005, Leland, E. S. and Wright, P. K, 2006; Sodano, H. et al., 2004; Choi, W. J et al., 2006). There are several main restrictions for real applications of the piezoelectric energy scavenger. Firstly, coupling coefficient values for piezoelectric materials is critical to improve the performance of piezoelectric energy harvesters. Secondly, sustainability of piezoelectric energy harvesters under severe vibrations from fatigue and cracking of these devices are crucial. Thirdly, an efficiency of the electronic circuitry for these harvesters in such small vibration energy needs to be developed (Heung Soo Kim et al., 2011). Lastly, operating frequency range is critical to be tuned for a specific real ambient vibration frequency.

1.2.2 Piezoelectric operating frequency tuning and bandwidth widening

Ambient vibration sources are unpredictable which a critical issue is for piezoelectric cantilever based energy harvesters. Resonant devices with high Q-factor has very narrow frequency bandwidth of operation, whereby with a minor shift of frequency in excitation will result in a drop in the output power (Kok et al., 2011). In other words, piezoelectric energy harvesters provide the maximum output power when working at resonance, which means that the harvesters are not efficient in environs with random vibrations (Hsu et al., 2014). To date there are, in general, two methodologies to solving this issue. The first is to alter the resonant frequency of a single harvester so that it matches the frequency of the ambient vibration.. This

can be verified by changing the mechanical characteristics of the structure or electrical load on the harvester and they are known as mechanical and electrical tuning approaches (Zhu et al., 2010). The second technique is to broaden the frequency bandwidth of the piezoelectric harvester and it can be achieved, for instance, by using an array of piezoelectric cantilevers with a diverse resonant frequency.

Mikael et al proposed a low-cost self-tuning technique (Mikael et al. 2010). It was based on the properties of systems driven at their natural frequency and on a non-linear, low-cost stiffness tuning scheme described by Guyomar et al. (2008) for the actuation. This technique permits an acceptable tuning of the resonance frequency on a wide range, whatever the vibration frequency is, while guaranteeing a net positive energy output that features a broader frequency spectrum than the uncontrolled system. Yu-Jen Wang et al. proposed a fine-weighted swing disk joined with a circular Halbach array magnetic disk for generating a steady power output in a broad wheel rotation speed band. A self-tuning mechanism was established, and it was revealed that several hundred micro-Watts of power could be scavenged from it Jen Wang et al. (2012). Zengtao Yang et al. suggested coupled bimorph beams whose resonant frequencies are very adjacent to each other are adjustable. It was shown that such a structure is wideband in the sense that it can collect vibration energy over a wider frequency spectrum than a single-beam harvester. This frequency wideband can be further broadened by using more than two beams Zengtao Yang et al. (2009). Wu et al presented a piezoelectric harvester utilizing mass adjusting. The tip mass of the suggested device consisted of two parts: a fixed mass fastened to the cantilever and a mobile screw (Wu et al., 2008). Wen-Jong Wu et al suggested and verified a tunable resonant frequency power scavenger in a cantilever beam form to move its resonant frequency to match that of the ambient vibration. This system utilizes an adjustable capacitive

load to change the gain curve of the beam and a low power microcontroller samples the ambient frequency and alters the capacitive load to match external vibration frequency (Wu et al., 2006).

Ferrari et al presented a multi-frequency piezoelectric harvester proposed for driving autonomous sensors from background vibrations. The harvester is consisted of multiple bimorph cantilevers with different natural frequencies, whose rectified outputs are fed to a storage capacitor. They revealed the possibility of utilizing the harvester with input vibrations across a wideband frequency range, improving the efficiency of the overall energy conversion system over the case of a single scavenger (Ferrari et al., 2008). S.M. Shahruz studied the performance of vibrational band-pass filters to be used in energy harvesters. Such a filter is consisting of several cantilever beams where at the end of each beam a tip mass, known as the proof mass, is attached. Shahruz raised two questions related to the performance of this filter: (i) what is the optimum expected performance of the filter? (ii) How can a system with such a performance be fabricated? Knowledge of such issues leads to a systematic process for evaluating dimensions of the cantilever beams and masses of the tip masses of the band-pass filters (Shahruz S.M., 2006). Weiqun Liu et al. suggested a bi-stable structure consisted of four thin cantilever beams, two piezoelectric stacks, and a dynamic mass is developed. The harvester performance was established for bandlimited noise excitations and an actual vibration signal from a driving car Weiqun Liu et al. (2014).

1.2.2.1 Mechanical tuning

Mechanical tuning can be satisfied by changing either the mass of the cantilever beam or the length which is also ultimately considered as cantilever mass changing. The resonant frequency of a spring mass structure is given by (Zhu et al., 2010):

$$f_r = \frac{1}{2\pi} \sqrt{\frac{k^*}{m}} \quad \text{Equation 1.3}$$

Where: k^* is the spring constant and m is the inertial mass. When tuning the natural frequency of the harvester the spring constant or the mass can be changed. For a cantilever with a mass at the free end in Figure 1.2 (adapted from Shahruz, 2006a) the resonant frequency is given by (Blevins, 1979):

$$f_r = \frac{1}{2\pi} \sqrt{\frac{Y w h_b^3}{4l^3(m+0.24m_b)}} \quad \text{Equation 1.4}$$

Where Y is Young's modulus of the beam material; w , h_b , m , l , and m_b , are the width, thickness, inertial mass, length, and the mass of the piezoelectric cantilever, respectively. When the length l is changed the mass of the cantilever m_c changes too as it is equal to $w h l_n \rho$ where l_n is the new length ($l + \Delta l$) and ρ is the density of the material of the cantilever. If the total mass is changed by both adding a proof mass m and changing the length, the new resonance frequency f_m equation changes to:

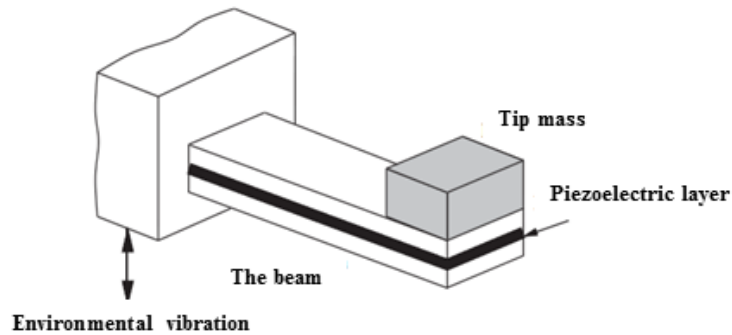


Figure1.2 a cantilever with a tip mass at the free end

1.2.2.2 Bandwidth widening

In order to harvest energy efficiently from different sources of vibration, an energy harvester should have wide bandwidth in nominated frequency ranges. A device with such characteristics is called a mechanical band-pass filter (Shahruz, 2006b). Figure 1.3 shows a beam–mass system (Shahruz, 2006a) that can be developed into a band-pass filter when dimensions of the cantilevers and masses of the tip masses are chosen properly:

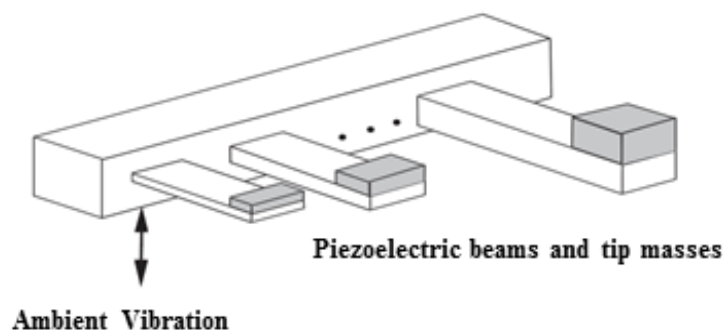


Figure 1.3 a band-pass filter of cantilever beams and proof masses

1.2.2.3 Electrical tuning

The main principle of electrical tuning is to alter the electrical damping by adjusting the load, which causes the power spectrum of the harvester to move (Zhu et al., 2010). By changing shunt circuit conditions applied across the piezoelectric layer, the elastic modulus of the layer changes and consequently the overall stiffness of the structure changes. Since the resonance frequency of the structure is dependent on its stiffness, by changing the shunt conditions, the natural frequency can be tuned to a required value. For a bimorph the upper, lower and in between natural frequency limits are denoted by the following three equations respectively (Charnegie, 2007).

$$\omega_{up} = \sqrt{\frac{3 \left(C_{11} - \frac{d_{31}^2}{\varepsilon^*} \right)^{-1} I}{L^3 m_{eff}}} \quad \text{Equation 1.6}$$

$$\omega_{low} = \sqrt{\frac{3 I}{L^3 C_{11} m_{eff}}} \quad \text{Equation 1.7}$$

$$\omega = \sqrt{\frac{3 \left(C_{11} - \frac{d_{31}^2 A}{t(C_p + C_{sh})} \right)^{-1} I}{L^3 m_{eff}}} \quad \text{Equation 1.8}$$

Where:

ω_{low} : Lower bound frequency

ω_{up} : Upper bound frequency

C_{11} : is the mechanical compliance of the piezoelectric cell

d_{31} : is the electromechanical coupling coefficient

ε^* : The permittivity of the material

A : Capacitor area

t : thickness

C : the capacitance

C_{sh} : The shunt capacitance

C_p : The inherent piezoelectric capacitance

In this study, a hybrid frequency tuning methodology using multiple piezoelectric bimorph cantilevers will be demonstrated. This is done to accomplish mechanical tuning, electrical

tuning, and bandwidth widening simultaneously to develop a significant growth in frequency spectrum for the piezoelectric energy scavenger. Rather than having three resonant frequencies the system has twelve natural frequencies and maximum power peaks.

In this study, a hybrid frequency tuning methodology using multiple piezoelectric bimorph cantilevers will be presented. This is done to accomplish mechanical tuning, electrical tuning, and bandwidth widening simultaneously to develop a significant growth in frequency spectrum for the piezoelectric energy scavenger. Rather than having three resonant frequencies the system has twelve natural frequencies and maximum power peaks.

It will be shown that this design which includes three cantilevers and four capacitors for each beam could deliver more power than the case if one bimorph cantilever is assumed to be used with 12 capacitors. The proposed hybrid tuning technique is feasible and the optimal method for wide broadband piezoelectric energy harvesting.

In addition, an experimental enhanced power harvester with hybrid tuning using multiple piezoelectric unimorph cantilevers will be described. This approach sought to enhance piezoelectric power and frequency spectrum using mechanical tuning, electrical tuning, and bandwidth widening techniques simultaneously with conjugate impedance matching. This approach aimed to enable piezoelectric energy harvesters to work efficiently in a variety of environments with random ambient vibrations frequencies. A small toroid inductor of 700 mH is connected in parallel to the load resistance and shunt capacitance. An extended frequency range of 12 resonance frequencies with 300% improvement is obtained experimentally with enhanced power density improvements of 19.7% to 197%.

1.3: Modeling for piezoelectric bimorph cantilever with RLC load

Some single degree of freedom SDOF models have been derived to analyze piezoelectric bimorph cantilevers (Du Toit N E et al. 2005; Stephen N G 2006; Erturk A and Inman D J 2008; Hagood N Wet al. 1990; Chen S-N et al., 2006, Sterken T 2004). Roundy S. developed a SDOF model for a piezoelectric harvester with two designs optimized within an overall space constraint of 1 cm^3 . These designs have been fabricated and tested with both resistive and capacitive loads. In this study a mathematical state space model for a piezoelectric bimorph cantilever beam with parallel resistance, capacitance, and inductance load has been developed considering the model demonstrated by Roundy S. 2004. This model can be utilized to evaluate the feasibility of shunting an inductive reactance with a small inductance value to improve the output power of piezoelectric scavengers with electrical tuning.

1.4: Hybrid Pyro-Piezoelectric energy harvesting

Hybrid energy harvesting devices can be defined as those which simultaneously harvest the numerous energies by utilizing an integrated system (Ya Yang et. al 2013).

Hybridizing different categories of energy systems into a single harvesting device will compensate the performance of each individual system. Moreover, this will allow the hybrid energy scavenger to harvest different kinds of energy simultaneously (Nayar C V et al., 1993; Xu C, Wang et al., 2008; Gonzalez, G. 2010, Iqbal M T 2003, and Challa, R 2009). The thermal, mechanical, and solar energies typically can be harvested from our living surroundings and this harvesting is of critical significance for our long-term energy desires. As these energies are not always obtainable at the same time, a hybrid energy cell is developed. Some materials, such as PVDF, PZT, and ZnO have both the pyroelectric and piezoelectric properties; they can be used for manufacturing both the pyroelectric and piezoelectric harvesters. These materials are used for

producing the hybrid energy scavenger since they can save the production cost and reduce the size of the energy harvesting device (S. B. Lang 2005). In some previous work (Ya Yang et. al 2014), a flexible hybrid energy harvester for simultaneously/individually harvesting heat, vibration, and solar energies was described. Dukhyun Choi proposed flexible hybrid Nano architecture that can be used as both an energy scavenger and a touch sensor on a single device. A hybrid cell was designed with a total thickness of less than 500 nm on a plastic substrate. This hybrid harvester can provide both solar and vibrational touching energies (Dukhyun Choi et al., 2010). Yonas Tadesse et al presented a hybrid energy scavenging device that uses electromagnetic and piezoelectric techniques. The device consists of piezoelectric crystals attached to a cantilever beam. The tip of the cantilever has an attached permanent magnet which vibrates within a coil fixed to the top of the system causing electric current by Faraday's effect. This harvesting package was optimized using the finite element software, ANSYS, and the output power was found to be 0.25W from the electromagnetic mechanism and 0.25mW using the vibration at 35 g vibration acceleration and 20 Hz frequency (Yonas Tadesse et al., 2009). Considering previous studies, there was no investigation for impedance matching and power maximization for a hybrid energy harvester combining pyroelectric and piezoelectric mechanisms on which we focused in this work.

1.5 Approach

Several techniques for power maximization will be presented in this study.

In the first approach, a simple method named PSLPF is used to characterize impedance for PVDF and PZT-5A cells at low frequencies has been invented such that the pyroelectric power harvested can be maximized. The PSLPF technique proposed here shows that impedance dependence on the average temperature and the heating rate are both key parameters when characterizing a pyroelectric material. This indicates obviously that to optimize impedance when exploiting the pyroelectric effect, both operating average working temperature and the rate of temperature change need to be considered when designing energy harvesting systems. Neglecting those parameters will result in inefficient and unpredictable systems.

In the second approach, a state space dynamics model of the piezoelectric cantilever with RLC load has been developed. This model can be utilized to analyze the feasibility of shunting an inductance with small value to improve the output power of vibration based scavengers with passive electrical tuning. A general dynamics model of the piezoelectric cantilever with RLC load has been developed, and test results from this generator were presented and discussed.

In the third approach, a hybrid frequency tuning methodology using multiple piezoelectric bimorph cantilevers is presented. This is done to accomplish mechanical tuning, electrical tuning, and bandwidth widening simultaneously to develop a significant increase in frequency range for the piezoelectric energy scavenger. The proposed hybrid tuning technique was feasible and the optimal method for wide broadband piezoelectric energy harvesting. An enhanced power hybrid tuning technique using multiple piezoelectric unimorph cantilevers with conjugate impedance has been presented.

Finally, a hybrid energy harvester has been designed and implemented. It was shown that to optimize impedance when utilizing the pyroelectric and piezoelectric effects simultaneously, both operating average working temperature and the rate of temperature change need to be considered when designing energy harvesting applications. Neglecting those parameters will result in inefficient and unpredictable hybrid energy harvesting systems. In addition, an impedance matching using a new voltage doubler circuit for rectifying and collecting pyroelectric and piezoelectric voltages individually is proposed and tested. The obtained results were significantly higher than harvested energy simultaneously from the same material.

Chapter 2 Pyroelectric Energy Maximization

2.1 Introduction

Energy harvesting systems are those which convert different types of ambient energy such as wind, heat, vibration, and light into useful electrical energy. The harvesting of ambient energy to power small electronic components has received tremendous attention over the last decade (Gambier et al., 2012). Among the most important phenomena utilized in energy harvesting is pyroelectricity which can be defined as the temperature reliance of the spontaneous polarization in certain anisotropic solids (Lang, 2005). The investigation of the feasibility of efficient heat energy harvesting using this pyroelectric effect and improving the effectiveness of the energy conversion from heat to electricity has become of importance (Guyomar et al., 2008). One of the pyroelectric materials that is easily available for energy harvesting is lead zirconate titanate (PZT) (Dalola et al., 201; Krishnan et al., 2014; Lee et al., 2012; Xie et al., 2008). Another material of interest, PVDF polymer as low cost, and flexible pyroelectric material has attracted interest for energy harvesting applications as shown by several researchers (Olsen et al., 1985; Yang, Zhang, et al., 2012; Navid et al., 2010).

All the research performed up to date on maximum power harvesting from pyroelectric devices indicate that material properties optimization, external circuitry power loss minimization, and impedance matching are three key factors on achieving efficient pyroelectric energy harvesting. Researchers have investigated generating currents from thermal fluctuations using pyroelectric cells based on fabricated screen-printed PZT and commercial PVDF films. Cuadras et al. (2006) showed that economical PZT films are useful in pyroelectric energy harvesting and the parallel association of different cells provided the opportunity to optimize the power output for a given combination of the cell internal resistance and load resistance. Currents in the order

of 0.1 μA and charges in the order of $10\mu\text{C}$ have been satisfied for a temperature gradient of 60K (Cuadras et al., 2010). Chang and Huang (2010) have proposed a PZT and stainless steel laminate composite with an 88% pyroelectric coefficient enhancement to increase its maximum power density, efficiency, and electro thermal coupling factor by 254%. Kandilian et al. (2011) showed that maximum energy density of $100 \text{ mJcm}^{-3}/\text{cycle}$ between temperatures of 80°C and 170°C by commercial PMN-32PT capacitors subjected to the Olsen cycle. Amokrane et al. (2012) showed a rectifier—using comparators and MOSFET as diodes—generated voltages ranging from 0.8 to 2.5 V which is higher than those obtained with conventional rectifiers. Sebald et al. (2008) studied methods for optimizing pyroelectric energy harvesting and described the most important parameters when choosing materials and designing a device. Krishnan et al. (2014) showed he could achieve a power density of $421.18 \mu\text{W}/\text{cm}^3$ with PZT-5H.

Impedance matching in general is very important to maximize power delivered to the load for piezoelectric energy harvesting. For example when the resistive load of the circuit exceeds the impedance of the piezoelectric material, lower efficiency power generation will be achieved (Sodano et al., 2004). In recent work, Kong et al. (2010) demonstrated an alternative method for impedance matching called resistive matching for piezoelectric energy harvesting. Since utilizing a large inductor value in order to complete the conjugate impedance matching is impractical, resistive impedance matching would be a better solution. However, impedance matching has not been thoroughly considered in pyroelectric studies on energy harvesting. Pyroelectric experimental work depends on trial and error or statistical approaches to choose the optimal load resistance. In a recent paper, as an illustrative example, the resistance is chosen to be $1 \text{ M}\Omega$ and it was not optimized for maximum pyroelectric power generation (Xie et al., 2010). Erturun et al., showed the effect of various resistances, up to $10 \text{ M}\Omega$, on stored energy for a

temperature rate of 0.1 Hz and capacitance of 100 μF . The optimum values for temperature rate, resistance, and capacitance were predicted to be 0.05 Hz, 7330 $\text{k}\Omega$, and 100 mF , respectively (Erturun et al., 2014). In another similar work, to optimize power, the resistance used in the circuit was tested for a range of values from 1 to 12 $\text{M}\Omega$, and based on these tests, the optimal value was determined to be 8 $\text{M}\Omega$ for a PZT sample (Mane et al., 2011a).

Some key points that previous published work in the area of pyroelectric energy harvesting show that the electrical part of the pyroelectric cell is modeled as a capacitor, while the inherent parallel resistor has been ignored. This parameter is usually neglected because common measurement techniques only show infinite resistance, which is not accurate. Hence if the equivalent circuit for a pyroelectric cell is incomplete, optimum impedance matching becomes impossible. Pyroelectric energy harvesters require equipment for impedance measurements at low frequencies, such as 1 Hz and lower. The most commonly available equipment to measure the impedance is an LCR precision meter, such as QuadTech 7400 with a range from 10 Hz and above, and the Impedance Analyzer, such as HP4194 with a range of 100 Hz to 40 MHz. Some spectroscopy equipment such as the Solartron 1296A Dielectric Interface System actually has the capability to do characterization for dielectric in the frequency range from 10 μHz up to 10 MHz, but it is not a stand-alone unit. It needs to interface with the 1260A impedance analyzer. It requires very long cycle times for samples due to the sub-hertz frequencies. All of these devices are costly and bulky.

This study aims to show a simple method to characterize impedance for PVDF and PZT-5A cells at low frequencies such that the pyroelectric power harvested can be maximized. This method utilizes a Pyroelectric Single pole Low Pass Filter, PSLPF, which consists of a pyroelectric cell instead of parallel R and C components in the feedback path of this common

filter. By applying a known input signal at low frequencies along with some simple calculations, the internal capacitance C_p and resistance R_p of the pyroelectric cell can be calculated. Once these parameters were calculated, the results were verified by measuring output pyroelectric energy at various values of load impedance. The maximum power corresponds to the calculated value of R_L using the PSLPF method within a 9.8 % difference for PVDF cell and a 1.4 % difference for PZT-5A cell.

The experiments highlighted the importance of the effect of ambient working temperature on the total pyroelectric impedance. When PVDF or PZT-5A is exposed to ambient working temperatures that are higher than 24°C, the inherent capacitance and resistance of the pyroelectric material change. For instance, in the case of PVDF impedance decreases approximately 10 times from 24 to 90°C. This order of magnitude change can have an adverse impact on application design specifically on energy harvesting applications. Hence the equivalent circuit of a pyroelectric material is reviewed in detail to highlight all of the effects observed in the experiments.

2.2 Pyroelectric equivalent circuit

The general approximate model of a pyroelectric cell is described in Figure 2.1 and was commonly used for many years. This circuit represents a current source connected in parallel with two parallel passive elements, a resistor R_p and a capacitor C_p (Cuadras, 2006).

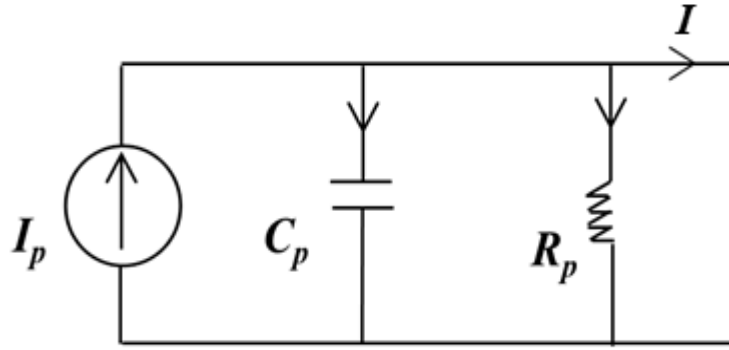


Figure 2.1. Equivalent circuit for a single pyroelectric cell

The pyroelectric equations can be written as (Guyomar et al., 2008):

$$D = \varepsilon E + pT \quad \text{Equation 2.1}$$

$$I = A \frac{dD}{dt} \quad \text{Equation 2.2}$$

$$I = p A \dot{T} - C_p \dot{V} \quad \text{Equation 2.3}$$

$$C_p = \frac{\varepsilon A}{b} \quad \text{Equation 2.4}$$

Where D , E , T , V , and I are the electrical displacement, electrical field, temperature, electric potential, and generated electric current respectively; \dot{T} and \dot{V} represent the first derivatives of temperature and electric potential; A , b , C_p , p , and ε are the surface area, thickness, inherent capacitance, the pyroelectric coefficient, and permittivity respectively.

Leakage current, usually neglected, has a value that is especially large at high temperatures. To include this effect, surface current density, J , is considered in the form shown in Equation 2.5 (Farmingdale University tutorial)

$$J = J_p + J_c \quad \text{Equation 2.5}$$

Where J_d , and, J_c are the two components of current density namely the displacement current density, J_d , and conduction current densities J_c

$$J = \frac{\partial D}{\partial t} + \sigma \cdot E \quad \text{Equation 2.6}$$

Where σ represents the conductivity of the material

$$I_p = A \cdot J = A \frac{\partial D}{\partial t} + A \cdot \sigma \cdot E \quad \text{Equation 2.7}$$

According to An-Shen Siao (An-Shen Siao et al., 2015), if the pyroelectric circuit is analyzed using Kirchhoff's current law, the sum of the currents entering into a node is equal to the sum of the currents leaving that node. Equation 2.7 shows this effect clearly when the outgoing current is mostly due to the pyroelectric effect and the other terms represent losses due to the internal capacitance and resistance.

The electric current in a pyroelectric cell depends on the temperature fluctuation which causes a polarization and a charge moving. There are not free carriers in the pyroelectric capacitor. The polarization of the charges induces an AC current in the electrodes if connected to an external circuit. The electric equivalent circuit can be considered as a parallel resistor-capacitor with no current source when there is no fluctuation in temperature.

Considering the described equivalent circuit, a new method to characterize a pyroelectric cell is proposed and described in the following section.

2.3 Pyroelectric Single Pole Low Pass Filter (PSLPF)

One of the most extensively used electronic circuits is the operational amplifier low pass filter circuit which simply consists of an operational amplifier, a resistor connected in series via the non-inverting input, and a parallel RC circuit connected to the feedback path. The function of this circuit is to undergo low pass filtering when an input signal is applied. This application can be effectively utilized in order to characterize any pyroelectric cell by connecting this cell across the feedback path instead of the RC parallel circuit as shown in Figure 2.2. The transfer function of PSLPF circuit would be written as:

$$\frac{V_o}{V_{in}} = \frac{-Z_p}{Z_1} = -\frac{\frac{R_p * X_p}{\sqrt{R_p^2 + X_p^2}}}{R_1} = -\frac{R_p * X_p}{R_1 \sqrt{R_p^2 + X_p^2}} \quad \text{Equation 2.8}$$

Where:

V_{in} and V_{out} are the input and output voltages respectively. R_p and X_p , and Z_p are pyroelectric resistance, capacitive reactance, and total impedance respectively.

At very low frequencies, the parallel feedback capacitive reactance can be considered as an open loop and the voltage gain is constant and equal to:

$$\frac{V_o}{V_{in}} = \frac{-R_2}{R_1} \quad \text{Equation 2.9}$$

The corner frequency for this low pass filter is:

$$\omega_{c1} = 1/R_p C_p \quad \text{Equation 2.10}$$

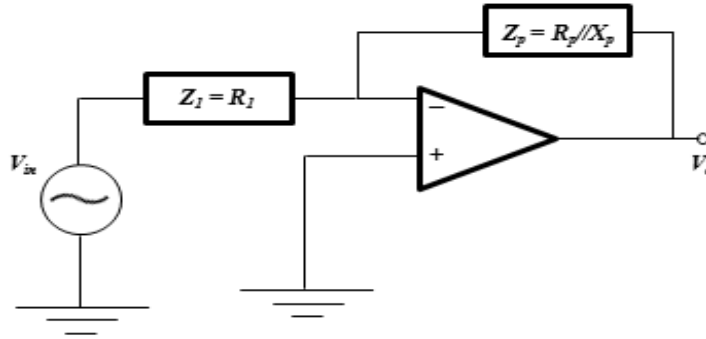


Figure 2.2. Pyroelectric single pole low pass filter PSLPF

To obtain the value of C_p and R_p using the PSLPF shown in Figure 2.2, first substitute Z_p with a pyroelectric material with inherent R_p and C_p (unknown values). DC voltages of -12V and +12V are applied on either side of the operational amplifier to have a voltage range of 24V across the circuit as a DC biasing voltage. Then, an input voltage, V_{in} , is applied such that it doesn't produce an output voltage that exceeds the rail-to-rail voltage that is equal to 24 V. The frequency of the input signal is chosen as low as possible until the output voltage reaches a constant sinusoidal wave that no longer increases. This is the maximum peak voltage. Then the frequency is adjusted until the peak voltage becomes 0.707 of the maximum peak voltage. This is the cutoff frequency for the pyroelectric material and will be the frequency used for Equation 2.13. The resistor in the circuit, R_p , needs to be shunted with a parallel resistor R_{sh} of 10 M Ω (See Figure2.3) so that it is significantly lower than the expected resistance of the pyroelectric material. This ensures that the current will all travel through the resistor R_{sh} instead of the highly resistant pyroelectric material. The capacitance C_p can then be calculated by using the cut off frequency and substituting R_{sh} instead of R_p in Equation 2.10. Once C_p is calculated, it can be

used to compute the capacitive reactance X_p . To calculate R_p at a particular frequency, the voltage gain, R_I , and X_p should be substituted in Equation 2.8. Once C_p and R_p are calculated, the total impedance Z_p can be easily computed using Equation 2.12 that is the same equation used for optimal load resistance.

To demonstrate that the optimal load resistance has been reached, an energy harvesting experiment is setup. It is a fact, that for maximum output power a resistive impedance matching method is required. Since the conjugate impedance requires a high inductance value, it becomes impractical in an energy harvesting application. Instead, the following section shows the principles for resistive impedance matching.

2.4 Resistive impedance matching

To extract the maximum power from an electric power source a conjugate impedance matching load is used. In order to cancel the capacitive impedance in a pyroelectric harvester, a large inductor value is needed which is impractical. An alternative method and suboptimal approach is to use only a resistive load and try to match the source impedance (Kong et al., 2010). If a load resistance R_L is connected in parallel to the circuit in Figure 2.1, the power delivered to the load can be calculated as follows:

$$P_0 = i_L^2 R_L \quad \text{Equation 2.11}$$

Where i_L is the load current:

The maximum power can be satisfied at the optimal load resistance R_{Lopt} which can be calculated by derivation of Equation 2.11 with respect to R_L and equating the result to zero.

$$R_{Lopt} = \frac{R_p * X_p}{\sqrt{R_p^2 + X_p^2}} \quad \text{Equation 2.12}$$

$$X_p = \frac{1}{j\omega C_p} \quad \text{Equation 2.13}$$

Equation 2.12 states that the optimal resistance for a maximum power is equal to the magnitude of the internal source impedance. By considering Figure 2.1, the optimal resistance for impedance matching is:

$$R_{Lopt} = \left| R_p // \frac{1}{j\omega C_p} \right| = \frac{R_p}{\sqrt{1 + \omega^2 C_p^2 R_p^2}} \quad \text{Equation 2.14}$$

Taking the limit of Equation 2.13 as follows:

$$\lim_{R_p \rightarrow \infty} \frac{R_p}{\sqrt{1 + \omega^2 C_p^2 R_p^2}} = \frac{1}{\omega C_p} \quad \text{Equation 2.15}$$

$$\lim_{\omega C_p \rightarrow 0} \frac{R_p}{\sqrt{1 + \omega^2 C_p^2 R_p^2}} = R_p \quad \text{Equation 2.16}$$

Equation 2.14 demonstrates the optimal load for a piezoelectric generator wherein the voltage frequency is higher than a pyroelectric generated voltage. For the case of pyroelectric energy scavenging, the frequency is usually less than 1 Hz. Hence, the capacitive reactance in a pyroelectric cell is very large and the optimal resistance should be equal to R_p as shown in Equation 2.15. An experimental study to prove the feasibility of the suggested method is presented in the next section.

2.5 Experimental setup for PVDF and PZT-5A PSLPF circuit

The main experimental circuit for characterization of two different pyroelectric cells is employed as shown in Figure 2.3. It has two general functional modes. In the first mode it is called a PVDF PSLPF, and in the second one it is called PZT-5A PSLPF. The general circuit contains an op-amp LM-348 chip, which is a quadruple, independent, and has high gain (Texas Instrument, 2002). The typical offset for the used op amp was about 4 nA and can be neglected. Input offset voltage of 1 mV between the input voltages is expected but it can be neglected too. It has a unity gain bandwidth of 1 MHz and input impedance of 2.5 M Ω . The load effect would be minor and can be ignored. The input bias currents i_+ and i_- are relatively small, so we treat them as though they don't present at all, and the contribution of bias voltages is still small and can be neglected. A National instrument DAQ was exploited to interface with a personal computer using LabVIEW to display and collect data. The materials utilized were PVDF and PZT. The geometry properties, manufacturer, and electrical characteristics of both samples are listed in Table 2.1. The circuit has three main modes as demonstrated in Table 2.1. By providing a sinusoidal voltage signal such that the output voltage is less than the rail-to-rail DC biasing voltage, measuring the output signal, and using Equations 2.8 and 2.10, parameters R_p , C_p , and Z_p can be calculated. The experimental setup has been tested using standard ceramic capacitors with known values as dummy cells and the performance has been validated successfully.

Table 2.1. Piezoelectric Materials Characteristics

Material	Manufacturer	Dimensions (cm)	Capacitance (nF)
PVDF (DT2-028K/L with rivets)	Measurement Specialties	Rectangular: 6.2 x 1.2 x 0.040	2.78
PZT5A4	Morgan Advanced Ceramics	Circular: D = 5cm, t = 0.0158cm	203.5

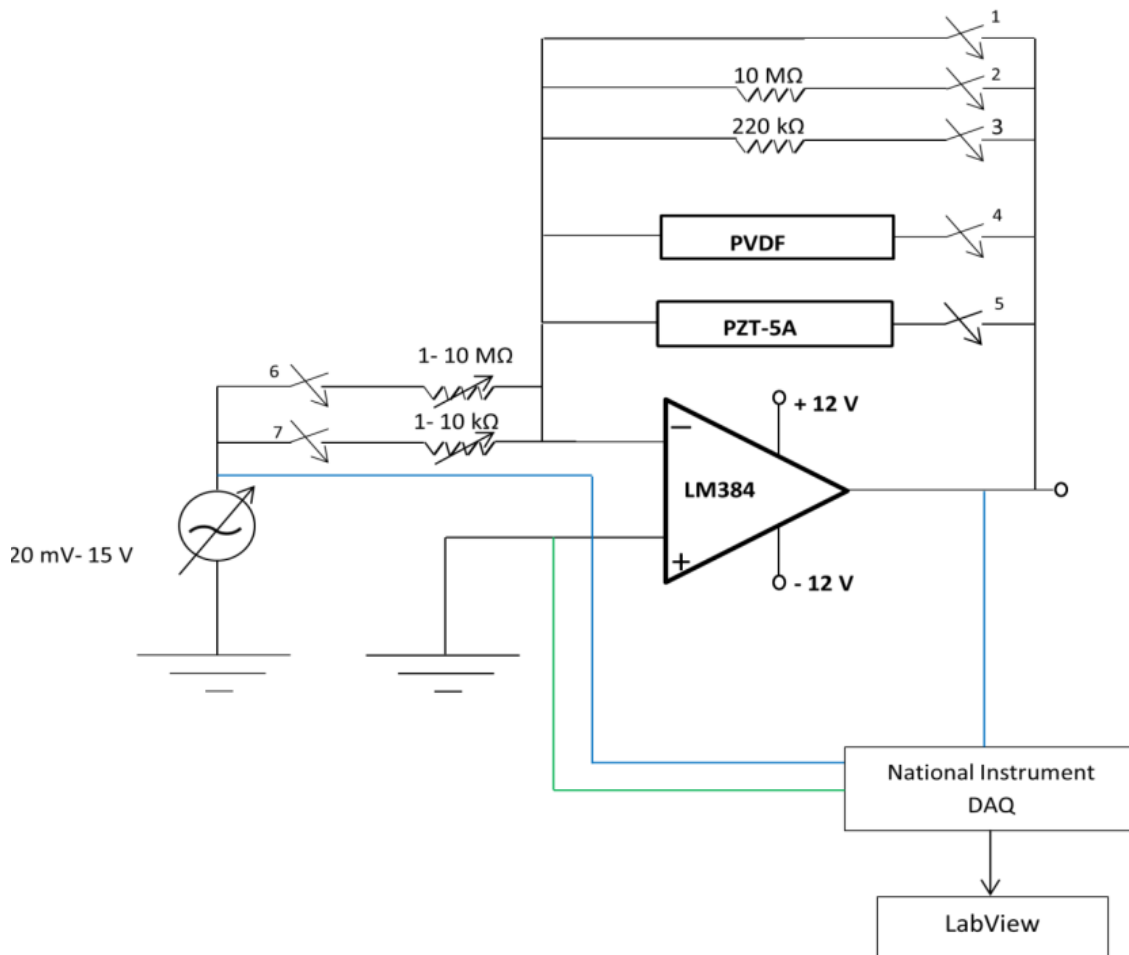


Figure 2.3. Experimental setup of PSLPF for both PVDF and PZT-5A cells

2.6 The PVDF single pole low pass filter circuit

The first main mode of the experimental circuit of Figure 2.3 is the PVDF PSLPF mode at which the switch 4 is in ON status and switch 5 is OFF. Generally two important values need to be considered, the input voltage V_{in} and the input resistance R_I . Both of these values need to be selected properly to have an output voltage less than the rail to rail span voltage of the operational amplifier at low frequencies such as 1 mHz in order to make sure that the voltage gain value at ultra-low frequencies is correct. Since the maximum output voltage cannot exceed the biasing DC voltage value, output voltage should be less than that for accurate measurements. Several of the chosen values are listed in Table 2.2 to show some functional modes of the PSLPF circuit. Comparison of the measurements is demonstrated in Table 2.3. It can be clearly noticed from Table 2.2 that there is a reverse correlation between resistance and frequency as it is already investigated by (Mathew W. Hooker, 1998).

For PVDF the results of R_p were in 8 % and 1.2 % differences as compared to the LCR meter for 10 Hz and 100 Hz respectively. There is a 3.1 % difference as compared to the IA at 100 Hz. The inherent capacitance C_p was measured to be in 1.9 %, 4.3 %, and 6.4 % differences as compared to LCR meter, IA and manufacturer measurements respectively. Measured pyroelectric resistance R_p , capacitive reactance X_p , and total impedance Z_p for PVDF using PSLPF are shown in Figure 2.4.

Table 2.2 Functional modes for the PSLPF

S_1	S_2	S_3	S_4	S_5	S_6	S_7	R_1 (M Ω)	V_{in} (mV)	f (Hz)	Parameter	Value
1	0	0	0	0	0	0	-	-	-	Reset	-
0	1	0	1	0	0	1	0.01	20	6	PVDF C_p	2.6 nF
0	0	0	1	0	1	0	10	180	0.001	PVDF R_p	1.3 G Ω
0	0	0	1	0	1	0	0.033	100	10	PVDF R_p	390 M Ω
0	0	1	0	1	0	1	10^{-3}	100	3.8	PZT-5A C_p	185 nF
0	0	0	0	1	1	0	1	100	10^{-3}	PZT-5A R_p	40 M Ω

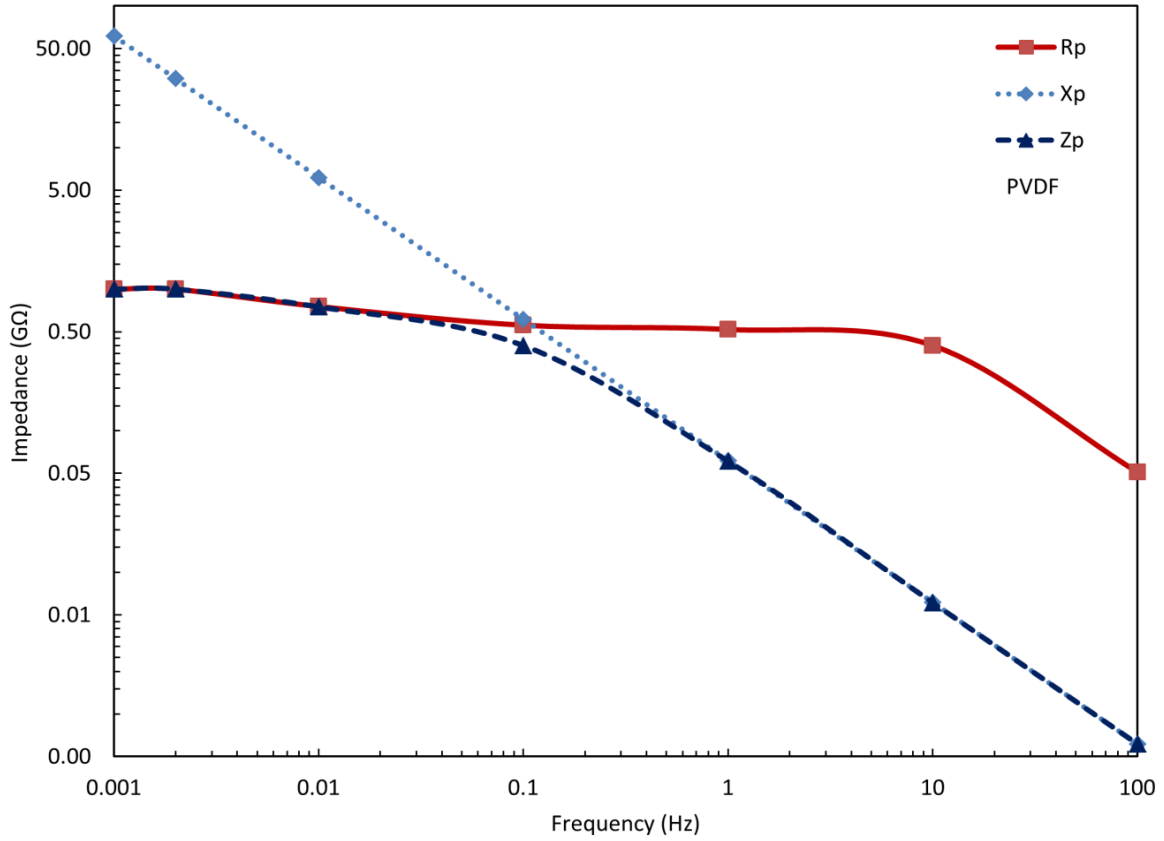


Figure 2.4. Measured pyroelectric R_p , X_p , and Z_p for PVDF using PSLPF

2.7 The PZT-5A single pole low pass filter circuit

The second main mode of the experimental circuit of Figure 2.3 is the PZT-5A PSLPF mode. The switch 5 is within ON status and switch 4 is within OFF as shown in Table 2.1. A comparison of PSLPF, LCR, and IA measurements is shown in Table 2.3. As compared to LCR meter the results of R_p were in 5.8% and 1.4% differences for 10 Hz and 100 Hz respectively and in 6.1% differences as compared to IA at 100 Hz. The inherent capacitance is measured to be in 0.5%, 7.5%, and 9.04 % differences with the LCR meter, IA, and manufacturer measurements respectively. The pyroelectric resistance R_p , capacitive reactance X_p , and total impedance Z_p for PZT-5A measured by PSLPF, in frequency range from 1 mHz to 100 Hz are shown in Figure 2.5.

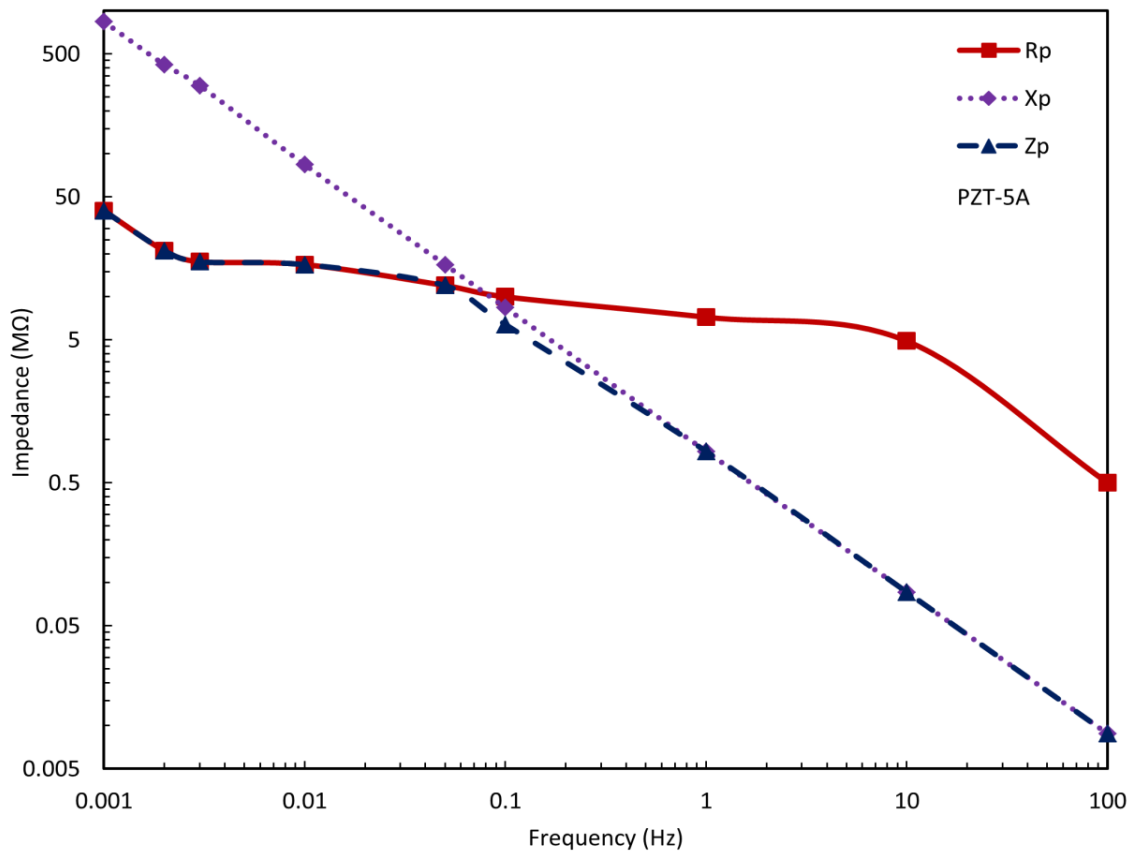


Figure 2.5. Measured pyroelectric R_p , X_p , and Z_p for PZT-5A using PSLPF

Table 2.3 Comparison of measured pyroelectric resistance R_p , capacitive reactance X_p , and total impedance Z_p using PSLPF, LCR meter, and IA

Pyro Cell	Freq.	R_p (M Ω)			X_p (M Ω)			Z_p (M Ω)		
		PSLPF	LCR	IA	PSLPF	LCR	IA	PSLPF	LCR	IA
PVDF	10 Hz	400	370	-	6.13	6.1	-	6.1	6.1	-
	100 Hz	51	50	65	0.61	0.59	0.64	0.61	0.59	0.64
PZT-5A	10 Hz	4.9	4.63	-	0.086	0.0855	-	0.086	0.0855	-
	100 Hz	0.5	0.5	0.53	0.0088	0.0087	0.0095	0.0088	0.0095	0.01

2.8 Effect of average working temperature on internal capacitance and resistance of a pyroelectric material

Ideally, the resistance of a pyroelectric element should be infinite since it is a dielectric material. This would correspond to zero leakage across the pyroelectric harvester. In reality, however, the resistance is finite and decreases as the applied electric field and temperature increase (Navid and Pilon, 2011). The total pyroelectric impedance is affected by heating as both parameters C_p and R_p do, so it is really important to consider the effect of heat on X_p , R_p , and Z_p to have an accurate impedance matching between the load resistance and the total internal pyroelectric impedance.

For this purpose, the same PSLPF circuit was used to characterize both PVDF and PZT-5A materials when radiation-based heating was applied. A halogen lamp (1 kW) was used for heating purposes and a thermometer (OMEGA HH506R) was utilized to measure the temperature of the samples. The measurements for PVDF and PZT-5A were performed in the

same procedure done previously and the results are demonstrated in Figure 2.6 and Figure 2.7 respectively. When a 100 mHz voltage signal is applied with different static temperature values the internal capacitance of the PVDF cell is found to be correlated directly to temperature as in Figure 2.6, hence the capacitive reactance correlates reversely while R_p directly. The total impedance Z_p is changed from a 400 M Ω to 40 M Ω in the temperature range from 25°C to 95°C for PVDF cell.

When a voltage signal with a 100 mHz is applied to the circuit and the same previous procedure of impedance measurement is followed at different temperature values, the internal capacitance of the PZT-5A cell is found to be correlated directly to temperature as in Figure 2.7; hence the capacitive reactance correlates reversely while R_p directly. The total impedance Z_p is changed from 8.7 M Ω to 6.4 M Ω in the temperature range from 25°C to 95°C for the PZT-5A cell. These results show that the operating average temperature of the pyroelectric material is vital to designing an application that utilizes the pyroelectric effect. The measurements have been taken at a room temperature of 23.9°C and the surrounding was kept as constant as possible. The different temperature values applied to the pyroelectric cells during the characterization process using the electric lamp were also kept as stable as possible.

2.9 Pyroelectric energy harvesting setup

The same cells of PVDF and PZT-5A cells which are characterized in the previous section are placed as a pyroelectric energy harvester. The complete set up is shown in Figure 2.8 and dimensions of the PVDF and PZT-5A cells are presented in Figure 2.9. A Function Generator (Hewlett Packard 15 MHz), a Solid State Relay (OMEGA SSR330 DC25) with 3-15 V_{dc} biasing voltage, a halogen lamp (110 V_{ac} and 1 kW), a thermometer (OMEGA HH506R), a Multimeter

(Fluke 189-True RMS), resistance decade box (0 to 10 M Ω), and a personal computer are used for measurements. The function generator provides a square voltage wave with different

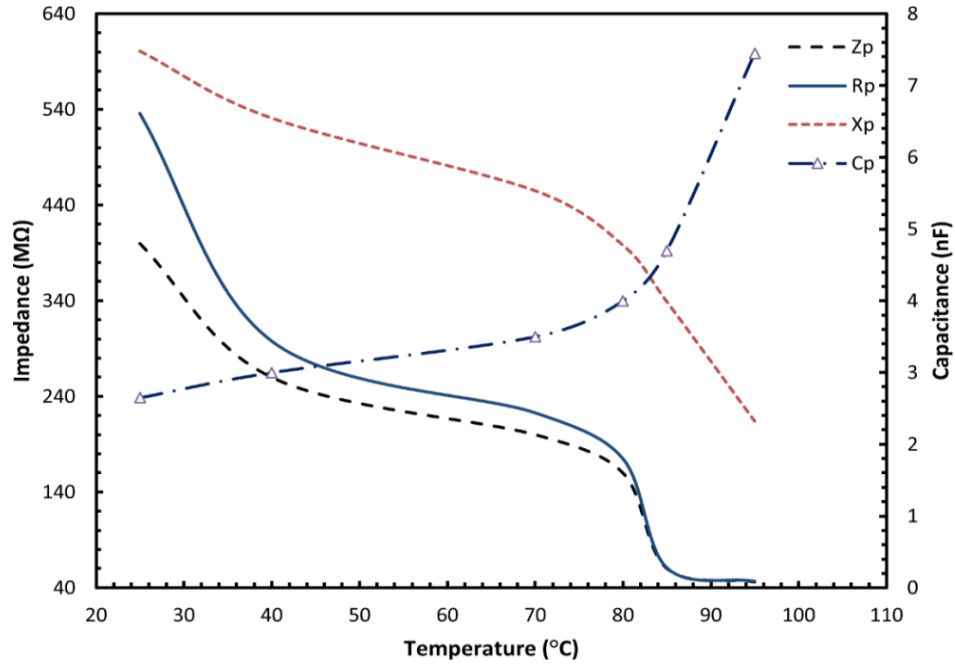


Figure 2.6. Measured total impedance Z_p , R_p , X_p and C_p values of PVDF for temperature changes at 100 mHz

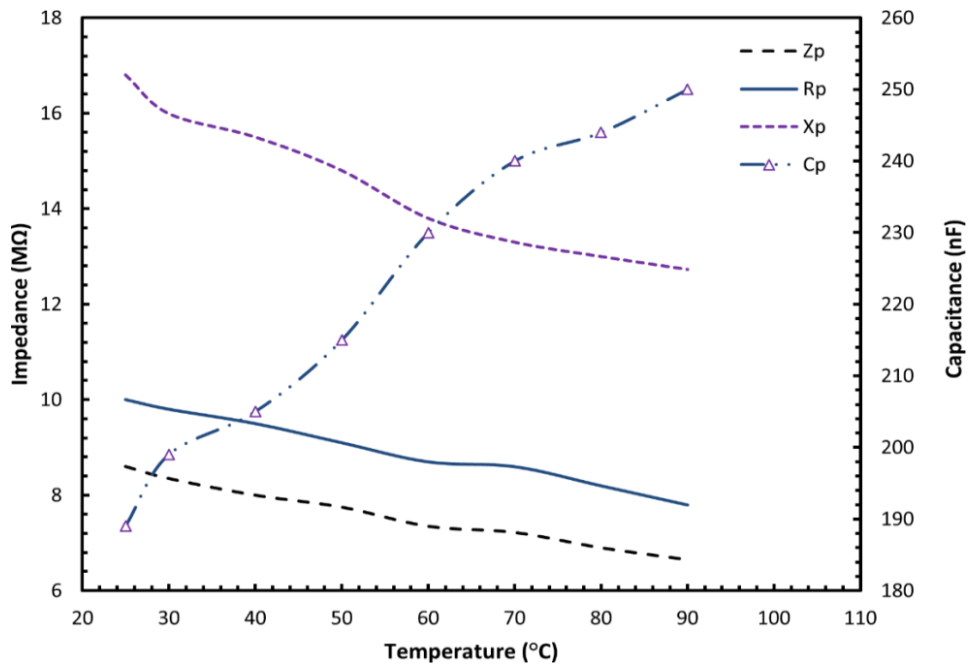


Figure 2.7. Measured total impedance Z_p , R_p , X_p and C_p of PZT-5A for temperature changes at 100 mHz

frequencies for the SSR which has two normally opened contacts used to supply a 110 V_{ac} voltage to the light bulb to get cyclic heating with 100 mHz frequency.

The load resistance is connected in parallel to the pyroelectric cell. It has a resistance value from 0 to 10 MΩ, and in some cases a series resistance is needed to have a higher load resistance. The thermometer and voltmeter with DAQ system are connected to the pyroelectric cell to record the periodic temperature and voltage values respectively.

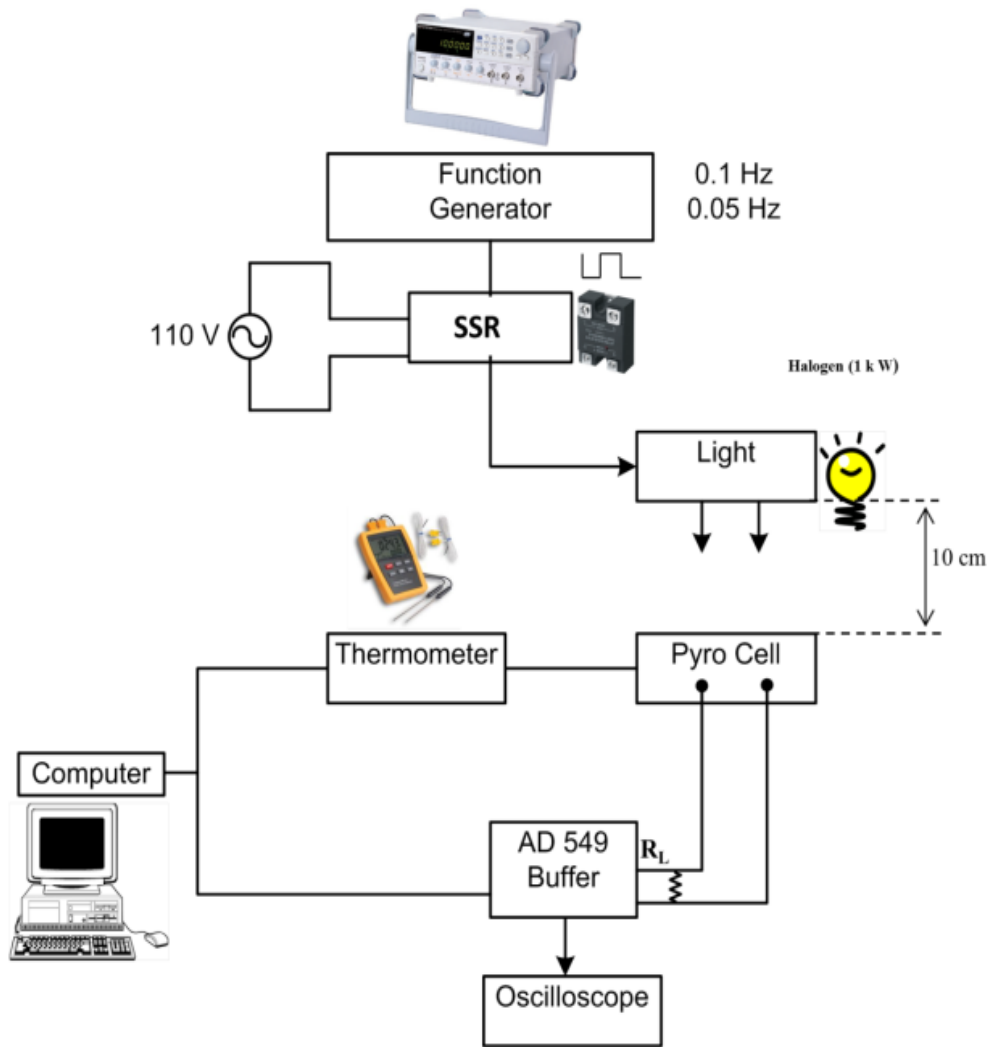


Figure 2.8. Experimental prototype for the cyclic pyroelectric energy harvester

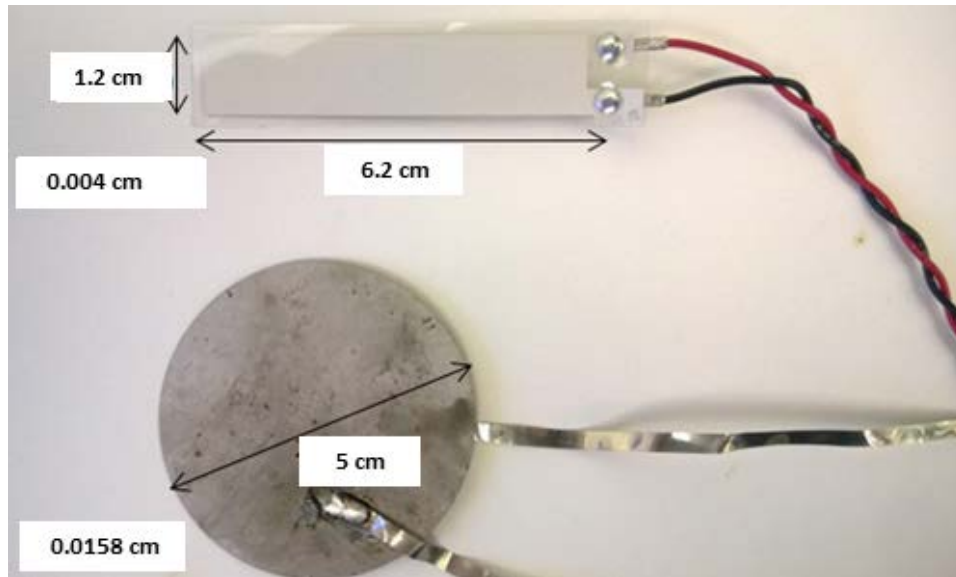


Figure 2.9. The PVDF and PZT-5A cells used for pyroelectric energy harvesting with cyclic heating

2.9.1 Energy harvesting with PVDF cell

The maximum pyroelectric energy harvesting in a PVDF cell can be extracted when the load resistance matches the total pyroelectric impedance at a particular temperature. The verification of inherent impedance values for the PVDF cell can be achieved by implementing the cyclic energy harvesting in this material and observing the load impedance value at which a maximum power value can be achieved. The cyclic temperature profile, the generated pyroelectric voltage, and power density for the PVDF cell for temperature changes (between 82.2°C and 88.3°C) at 100 mHz and R_L of 150 M Ω are shown in Figure 2.10. Since simple equipment is used to provide cyclic heating, the resulted periodic temperature signal has a high frequency component. In a real environment the heat signal is random so it is important to have a cyclic temperature signal. The load resistance has been changed from 5 M Ω to 120 M Ω at 100 mHz and the pyroelectric voltage and power density have been plotted as presented in

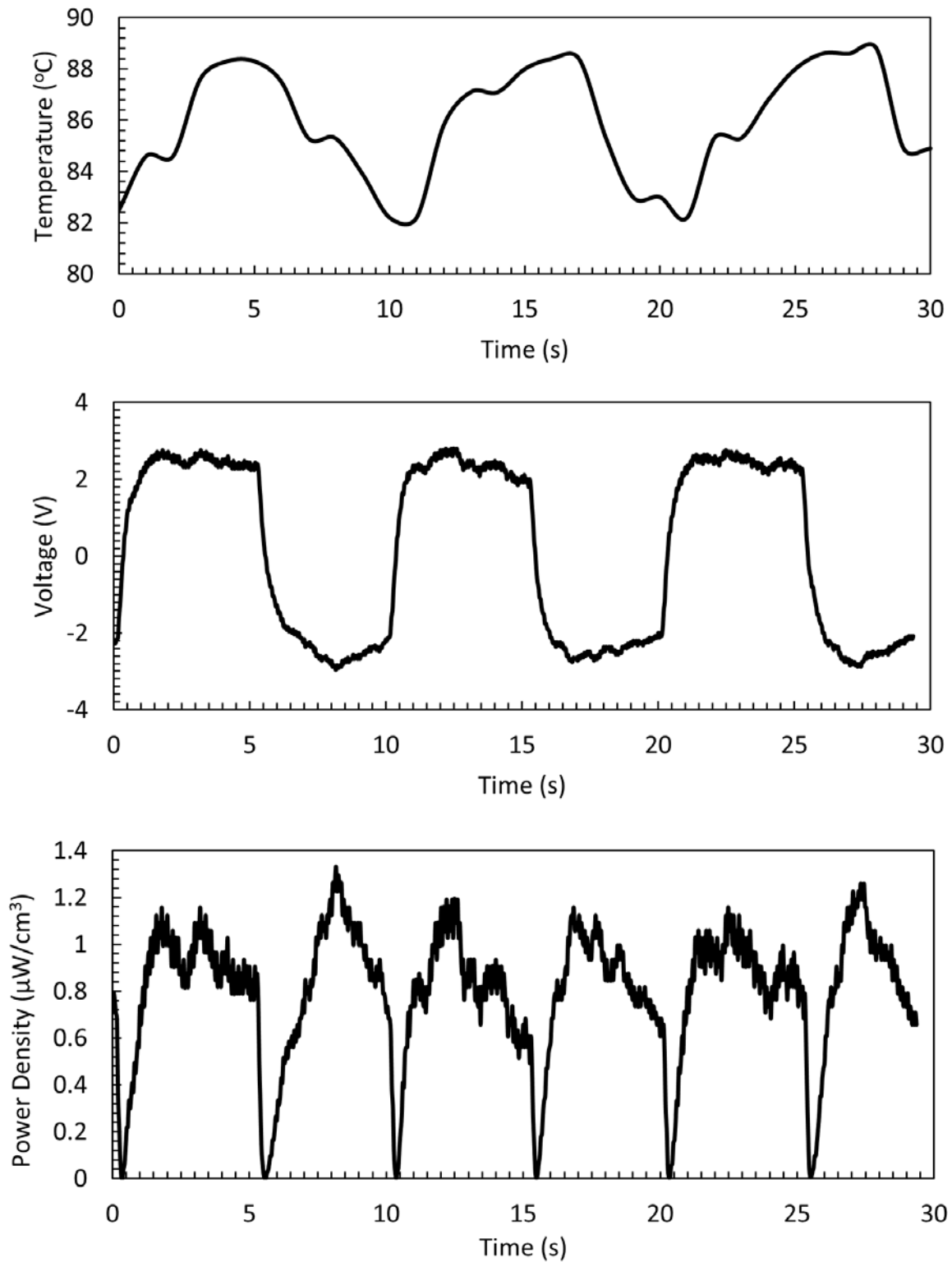


Figure 2.10. Instantaneous waveform of temperature, voltage, and power density changes of PVDF cell for temperature changes at 100 mHz and R_L of 150 M Ω

Figure 2.11. The maximum power density was $1.25 \mu\text{W}/\text{cm}^3$ when R_L of $55 \text{ M}\Omega$ and ΔT of $6.2 \text{ }^\circ\text{C}$. When Figure 2.6 is considered it can be noticed that the total PVDF impedance Z_p at a temperature of 83.5°C is about $61 \text{ M}\Omega$ which is in good coincidence with the resulted optimal load resistance. Results should be more consistent if the electric field effect on PVDF inherent capacitance and resistance are considered in addition to the temperature effect. The pyroelectric capacitive reactance X_p measured at temperature of 83.5°C was $400 \text{ M}\Omega$, as shown in Figure 2.6, which is very large and not optimal for maximum power.

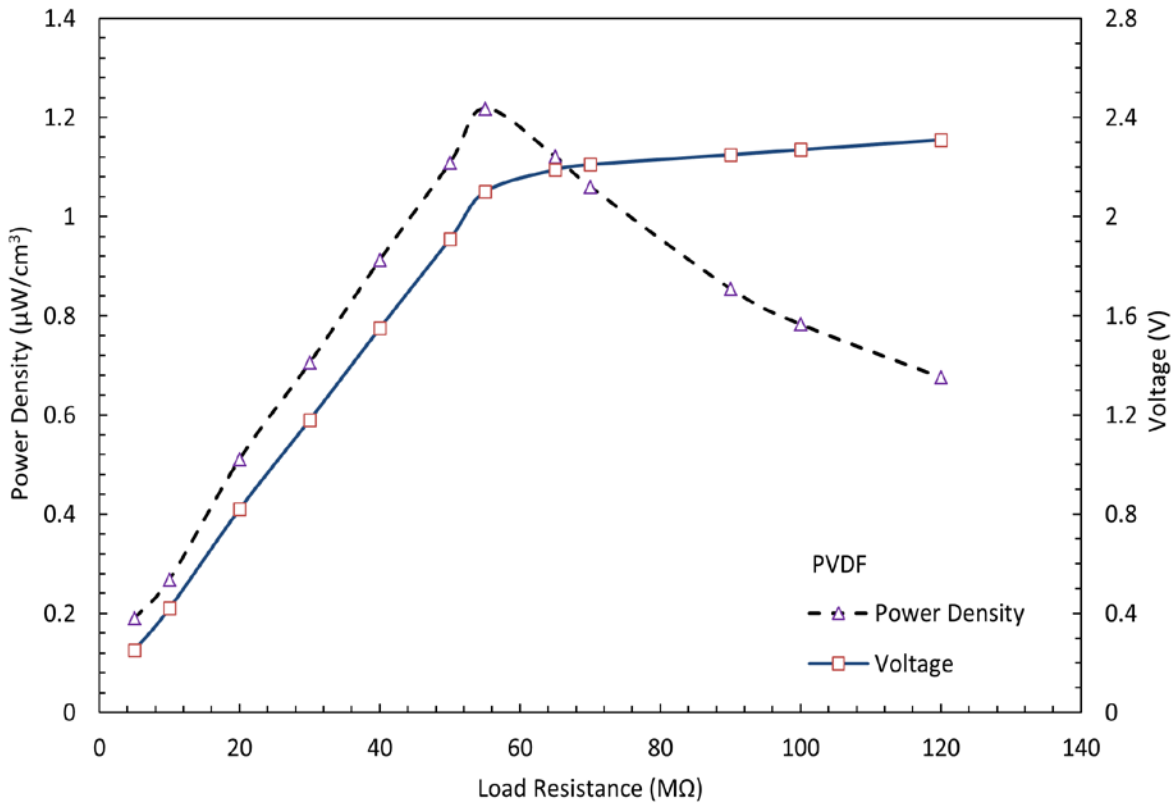


Figure 2.11. Pyroelectric voltage and power density versus load resistance for PVDF at 100 mHz

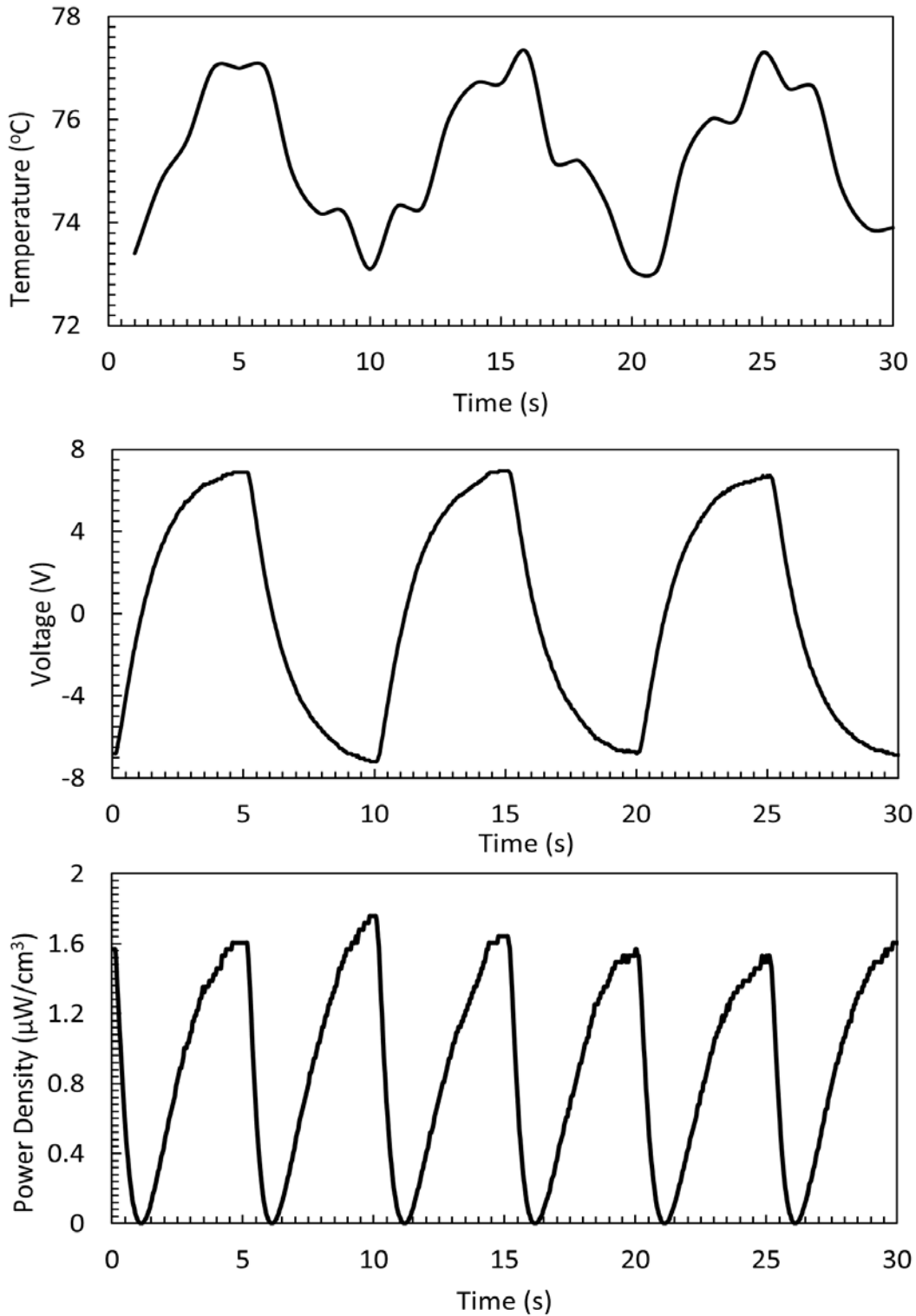


Figure 2.12. Instantaneous waveform of temperature, voltage, and power density changes of PZT-5A cell for temperature changes at 100 mHz and R_L of 50 M Ω

2.9.2 Energy harvesting with PZT-5A cell

A similar experimental circuit and procedure are used to harvest pyroelectric energy by cyclic heating of the PZT-5A pyroelectric cell at 100 mHz. The cyclic temperature, voltage and the power density at 100 mHz temperature (between 73°C and 77°C) and R_L of 100 M Ω are shown in Figure 2.12. The irregularities and high frequency components in the temperature wave were due to the simple equipment used for cyclic heating and the resolution of the thermometer which is equal to 0.2°F. The load resistance has been changed from 10 M Ω to 120 M Ω at 100 mHz and the pyroelectric voltage and power density have been plotted as presented in Figure 2.13. The maximum power density was 5.2 $\mu\text{W}/\text{cm}^3$ measured at optimal load resistance of 7 M Ω and a temperature of about 75°C.

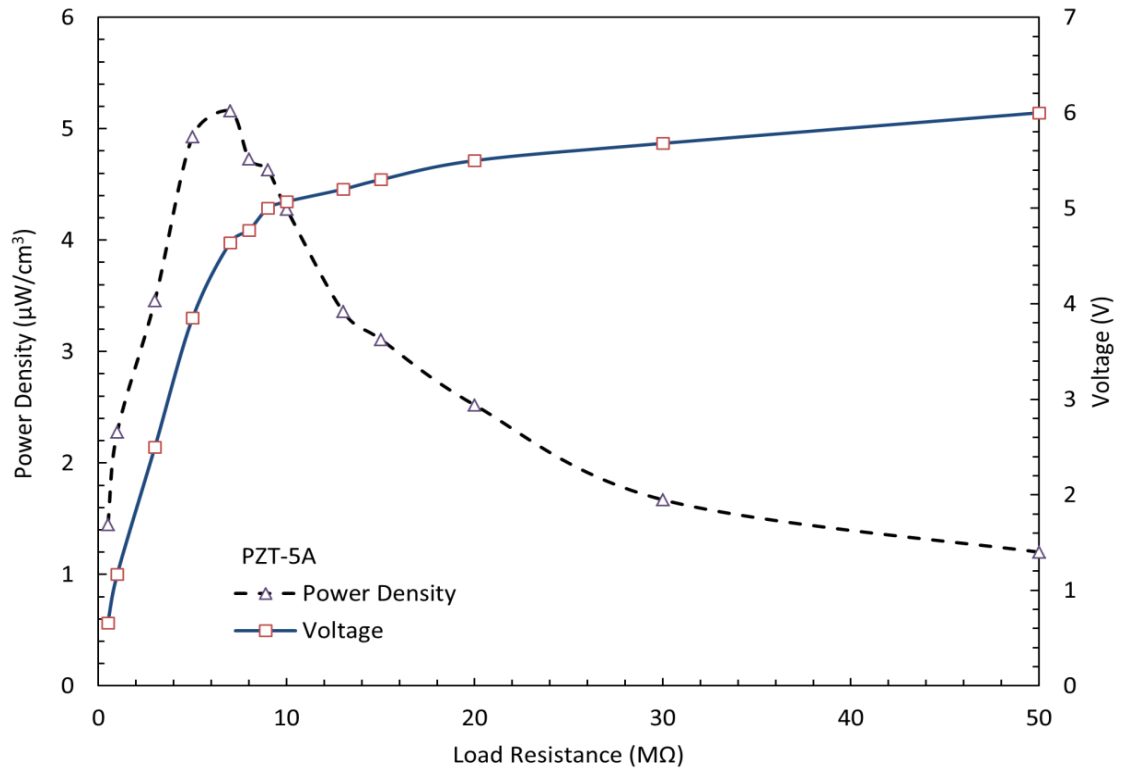


Figure 2.13. Pyroelectric voltage and power density versus load resistance for PZT-5A at 100 mHz

When Figure 2.7 is considered it can be noticed that the total PZT-5A impedance at 75°C is about 7.1 MΩ which is in good correspondence with the optimal load resistance. The pyroelectric capacitive reactance X_p measured at 75°C was 13.4 MΩ as shown in Figure 2.7 and it is large and not optimal for maximum power.

2.10 Results and discussion

A new methodology based on electronic signal filtering called PSLPF is proposed to characterize pyroelectric impedance. Results are compared to existing instrumentation. To stress the importance of impedance matching, energy harvesting experiments using pyroelectric cells are conducted. The results corroborate the impedance values calculated by experimentation and the ones measured by the proposed PLSPF method.

Two pyroelectric cells, PVDF and PZT-5A, were characterized in a frequency range from 1 mHz to 100 Hz. For PVDF the results of R_p were in 8% and 1.2% differences as compared to LCR meter for 10 Hz and 100 Hz respectively, and in 3.1% difference as compared to IA at 100 Hz. The inherent capacitance C_p was measured to be in 1.9 %, 4.3%, and 6.4 % differences with the LCR meter, IA, and manufacturer measurements respectively. For PZT-5A the results of R_p were in 5.8 % and 1.4 % differences as compared to LCR meter for 10 Hz and 100 Hz respectively, and in 6.1% difference as compared to IA at 100 Hz. The inherent capacitance C_p was measured to be in 0.5 %, 7.5 %, and 9.04 % differences with the LCR meter, IA, and manufacturer measurements respectively.

The proposed method is used with a pyroelectric cyclic heating at a temperature rate of 0.6 degrees per second for PVDF. For PZT-5A a temperature rate of 0.44 degrees per second has been presented. The optimal load for PVDF and PZT-5A samples were 55 MΩ and 7 MΩ at the mentioned temperature rates respectively. The optimal load resistances for PVDF and PZT-5A

were consistent with the measured pyroelectric impedance at the particular heat range with 10.9 % and 1.4% differences respectively. In addition, the dependence of impedance on operating median temperature was also measured. For PVDF sample, the results show impedance values can range from 400M Ω to 40M Ω with temperatures between 25 to 95 °C. In the case of PZT-5A the changes are smaller and are in the order of a 3M Ω at the same temperature ranges.

The PSLPF method presented here shows that impedance dependence on the average temperature and the heating rate are both key parameters when characterizing a pyroelectric material. This indicates clearly that to optimize impedance when utilizing the pyroelectric effect, both operating average working temperature and the rate of temperature change need to be considered when designing energy harvesting applications. Neglecting those parameters will result in inefficient and unpredictable systems.

Chapter 3. Piezoelectric energy scavenger modeling

3.1 Introduction

Recent two decades have noticed a dramatic increase in energy scavenging research applied to wireless sensors' nodes. This research attention has been motivated by the huge reduction in power and size of electronic circuits of wireless sensor devices. For instance, the required power for wireless sensor devices has been reduced to less than 1mW (Shad Roundy and Yang Zhang, 2005, Ajitsaria, J. 2007 , Culler D, 2002, Glynne-Jones P et al., 2001), opening up the possibility of driving the device from energy scavenged from the environment.

A major amount of research has been presented on piezoelectric energy harvesters which depend on the conversion of vibrations to electric power. (Roundy S et al., 2003, Amirtharajah R and P. Chandrakasan 1998, Williams CB et al., Tayahi M B et al., 1995, and Erturk A and Inman D J 2008, Taylor G et al., 2001). An important feature of the piezoelectric generators is that they deliver maximum output power when the natural frequency of the harvester is matched with the frequency of the environmental vibrations. Therefore, if there is an incompatibility between ambient vibration and resonance frequencies, the power output drops very rapidly.

This property is the main constraint to developing many applications. To address this issue, it has been suggested by several investigators that a capacitor could be shunted in parallel to a piezoelectric cantilever as a method of electrical tuning (Charnegie D 2007). When such a passive element is connected in parallel the total capacitance will be equal to the sum of the inherent piezoelectric capacitance C_p and the shunt capacitance, and the power decreases significantly from its original value. To resolve that, an enhanced adjusting capacitor method for electrical piezoelectric tuning and power maximization is developed. Utilizing this new

technique, an enhanced output power and piezoelectric resonance frequency matching to the ambient vibration frequency can be gained simultaneously. This method is performed by connecting a toroid inductor with a small value in parallel to the shunt capacitor to improve the output power. All researchers don't consider such a method as they know that satisfying such an improvement needs an inductor with a huge value. The reason behind using the shunt inductor with a small value is the relatively high total capacitance resulted from the shunted and inherent capacitance.

The aim of this chapter is to develop state space dynamics model of the piezoelectric cantilever with RLC load. This model can be used to analyze the feasibility of shunting an inductance with small value to improve the output power of vibration based scavengers with passive electrical tuning. A general dynamics model of the piezoelectric bimorph with RLC load has been developed. Results will be presented and discussed.

3.2 Modeling of piezoelectric bimorph with RLC load

The general theory developed in this section will provide general expressions for the piezoelectric cantilever generator with RLC load (resistor, inductor, and capacitor). The aim is to analytically determine the output voltage and power delivered to the load resistance R_L before and after connecting the shunt inductance in parallel to the output of the piezoelectric scavenger. The net power output when L_{sh} is connected should be greater than would be obtained without the use of L_{sh} .

3.2.1 State space modeling for piezoelectric bimorph harvester with conjugate impedance matching (RLC load)

The modeling of the piezoelectric bimorph harvester presented in this section is based on the linear vibration based generator model presented by Shad Roundy 2004.

Figure 3.1 shows the piezoelectric electromechanical equivalent circuit of the system. The voltage generator ma^* represents the effective force induced by the base vibration and is the only source in the electrical side, where m is the effective mass term and a^* is the base acceleration amplitude. The circuit consists of two parts, mechanical and electrical which are combined electromechanically via a transformer with a turn ratio n which represents the piezoelectric coupling vector. The resistance R in the mechanical side represents the mechanical damping. The inductance L and the capacitance C represent the modal mass of the first mode and the compliance respectively. The capacitance C_p on the electrical side is the equivalent inherent capacitance of the piezoelectric layer. The bimorph cantilever has a natural frequency which should be matched by the environmental vibration frequency by using frequency tuning to scavenge the maximum power. Electrical tuning can be verified by connecting a shunt capacitor C_{shn} in parallel to the inherent capacitor on the right side of the electromechanical coupling transformer as shown in Figure 3.2.

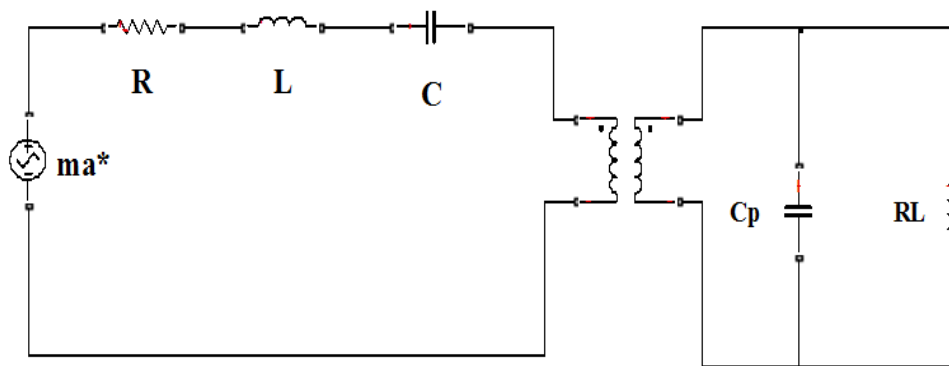


Figure 3.1. the equivalent circuit for a piezoelectric energy harvester with a resistive load.

The system model for the piezoelectric bimorph cantilever without shunt capacitor and resistive load in state space form can be written as (Shad Roundy 2004):

$$\begin{bmatrix} \dot{f} \\ \ddot{f} \\ \dot{V} \end{bmatrix} = \begin{bmatrix} 0 & 1 & 0 \\ -k & \frac{-b_m \dot{b}}{m} & \frac{kd}{2mt_c} \\ 0 & \frac{-2dY_c t_c}{\varepsilon} & \frac{-1}{R C_p} \end{bmatrix} \begin{bmatrix} \delta \\ \dot{\delta} \\ V \end{bmatrix} + \begin{bmatrix} 0 \\ \dot{b} \\ 0 \end{bmatrix} \ddot{u}$$

Equation 3.1

Where:

f : Strain.

\dot{f} : First derivative for strain.

\ddot{f} : Second derivative for strain.

V : Output Voltage.

\dot{V} : First derivative of the output voltage.

v : vertical beam tip deflection

k : effective spring constant.

m : mass.

b_m : damping coefficient.

\dot{b} : A constant relates vertical force to stress.

d : piezoelectric strain coefficient.

ε : dielectric constant of the piezoelectric material.

Y_c : Young modulus of the piezoelectric ceramic layer.

t_c : Thickness of the piezoelectric material layer

R : Load resistance.

C_p : Inherent piezoelectric capacitance

C_{sh} : The shunt capacitance.

L_{sh} : shunt inductor.

\ddot{u} : Input vibration in terms of acceleration.

When a shunt capacitance C_{sh} is connected, Equation 3.1 can be modified as in Equation 3.2.

$$\begin{bmatrix} \dot{\delta} \\ \ddot{\delta} \\ \dot{V} \end{bmatrix} = \begin{bmatrix} 0 & 1 & 0 \\ \frac{-k}{m} & \frac{-b_m \ddot{b}}{m} & \frac{kd}{2mt_c} \\ 0 & \frac{-2dY_c t_c}{\varepsilon} & \frac{-1}{R(C_p + C_{sh})} \end{bmatrix} \begin{bmatrix} \delta \\ \dot{\delta} \\ V \end{bmatrix} + \begin{bmatrix} 0 \\ \dot{b} \\ 0 \end{bmatrix} \ddot{u} \quad \text{Equation 3.2}$$

In the case of connecting a parallel inductor as in Figure 3.2 via its switch to the system to improve the extracted power at a resonance frequency

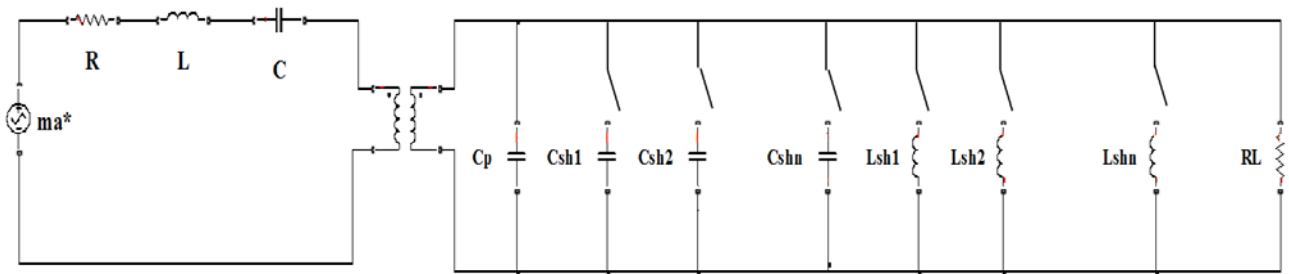


Figure 3.2. Equivalent circuit for the proposed piezoelectric energy harvester with RLC load

Using Kirchoff's current law for the circuit on the right side of the equivalent circuit, the dynamic system model will be modified as:

$$\begin{bmatrix} \dot{\delta} \\ \ddot{\delta} \\ \dot{V} \\ \ddot{i}_L \end{bmatrix} = \begin{bmatrix} 0 & 1 & 0 & 0 \\ \frac{-k}{m} & \frac{-b_m \ddot{b}}{m} & \frac{kd}{2mt_c} & 0 \\ 0 & \frac{-2dY_c t_c}{\varepsilon} & \frac{-1}{R(C_p + C_{sh})} & \frac{1}{(C_p + C_{sh})} \\ 0 & 0 & \frac{-1}{L_{sh}} & 0 \end{bmatrix} \begin{bmatrix} \delta \\ \dot{\delta} \\ V \\ i_L \end{bmatrix} + \begin{bmatrix} 0 \\ \dot{b} \\ 0 \\ 0 \end{bmatrix} \ddot{u} \quad \text{Equation 3.3}$$

Equation 3.3 can be derived as follow:

The effective moment of inertia can be calculated as:

$$I = 2 \left[\frac{wt_c^3}{12} + wt_c b^2 \right] + \frac{\eta wt_{sh}^3}{12} \quad \text{Equation 3.4}$$

Where:

I : effective moment of inertia

w : width of the beam.

t_c : thickness of individual piezoelectric ceramic layer.

t_{sh} : thickness of the center shim.

η : ratio between Y_c and Y_{sh}

$$\eta = \frac{Y_c}{Y_{sh}} \quad \text{Equation 3.5}$$

Y_{sh} : Young modulus of the piezoelectric ceramic layer (Beer and Johnston 1992)

The constitutive equations will be written in term of stress and strain instead of force and tip deflection.

Assuming that $l_e \leq l_b$.

Where l_e and l_b are the lengths of electrode and the bending respectively

Average stress and strains are used as state space variables.

$$\sigma = \frac{1}{l_e} \int_0^{l_e} \frac{\vartheta(x)b}{I} dx \quad \text{Equation 3.6}$$

Where:

σ : is the stress.

x : distance from the base of the beam.

$\emptyset(x)$: Moment of the beam as a function of distance x .

Moment can be defined as the result of vertical force ($m(\ddot{u} + \ddot{v})$) with force hand ($l_b + \frac{l_m}{2} - x$) as follows:

$$\emptyset(x) = m(\ddot{u} + \ddot{v}) \left(l_b + \frac{l_m}{2} - x \right) \quad \text{Equation 3.7}$$

Where v is the vertical displacement

Substituting Equation 3.7 in Equation 3.6 yields:

$$\sigma = \frac{1}{l_e} \int_0^{l_e} \left[\frac{m(\ddot{u} + \ddot{v}) \left(l_b + \frac{l_m}{2} - x \right) b}{I} \right] dx = \frac{m(\ddot{u} + \ddot{v}) b}{I l_e} l_e \left[l_b + \frac{1}{2} l_m - \frac{1}{2} l_e \right] \quad \text{Equation 3.8}$$

Or,

$$\sigma = \frac{m(\ddot{u}) b (2l_b + l_m - l_e)}{2I} + \frac{m(\ddot{v}) b (2l_b + l_m - l_e)}{2I} = \sigma_{in} + \sigma_m \quad \text{Equation 3.9}$$

Where σ_{in} and σ_m are the stresses resulting from input vibration and inertial element mass respectively.

Assume:

$$\ddot{b} = \frac{2I}{b(2l_b + l_m + l_e)} \quad \text{Equation 3.10}$$

From Equation 3.9 and Equation 3.10:

$$\sigma_{in} = \frac{m\ddot{u}}{\ddot{b}} \quad \text{Equation 3.11}$$

$$\sigma_m = \frac{m\ddot{v}}{b} \quad \text{Equation 3.12}$$

Where l_b , l_m , and l_e :

The lengths of the bending cantilever, mass, and electrode respectively

b : the distance between the centers of the shim and the center of piezoelectric layers.

So,

$$\sigma = \frac{m(\ddot{u} + \ddot{v})}{b} \quad \text{Equation 3.13}$$

To relate a deflection to the average strain lets write the Euler beam equation as follows:

$$\frac{d^2 v}{dx^2} = \frac{\sigma(x)}{Y_c I} \quad \text{Equation 3.14}$$

Substituting Equation 3.7 in Equation 3.14 yields:

$$\frac{d^2 v}{dx^2} = \frac{m(\ddot{u} + \ddot{v}) (l_b + \frac{l_m}{2} - x)}{Y_c I} \quad \text{Equation 3.15}$$

By integrating Equation 3.15 yields:

$$\frac{dv}{dx} = \frac{m(\ddot{u} + \ddot{v}) (l_b x + \frac{l_m}{2} x - \frac{x^2}{2})}{Y_c I} \quad \text{Equation 3.16}$$

$$v = \frac{m(\ddot{u} + \ddot{v}) \left(l_b \frac{x^2}{2} + \frac{l_m}{4} x^2 - \frac{x^3}{6} \right)}{Y_c I} = \frac{m(\ddot{u} + \ddot{v}) \left(l_b x^2 + \frac{l_m}{2} x^2 - \frac{x^3}{3} \right)}{2Y_c I} \quad \text{Equation 3.17}$$

When $x = l_b$:

$$v = \frac{m(\ddot{u} + \ddot{v}) \left(l_b^3 + \frac{l_m}{2} l_b^2 - \frac{l_b^3}{3} \right)}{2Y_c I} = \frac{m(\ddot{u} + \ddot{v}) \left(\frac{2l_b^3}{3} + \frac{l_m}{2} l_b^2 \right)}{2Y_c I} \quad \text{Equation 3.18}$$

Or,

$$v = \frac{m(\ddot{u} + \ddot{v}) l_b^2 \left(\frac{2l_b}{3} + \frac{l_m}{2} \right)}{2Y_c I} \quad \text{Equation 3.19}$$

It is known that:

$$f = \frac{\sigma}{Y} \quad \text{Equation 3.20}$$

Substituting Equation 3.9 into Equation 3.19 yields:

$$f = \frac{m(\ddot{u} + \ddot{v}) b (2l_b + l_m - l_e)}{2I Y_c} \quad \text{Equation 3.21}$$

$$m(\ddot{u} + \ddot{v}) \frac{2I Y_c f}{b(2l_b + l_m - l_e)} \quad \text{Equation 3.22}$$

By substituting Equation 3.22 into Equation 3.19 yields:

$$v = \frac{\frac{2I Y_c f}{b(2l_b + l_m - l_e)} l_b^2 \left(\frac{2l_b}{3} + \frac{l_m}{2} \right)}{2Y_c I} = \frac{l_b^2 \left(\frac{2l_b}{3} + \frac{l_m}{2} \right) f}{b(2l_b + l_m - l_e)} \quad \text{Equation 3.23}$$

Let's define \hat{b} as a parameter that relates the strain to the vertical displacement:

$$\dot{b} = \frac{\dot{d}}{v} = \frac{b(2l_b + l_m - l_e)}{l_b^2 \left(\frac{2l_b + l_m}{3} + \frac{l_m}{2}\right)} \quad \text{Equation 3.24}$$

From Equation 3.12, Equation 3.23, and Equation 3.24

$$\sigma_m = \frac{m \frac{l_b^2 \left(\frac{2l_b + l_m}{3} + \frac{l_m}{2}\right) \ddot{d}}{b(2l_b + l_m - l_e)}}{\dot{b}} = \frac{m \ddot{d}}{\dot{b} \frac{b(2l_b + l_m - l_e)}{l_b^2 \left(\frac{2l_b + l_m}{3} + \frac{l_m}{2}\right)}} \quad \text{Equation 3.25}$$

$$\sigma_m = \frac{m}{b\dot{b}} \ddot{d} \quad \text{Equation 3.26}$$

$$\sigma_{bm} = \frac{b_m}{b} \dot{d} \quad \text{Equation 3.27}$$

Where: σ_{bm} represents the effective stress.

$$\sigma_Y = Y_c \dot{d} \quad \text{Equation 3.28}$$

The constitutive piezoelectric equations can be described as:

$$\dot{d} = \frac{\sigma}{Y} + dE \quad \text{Equation 3.29}$$

$$D = \epsilon E + d\sigma \quad \text{Equation 3.30}$$

D : Electric displacement.

E : Electric field.

d : piezoelectric strain coefficient.

ϵ : dielectric constant of the piezoelectric material.

$$\sigma_t = -dY_c E \quad \text{Equation 3.31}$$

$$D_t = -dY_c \dot{\delta} \quad \text{Equation 3.32}$$

For unimorph cantilever the charge is:

$$q = l_e w D \quad \text{Equation 3.33}$$

For bimorph cantilever:

$$q = 2l_e w D \quad \text{Equation 3.34}$$

Voltage across the bimorph will be:

$$V = 2Et_c \quad \text{Equation 3.35}$$

$$\sigma_t = \frac{-adY_c}{2t_c} V \quad \text{Equation 3.36}$$

$$i_T = -dY_c a l_e w \dot{\delta} \quad \text{Equation 3.37}$$

Where

a =1 for series wiring and a =2 for parallel wiring.

The total stress resulted from input base vibration is:

$$\sigma_{in} = \sigma_m + \sigma_{bm} + \sigma_t + \sigma_Y \quad \text{Equation 3.38}$$

Substituting Equations 3.11, 3.12, 3.26, 3.27, and 3.28 into Equation 3.38 yields:

$$\frac{m}{b} \ddot{u} = \frac{m}{b\ddot{b}} \ddot{\delta} + \frac{bm}{b} \dot{\delta} + \left(\frac{-adY_c}{2t_c} V \right) + Y_c \dot{\delta} \quad \text{Equation 3.39}$$

Arrange Equation 3.39 to have:

$$\ddot{\delta} = \ddot{b} \ddot{u} - \frac{bm\ddot{b}}{m} \dot{\delta} + \left(\frac{b\ddot{b}}{m} \right) \left(\frac{adY_c}{2t_c} \right) V - \frac{b\ddot{b}}{m} Y_c \dot{\delta} \quad \text{Equation 3.40}$$

Let $k = \dot{b}\ddot{b}Y_c$ and substituting in Equation 3.40 yields:

$$\ddot{f} = -\frac{k}{m} \delta - \frac{b_m \ddot{b}}{m} \dot{f} + \frac{kda}{2mt_c} V + \dot{b} \ddot{u} \quad \text{Equation 3.41}$$

Applying KCL to the electrical side of the transformer yields:

$$i_T = i_C + i_L + i_R \quad \text{Equation 3.42}$$

Where i_T : total current

i_C , i_L and i_R : the current of capacitance, inductance, and resistance respectively.

$$i_T = C_T \dot{V} + i_L + \frac{V}{R} \quad \text{Equation 3.43}$$

The inherent capacitance of the piezoelectric layer can be computed as follow:

$$C_p = \frac{a^2 \varepsilon w l_e}{2t_c} \quad \text{Equation 3.44}$$

The total capacitance is equal to the sum of inherent and shunts capacitances as follow:

$$C_T = C_p + C_{shn} \quad \text{Equation 3.45}$$

By Substituting Equation 3.37 into Equation 3.43 and using C_p expression in Equation 3.2

yields:

For $C_T = C_p$ only

$$-dY_c a l_e w \dot{f} = \frac{a^2 \varepsilon w l_e}{2t_c} \dot{V} + i_L + \frac{V}{R} \quad \text{Equation 3.46}$$

For $C_T = C_p + C_{shn}$

$$dY_c a l_e w \dot{\int} = \left(\frac{a^2 \varepsilon w l_e}{2t_c} + C_{shn} \right) \dot{V} + i_{Lshn} + \frac{V}{R} \quad \text{Equation 3.47}$$

For $C_T = C_p$ only

$$\dot{V} = \left(-dY_c a l_e w \dot{\int} - i_L - \frac{V}{R} \right) \frac{2t_c}{a^2 \varepsilon w l_e} = \frac{-2t_c dY_c}{a\varepsilon} \dot{\int} - \frac{V}{RC_p} - i_L \quad \text{Equation 3.48}$$

For $C_T = C_p + C_{shn}$

$$\dot{V} = \frac{-dY_c a l_e w}{\frac{a^2 \varepsilon w l_e}{2t_c} + C_{shn}} \dot{\int} - \frac{V}{R \left(\frac{a^2 \varepsilon w l_e}{2t_c} + C_{shn} \right)} - \frac{1}{\frac{a^2 \varepsilon w l_e}{2t_c} + C_{shn}} i_L \quad \text{Equation 3.49}$$

$$V = V_L = -L_{shn} \frac{di_L}{dt} = -L_{shn} \ddot{i}_L \quad \text{Equation 3.50}$$

The new system model can be written as:

$$\begin{bmatrix} \dot{\int} \\ \ddot{\int} \\ \dot{V} \\ \ddot{i}_L \end{bmatrix} = \begin{bmatrix} 0 & 1 & 0 & 0 \\ \frac{-k}{m} & \frac{-b_m \ddot{b}}{m} & \frac{kd}{2mt_c} & 0 \\ 0 & \frac{-dY_c a l_e w}{\frac{a^2 \varepsilon w l_e}{2t_c} + C_{shn}} & \frac{-1}{R \left(\frac{a^2 \varepsilon w l_e}{2t_c} + C_{shn} \right)} & \frac{1}{\frac{a^2 \varepsilon w l_e}{2t_c} + C_{shn}} \\ 0 & 0 & \frac{-1}{L_{sh}} & 0 \end{bmatrix} \begin{bmatrix} \int \\ \dot{\int} \\ V \\ i_L \end{bmatrix} + \begin{bmatrix} 0 \\ \dot{b} \\ 0 \\ 0 \end{bmatrix} \ddot{y} \quad \text{Equation 3.51}$$

Now let:

$$z_1 = \int, z_2 = \dot{\int}, z_3 = V, \quad \text{so } \dot{z}_3 = \dot{V}, z_4 = i_L, \text{ and } \dot{z}_4 = \dot{i}_L$$

Then Equation 3.51 will be:

$$\begin{bmatrix} \dot{z}_1 \\ \dot{z}_2 \\ \dot{z}_3 \\ \dot{z}_4 \end{bmatrix} = \begin{bmatrix} 0 & 1 & 0 & 0 \\ \frac{-k}{m} & \frac{-b_m \dot{b}}{m} & \frac{kd}{2mt_c} & 0 \\ 0 & \frac{-dY_c a l_e w}{\frac{a^2 \epsilon w l_e}{2t_c} + C_{shn}} & \frac{-1}{R \left(\frac{a^2 \epsilon w l_e}{2t_c} + C_{shn} \right)} & \frac{1}{\frac{a^2 \epsilon w l_e}{2t_c} + C_{shn}} \\ 0 & 0 & \frac{-1}{L_{sh}} & 0 \end{bmatrix} \begin{bmatrix} z_1 \\ z_2 \\ z_3 \\ z_4 \end{bmatrix} + \begin{bmatrix} 0 \\ \dot{b} \\ 0 \\ 0 \end{bmatrix} \ddot{y} \quad \text{Equation 3.52}$$

3.3. Experimental Set up

The implementation for the proposed method has been performed using some equipment such as Arbitrary Function Generator (Tektronix AFG 2021, 20 MHz) Shaker (vibration exciter Type 4809), Power amplifier (Type 2718), piezoelectric bimorph cantilever (manufactured by Piezo Systems, Inc. with model number T226-A4-503X is consisted of two oppositely poled PZT-5A piezoelectric layers bracketing a brass substructure element, and the two piezoelectric layers are connected in series), resistance decade box with resistance values 1Ω to 11 MΩ, (TENMA 72-7270), Ceramic Capacitors (0.47 to 3μF), toroid inductor TE-4Q3TA with 2.7 H and 3H, Oscilloscope (Type TDS2012B, 100 MHz), and PCB PIEZOTRONICS Accelerometer, Model # 352C33, 102.9 mV/g, and 0.5-10kHz

The function generator has been used to provide a sinusoidal voltage to the power amplifier whose output supplies the shaker to have a vibration with different level of accelerations which can be measured using the PCB accelerometer. The piezoelectric bimorph cantilever with the mentioned characteristics has been placed properly to a thick plastic piece on the top of a bar screwed to the shaker. The load resistance has been connected in parallel with the unimorph output, the shunted capacitors, and inductors via serial switches to have different collections of R_L-C_p , $R_L-C_p-C_{sh}$, and $R_L-C_p-C_{sh}-L_{sh}$ parallel circuits as shown in Figure 3.2.

A single piezoelectric bimorph T226-A4-503X with characteristics described below has been attached to the top of a bar connected to the shaker to be vibrated at based vibration acceleration of 0.3 m/s^2 with frequencies' range of 93.3 to 97 Hz.

Table 3.1 Material properties of the piezoelectric bimorph: T226-A4-503X (source: www.piezo.com)

Brass	Effective length(L_{sh})	$50 \times 10^{-3} \text{ m}$
	Effective width (b)	$31.8 \times 10^{-3} \text{ m}$
	Density ρ_s	8700 kg/m^3
	Thickness(t_{sh})	$0.127 \times 10^{-3} \text{ m}$
	Elastic modulus(Y_{sh})	95 GPa
Piezoceramic	Density ρ_p	7800 kg/m^3
	d constant (d_{31})	$-190 \times 10^{-12} \text{ m/V}$
	Capacitance C_p	50 nF
	Effective length(L_c)	$51.0 \times 10^{-3} \text{ m}$
	Effective width (t_c)	$31.8 \times 10^{-3} \text{ m}$

3.4 Results and Discussion

The maximum piezoelectric power can be extracted from the bimorph cantilever when its natural frequency matches the vibration frequency which can be satisfied by an electrical tuning technique. The electrical tuning could be verified by adjusting the output capacitance of the piezo-ceramic layer which changes the stiffness of the cantilever and then the resonance frequency will be shifted. To demonstrate the electrical tuning for the piezoelectric unimorph cantilever, several shunt capacitors (0.47 to $3 \mu\text{F}$) have been connected individually in parallel to have different operating resonance frequencies (97Hz to 93.3Hz). The electric peak to peak voltage and power have been measured at load resistance of $35 \text{ k}\Omega$ to validate the influence of

shunt capacitance on the natural frequency and power delivered to the load resistance. The resonance frequency has been shifted from 97 Hz at no shunt capacitance to 93.3 Hz at a 3 μ F shunt capacitor. Although a good resonance frequency range has been obtained, the inverse correlation between a shunt capacitance and the output power is a real limitation which needs to be addressed. The maximum extracted power values at base vibration acceleration of 0.3 m²/s (as shown in Figure 3.3) were 5.3 μ W and 0.012 μ W at C_{sh} equal to zero and 3 μ F respectively.

3.5 Model Validation

When there is no shunt capacitance and inductance connected to the load resistance, the output voltages are shown in Figure 3.4. There is good correspondence between experimental and simulated waveforms of the output voltages which have peak values of 0.48 V and 0.43 respectively.

As mentioned previously the issue of output power decrement needs to be resolved and hence shunt inductors were connected in parallel to the system for three different shunt capacitors.

By considering Figure 3.5 it can be noticed that there is a significant improvement in the harvested power of the circuit with the shunt inductor. For the case of the shunt C_{sh} of 0.47 μ F, an inductive impedance of 2.7 H is connected. An inductive shunt reactance with inductor L_{sh} of 3H has been connected to the system to improve the generated power when the shunt capacitance was equal to 1.47 μ F and 3 μ F. Generally, the gained power percentages were (10 % - 60 %). The maximum difference between the simulated and experimental results was 7.5 %. Experimental and simulated data for output peak power P_p of the piezoelectric generator for different cases of shunt capacitance and resonance frequency have been demonstrated in Table 3.2.

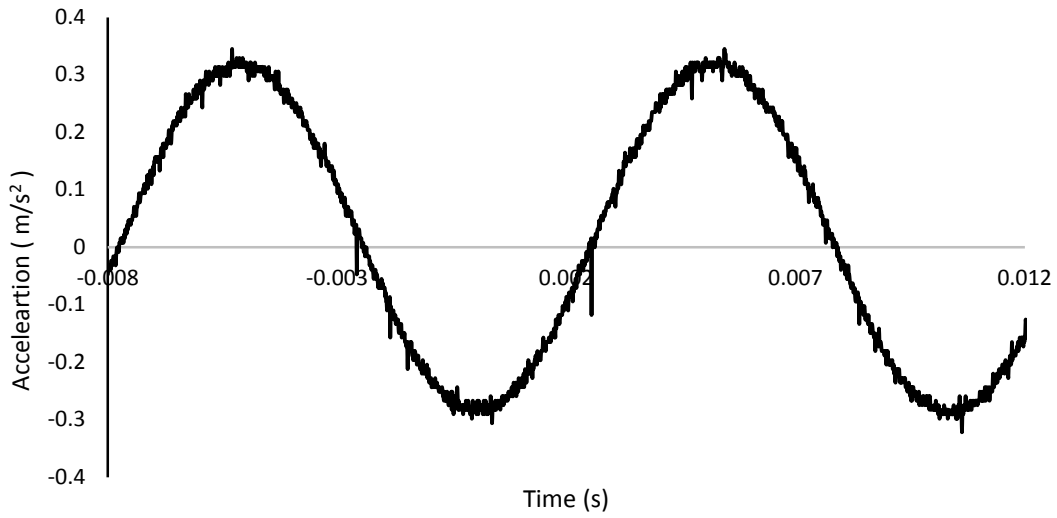


Figure 3.3 the input base vibration acceleration

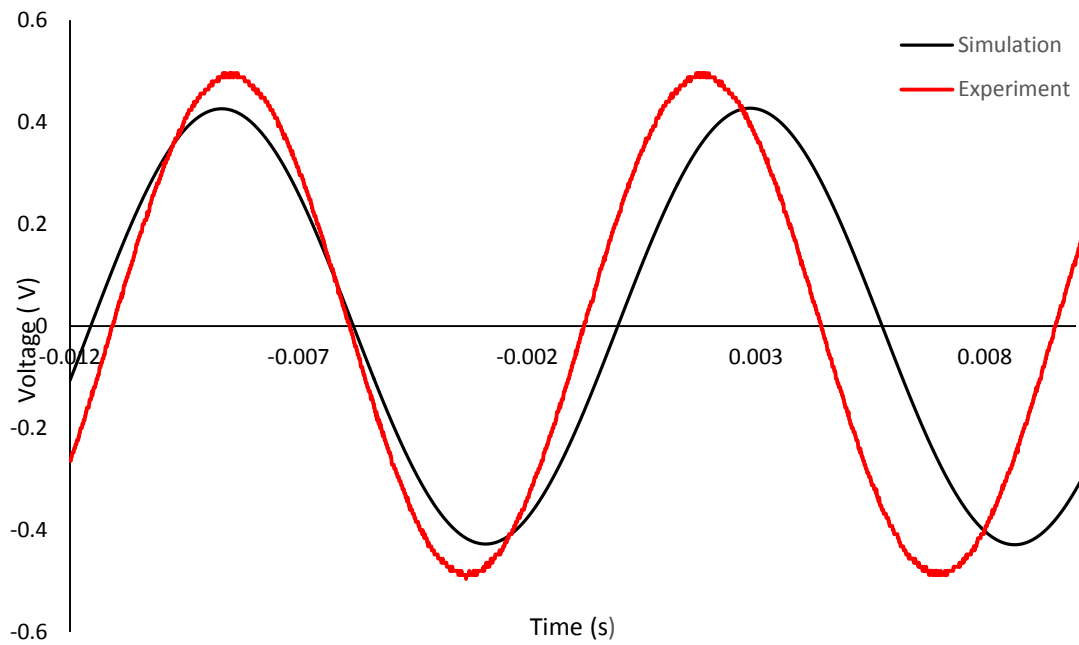


Figure 3.4 the experimental and simulated output voltages at C_{sh} equals to zero

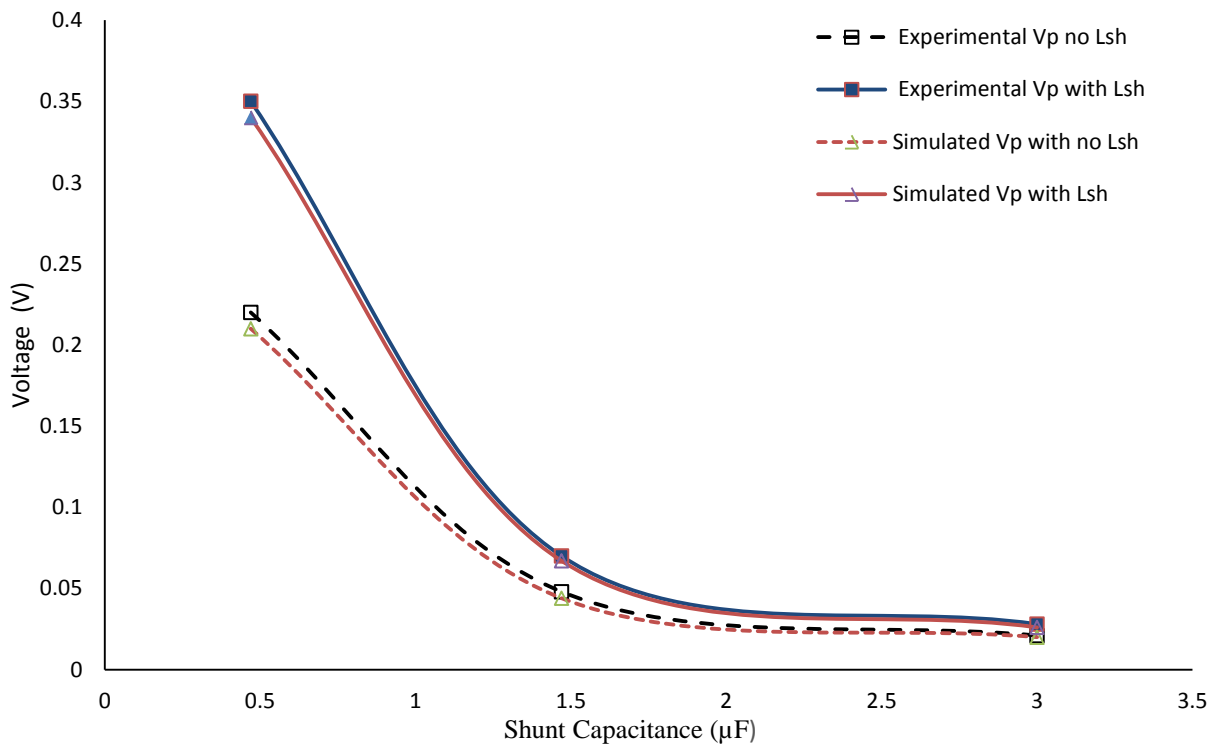


Figure 3.5 the experimental and simulated output peak voltages for the cases of shunted inductance L_{sh} and no shunted inductance L_{sh}

Table 3.2 Experimental and simulated data for output peak power P_p of the piezoelectric generator

C_{sh} (μF)	ω_n (Hz)	Experimental P_p with no L_{sh} (μW)	Simulated P_p with no L_{sh} (μW)	Experimental P_p with L_{sh} (μW)	Simulated P_p with L_{sh} (μW)
0.0	97	5.3	5.7	-	-
0.47	95.8	1.38	1.28	3.5	3.3
1.47	94	0.065	0.055	0.14	0.13
3	93.5	0.012	0.011	0.022	0.022

Chapter 4. Piezoelectric Operating Frequency Tuning and Bandwidth

Widening

4.1 Introduction

A diversity of wireless applications have been developed in recent years providing new communication abilities. However, the batteries used to power such devices require tedious charging or replacement, and often result in excess volume requirements (N A Kong et al, 2010). Variety of energy sources in the surroundings around the wireless devices, such as light, heat, and vibration, can be utilized for energy harvesting. Among them, vibration can be found in numerous applications in our daily life and has therefore fascinated much research consideration (Lihua Tang, et al 2010). Vibration energy scavengers provide the maximum power when working at resonance, which means that the harvesters are not efficient in environment vibrations with random frequencies (Jin-Chen Hsu et al 2014). Ambient vibration sources, however, are unpredictable, which is a critical issue for piezoelectric harvesters. Resonant devices with a high Q-factor have a very narrow frequency spectrum of operation. A minor move in excitation frequency (for instance ± 2 Hz) around the resonant frequency will lead to a big reduction in the output power (-3 dB) (Swee-Leong et al, 2011).

There are some proposed approaches used as a remedy to such a problem and increase the bandwidth of piezoelectric energy harvesters. To date there are generally two methods to resolving this issue. The first is to adjust the natural frequency of a piezoelectric generator so that it matches the frequency of the environmental vibration at all times. This can be satisfied by changing the mechanical characteristics of the structure or electrical load on the harvester (Dibin Zhu et al 2010 and Xiaoming Wu et al 2008). The second method is to widen the bandwidth of the piezoelectric scavenger by utilizing an array of piezoelectric beams with diverse resonant

frequencies. Wu et al presented a piezoelectric generator using mass adjusting. The proof mass of the suggested device consisted of two parts: a fixed mass fixed to the cantilever and a movable screw. Including such moveable parts in a piezoelectric harvester could be considered as a drawback (Xiaoming Wu et al 2008). Wing-Wen Wu et al developed and verified a tunable resonant frequency power harvesting device in cantilever beam form to change its natural frequency to match that of the ambient vibration (Wen-Jong Wu et al 2006). This harvester exploits a variable capacitive load to shift the gain curve of the cantilever and a low power microcontroller samples the ambient frequency and modifies the capacitive load accordingly to match ambient vibration frequency in real-time.

Marco Ferrari et al presented a multi-frequency piezoelectric scavenger envisioned for driving autonomous sensors from background vibrations. The harvester is consisted of multiple bimorph cantilevers with different resonance frequencies, whose rectified voltages are fed to a storage capacitor. The efficiency of the energy harvester was higher than the case of a single converter (Macro Ferrari et al 2008). S.M. Shahruz studied the performance of mechanical band-pass filters to be utilized in energy scavengers. Such a filter consists of an array of cantilever beams where at the tip of each beam a proof mass is attached. Two issues are discussed regarding the performance of the filter: (i) the optimal performance of the filter (ii) the design of the filter to get such performance (S.M. Shahruz 2006).

In this chapter, a hybrid approach using multiple piezoelectric bimorph cantilevers is presented. This is done to achieve mechanical tuning, electrical tuning, and bandwidth widening simultaneously to develop a significant increase in frequency range for the vibration-based energy harvester. In this innovative work three bimorph cantilevers with the same characteristics have been used. Each one has the same natural frequency, but mechanically tuning by using two

different tip (proof) masses and different lengths will result in three different natural frequencies. These three cantilevers are connected electrically in series to create a wide bandwidth energy harvester. Using three different ceramic capacitors for each cantilever, each one will have an extended operating frequency range of several hertz around each individual natural frequency. Hence rather than having three resonant frequencies the system has twelve natural frequencies and maximum power peaks.

The goal behind such a hybrid system is to develop a significant increase in frequency bandwidth for the piezoelectric energy harvester using three techniques of mechanical tuning, electrical tuning, and bandwidth widening simultaneously. Using three similar bimorph beams connected in series and having different tip masses will result in three different natural frequencies. Shunting three different ceramic capacitors, each cantilever will have an extended range of four frequencies. A total of 12 resonance frequencies are achieved. This design, which includes three cantilevers and four capacitors for each beam, could deliver more power than the case if one bimorph cantilever is assumed to be used with 12 capacitors. It is presented that the output power corresponding to the largest shunt capacitor of 470 nF is less than 0.5 mW. In order to have a wider frequency band, capacitors with values more than 470 nF should be used, and accordingly the power achieved could be estimated to be even less and less than 0.1 mW. Also, if 12 beams are used to get 12 resonance frequencies by mechanical tuning, the size limitation would be a serious issue. Based on that, the proposed hybrid tuning technique is more feasible and the optimal method for wide broadband piezoelectric energy harvesting.

4.2 Frequency Tuning Techniques

4.2.1 Mechanical tuning

Mechanical tuning can be accomplished by changing the mass of the cantilever. This can be accomplished by changing its length, or by adding tip masses.

The resonant frequency of a spring-mass structure is given by (Dibin Zhu et al 2010):

$$f_r = \frac{1}{2\pi} \sqrt{\frac{k}{m}} \quad \text{Equation 4.1}$$

Where: k is the spring constant and m is the inertial mass.

When tuning the resonant frequency of the generator, one can change either the spring constant or the mass. For a cantilever with a mass at the free end (Figure 4.1) the resonant frequency is given by (Blevins R D 1979).

$$f_r = \frac{1}{2\pi} \sqrt{\frac{Ywh^3}{4l^3(m+0.24m_c)}} \quad \text{Equation 4.2}$$

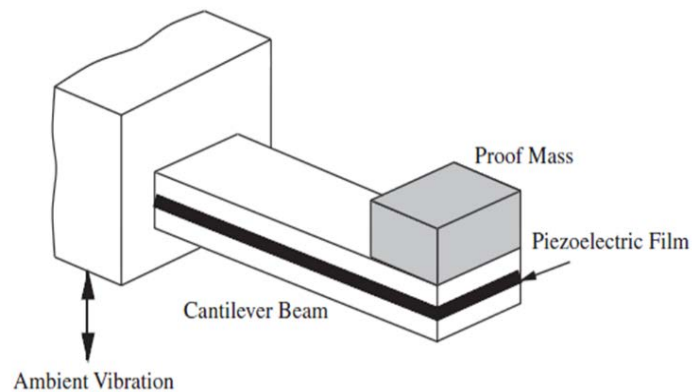


Figure 4.1. Cantilever with a proof mass at the free end (S.M. Shahruz 2006).

Where Y is Young's modulus of the cantilever material; w , h , m , l , and m_c , are the width, thickness, inertial mass, length, and the mass of the cantilever, respectively. When the length of the cantilever is changed, the mass of the cantilever m_c changes too, as it is equal to $(w h l_n \rho)$ where l_n is the new length $(l + \Delta l)$ and ρ is the density of the material of the cantilever. If the total mass is changed by both adding a proof mass m and changing the length, the new resonance frequency f_{rn} equation changes to that described in Equation 1.5.

4.2.2 Bandwidth Widening

In order to harvest energy efficiently from numerous vibration sources, energy scavengers should have wide bandwidth in designated frequency intervals. A device with such a property is called a mechanical band-pass filter (S.M. Shahruz 2006). In S.M. Shahruz 2005, a mechanical band-pass filter is proposed. The proposed filter consists of several beam-mass systems; see Figure 4.2. It is shown that such a prototype can be used as a band-pass filter when dimensions of the beams and the proof masses are chosen suitably

4.2.3 Electrical Tuning

The main principle of electrical tuning is to change the electrical damping by altering the load, which causes the power spectrum of the harvester to shift (Dibin Zhu et al 2010). By adjusting electrical load characteristics of the shunt circuit applied across the piezoelectric layer, the effective elastic modulus of this layer changes and therefore the overall stiffness of the structure changes. Since the natural frequency of the structure is dependent on its stiffness, by changing the shunt characteristics, this frequency can be tuned to a desired value.

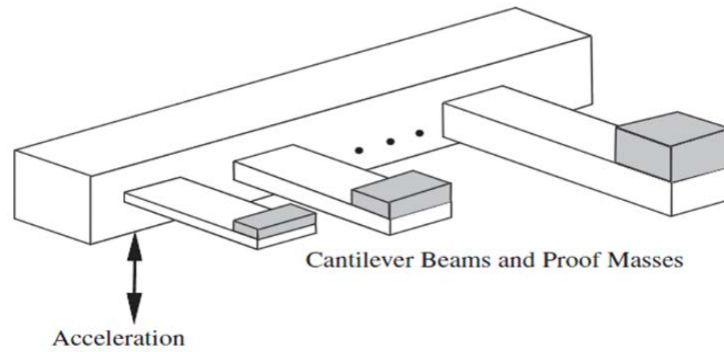


Figure 4.2. Band-pass filter of cantilever beams and proof masses (S.M. Shahrucz 2005).

4.3 Hybrid Technique for PH frequency tuning and bandwidth widening

By combining the three aforementioned frequency tuning techniques in one system, a new hybrid technique can be developed to create a broadband piezoelectric operating frequency spectrum. The electrical equivalent circuit for this system is shown in Figure 4.3. It has been implemented by using three bimorph cantilevers using different tip masses and lengths resulting in three natural frequencies. The three cantilevers were connected in series and three different ceramic capacitors for each cantilever have been used. Each capacitor causes a frequency shift to get a particular resonance frequency. The system has an extra range of operating frequency around each individual natural frequency. A total number of 12 resonance frequencies have been developed using this hybrid system.

4.4 Experimental setup of hybrid tuning system

An arbitrary Function Generator (Tektronix AFG 2021, 20 MHz) has been used to supply a sinusoidal 80 mV peak-to-peak voltage to a power amplifier (Type 2718), which provides

enough power to drive a shaker (vibration exciter Type 4809). The shaker provides different levels of vibration acceleration, which can be measured using the PCB accelerometer of the type PCB Piezotronics Accelerometer, Model # 352C33, 102.9 mV/g, and 0.5-10kHz. Three similar bimorphs (manufactured by Piezo Systems, Inc. with model number T226-A4-503X and consisting of two oppositely poled PZT-5A piezoelectric elements bracketing a brass substructure layer, with the two piezoelectric elements connected in series (NA Kong et al, 2010)) have been placed properly to a thick plastic piece on top of a bar fastened to the shaker as shown in Figure 4.4. A resistance decade box with resistance values of 1Ω to $11\text{ M}\Omega$, (TENMA 72-7270) was used to have different load resistance values. The load resistance has been connected in parallel with the bimorph cantilever outputs and the shunted capacitors through serial switches to have different collections of RC parallel circuits. A Digital Storage Oscilloscope (Type TDS2012B, 100 MHz, 1 GS/s) was used to measure the output peak-to-peak potential across the load resistor, and then the measured voltage was used to calculate the peak-to-peak output power.

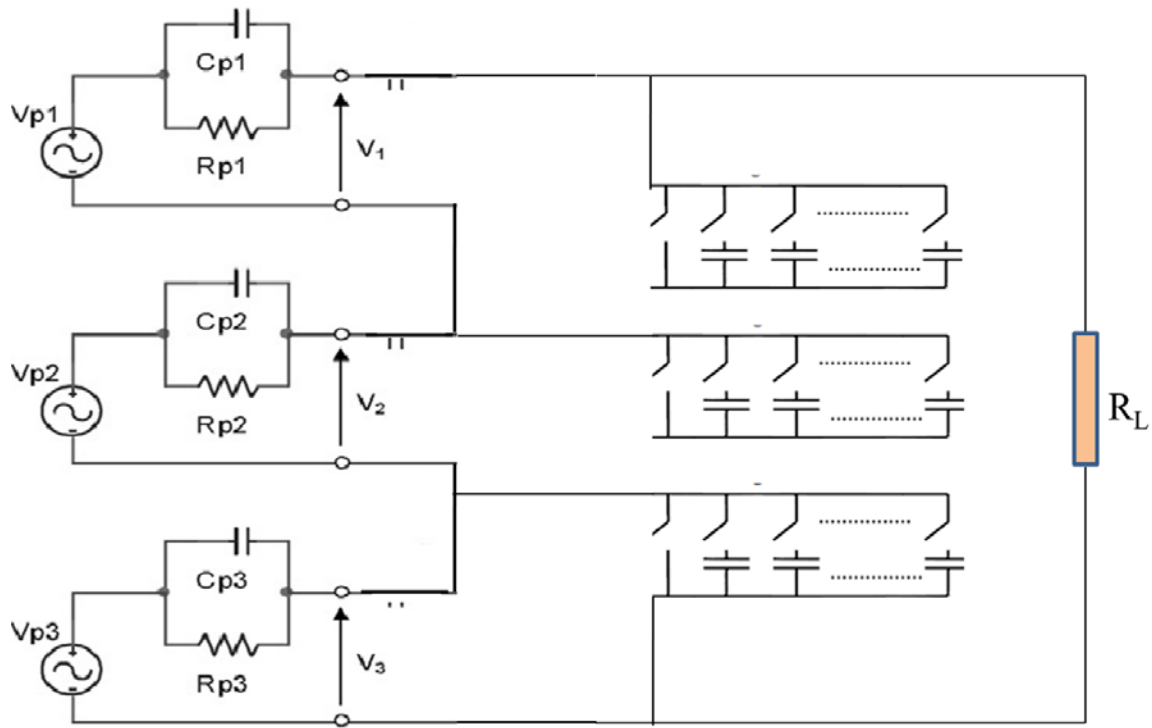


Figure 4.3. Electrical equivalent circuits for the developed hybrid piezoelectric frequency tuning system

Each one of the three bimorphs has a 110 Hz resonance frequency at its full length (6.35 cm) with no mechanical or electrical tuning. In this work the first cantilever is tuned mechanically by adjusting its length to 5.35 cm to have a resonance frequency of 93.5 Hz. No tip mass is used on the first cantilever. Mechanical tuning is applied to the second bimorph by changing its length to 5.05 cm and using a 0.65 g tip mass to get a 99.5 Hz resonance frequency. A length of 4.85 cm and tip mass of 1.1 g were chosen for the third cantilever to give a resonance frequency of 114 Hz. These three piezoelectric bimorph cantilevers were connected in series to develop a bandwidth widening tuning system with three main resonance frequencies: 93.5 Hz, 99.5 Hz, and 114 Hz. To extend the operating frequency spectrum to 12 resonance frequencies

instead of 3, three different capacitors with values of 55, 100, and 470 nF were shunted to the load resistance through manual series switches to adjust the stiffness for each bimorph.

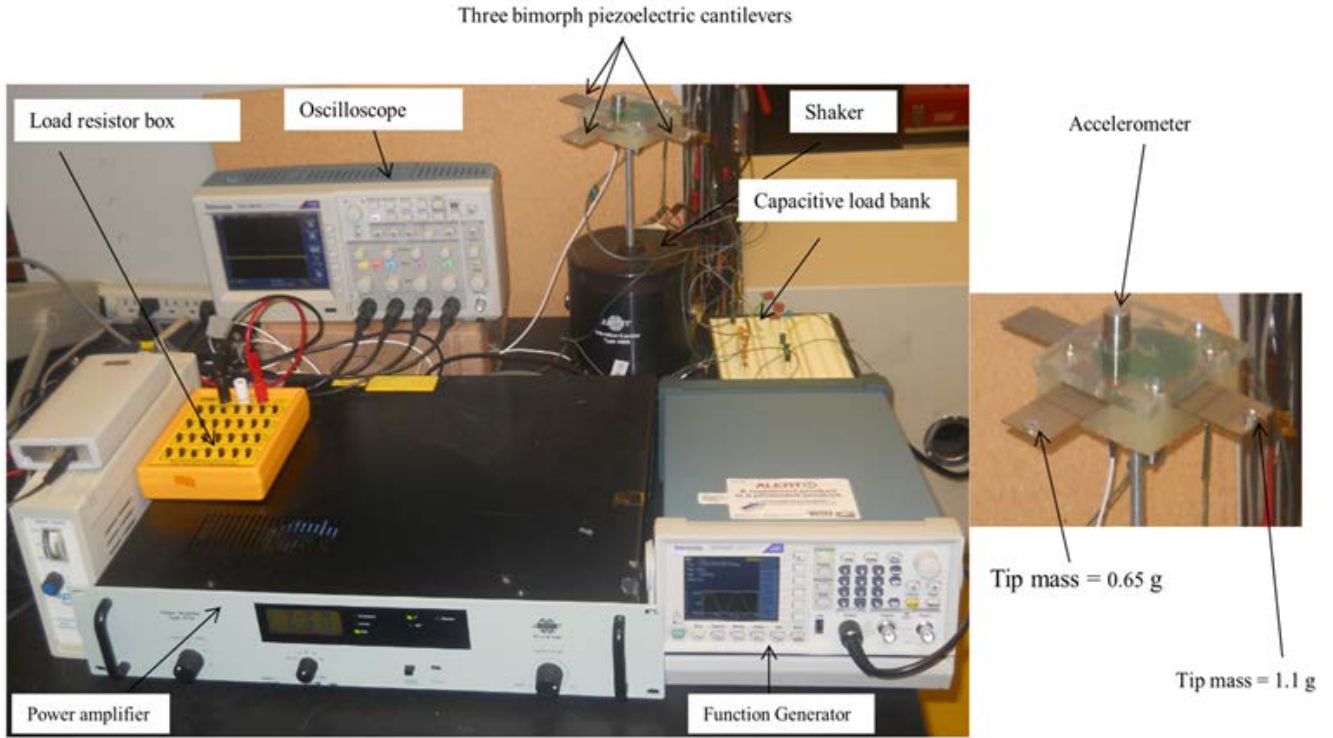


Figure 4.4. Experimental setup for the developed hybrid piezoelectric frequency tuning system

4.5 Results and discussion

Figure 4.5 shows the output voltage versus frequency of the first bimorph for load resistances of 20 k Ω , 35 k Ω , 50 k Ω , 100 k Ω , 200 k Ω , and 1 M Ω respectively. The maximum voltage of 24 V is obtained at an acceleration rate of 3.5 g and load resistance of 1 M Ω at a resonance frequency of 93.5 Hz. A maximum power of 4.25 mW (as shown in Figure 4.6) has been gained at the same frequency with a 35 k Ω load resistance. This load impedance is exactly equal to the inherent capacitive reactance of the piezoelectric cantilever ($1/\omega C_p$). The second

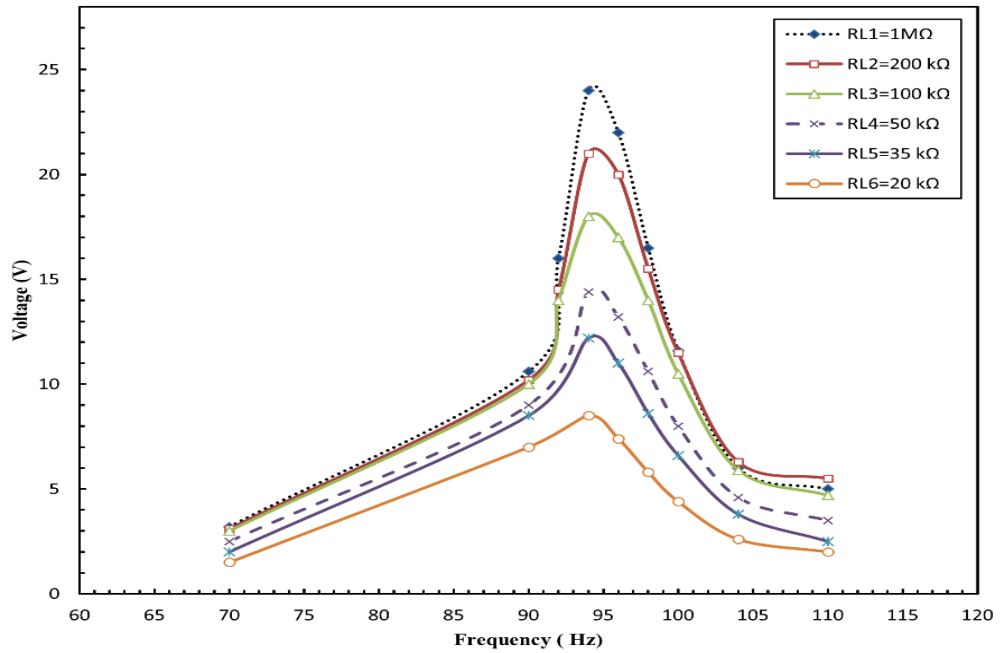


Figure 4.5. Output voltages versus frequency of the first bimorph cantilever with resonance of 93.5 Hz.

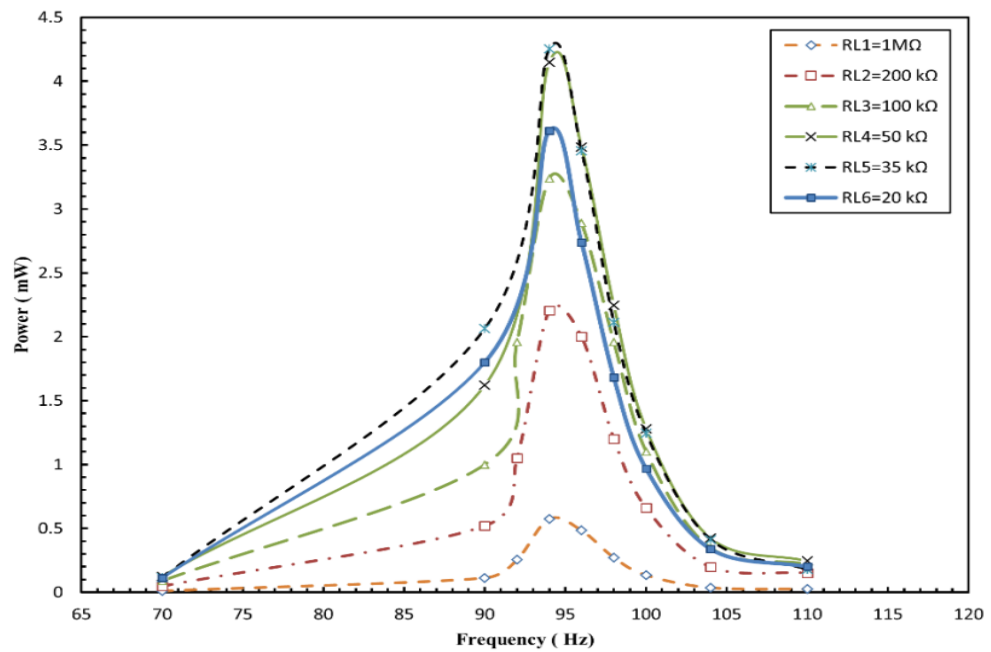


Figure 4.6. Output powers versus frequency of the first bimorph cantilever with resonance of 93.5 Hz.

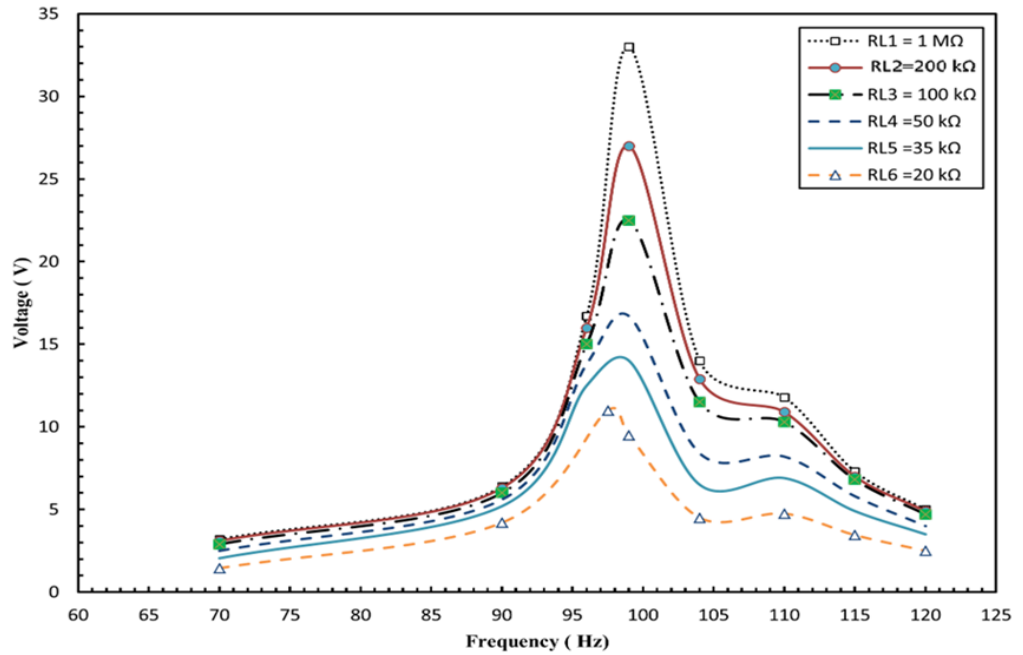


Figure 4.7. Output voltages versus frequency of the 2nd bimorph with resonance of 99.5 Hz.

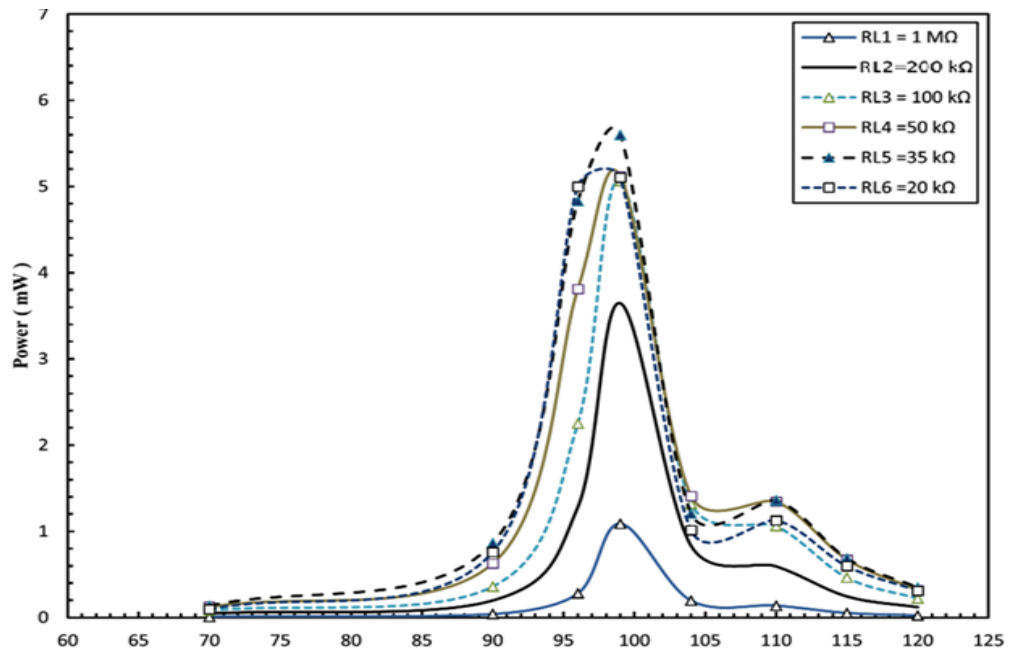


Figure 4.8. Output powers versus frequency of the 2nd bimorph with resonance of 99.5 Hz.

cantilever output voltage and power curves are shown in Figure 4.7 and Figure 4.8 respectively. At a resonance frequency of 99.5 Hz, the maximum voltage of 33 V and maximum power of 5.6 mW were measured at load resistances of 1 M Ω and 35 k Ω respectively. Figure 4.9 and Figure 4.10 show peak output voltage and maximum power for the third piezoelectric cantilever, which are 29.5 V and 6.86 mW at a resonance frequency of 114 Hz, and load resistances of 1 M Ω and 35 k Ω respectively.

The series piezoelectric system of three successive cantilevers provides three voltage peaks, which can be observed at resonance frequencies of 93.5 Hz, 99.5 Hz, and 114 Hz, as shown in Figure 4.11. The maximum voltage peaks were 22.7 V, 40 V, and 38.8 V at the mentioned frequencies respectively at a load resistance of 1 M Ω , while the maximum output power values of 2.65 mW, 5.76 mW, and 5.29 mW were measured using a load resistor of 100 k Ω . This is equal to the sum of the three series inherent piezoelectric capacitive impedance values as shown in Figure 4.12. In addition to the mechanical tuning and the bandwidth widening, an electrical tuning has been applied and 12 resonance frequencies have been gained. The first three frequencies resulted from the original case (no capacitor connected): 93.5 Hz, 99.5 Hz, and 114 Hz. The next three resonance frequencies of 91 Hz, 98 Hz, and 113 Hz resulted from shunting a 55 nF capacitor to the load resistance. Resonance frequencies of 90 Hz, 97 Hz, and 112 Hz were gained using a shunt capacitor of 100 nF. The fourth group of frequencies of 89 Hz, 96 Hz, and 111 Hz resulted from a parallel capacitor of 470 nF. It is clear that there is a significant increase in the number of resonance frequencies using the hybrid technique for frequency tuning. The 12 average power peaks for the system with a load resistance of 100 k Ω and 20 k Ω are shown in Figure 4.13 and Figure 4.14 respectively.

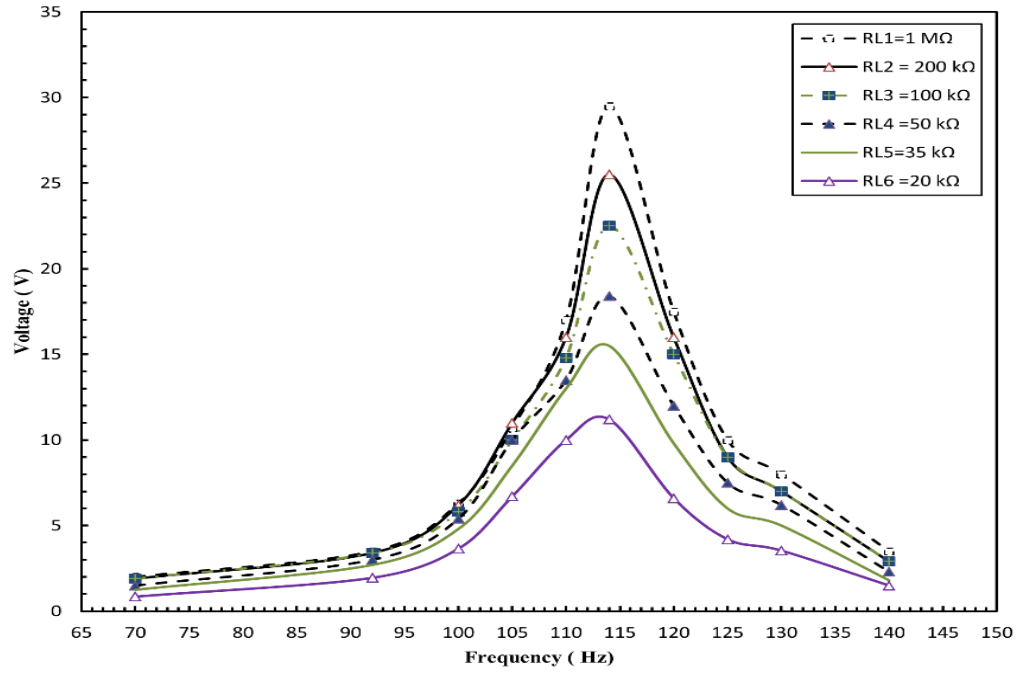


Figure 4.9. Output voltages for 3rd piezoelectric cantilever for different load resistors at resonance of 114 Hz

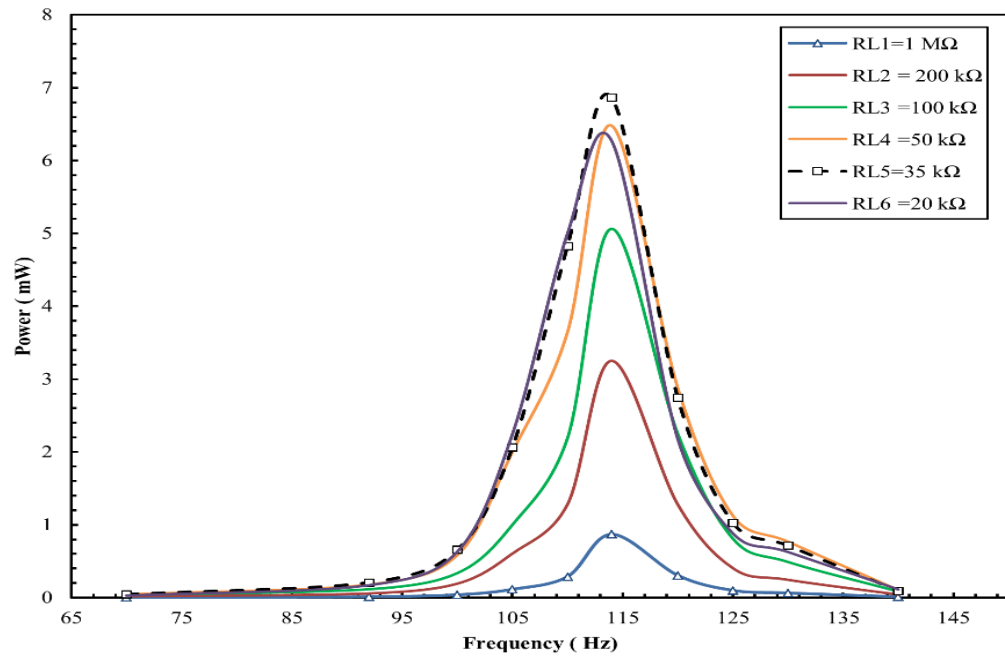


Figure 4.10. Output powers for 3rd piezoelectric cantilever for different load resistors at resonance of 114 Hz

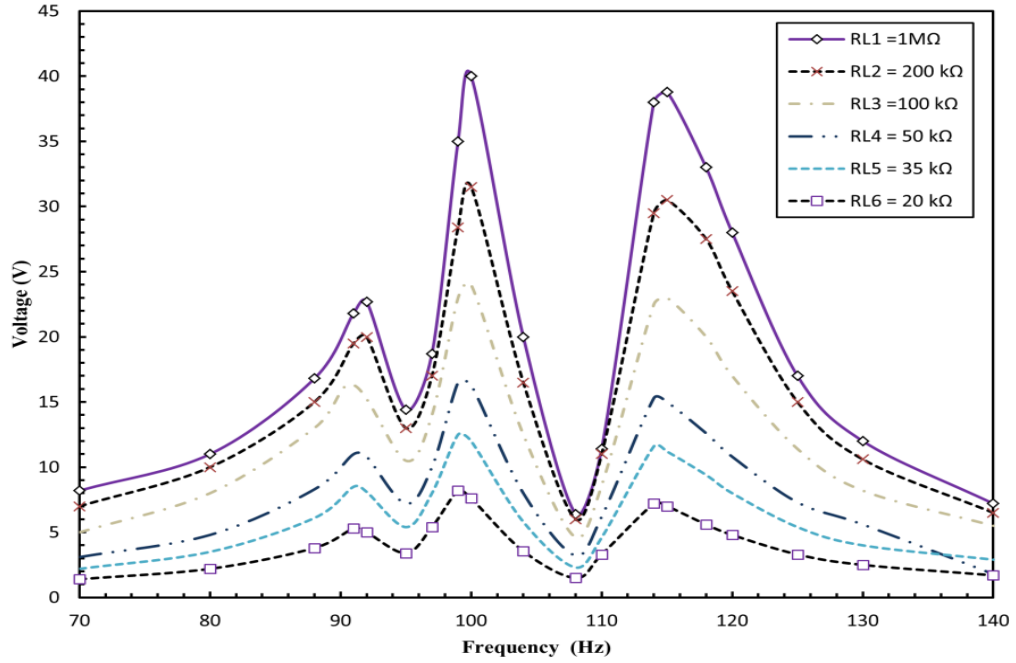


Figure 4.11. Voltage of the series piezoelectric system at of 93.5 Hz, 99.5 Hz, and 114 Hz

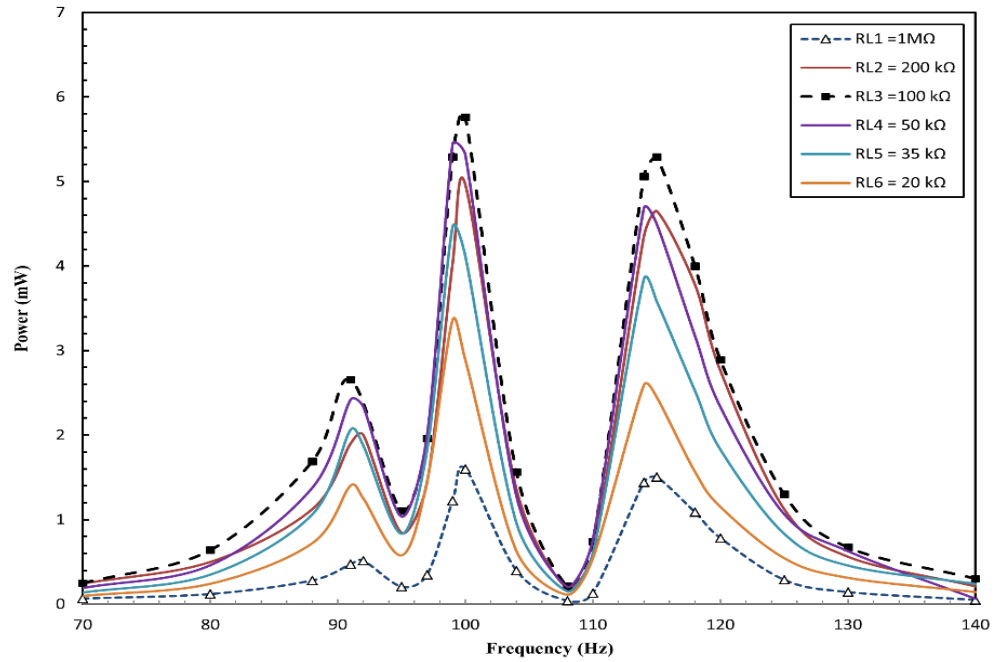


Figure 4.12. Power of the series piezoelectric system at of 93.5 Hz, 99.5 Hz, and 114 Hz

This design which includes three cantilevers and four capacitors for each beam could deliver more power than the case if one bimorph cantilever is assumed to be used with twelve capacitors. It is clear from Figure 4.13 that the output power corresponding to the shunted capacitor of 470 nF is less than 0.5 mW for each of the three resonance frequencies. In order to have a wider operating frequency band, capacitors with values of more than 470 nF should be used, and accordingly the power achieved could be estimated to be even less and less than 0.1 mW. Also, if as an alternative method twelve cantilevers are used to get 12 resonance frequencies by mechanical tuning technique, the size limitation can be a serious issue. Based on that, the proposed hybrid tuning technique is more feasible and optimal method for wide broadband piezoelectric energy harvesting.

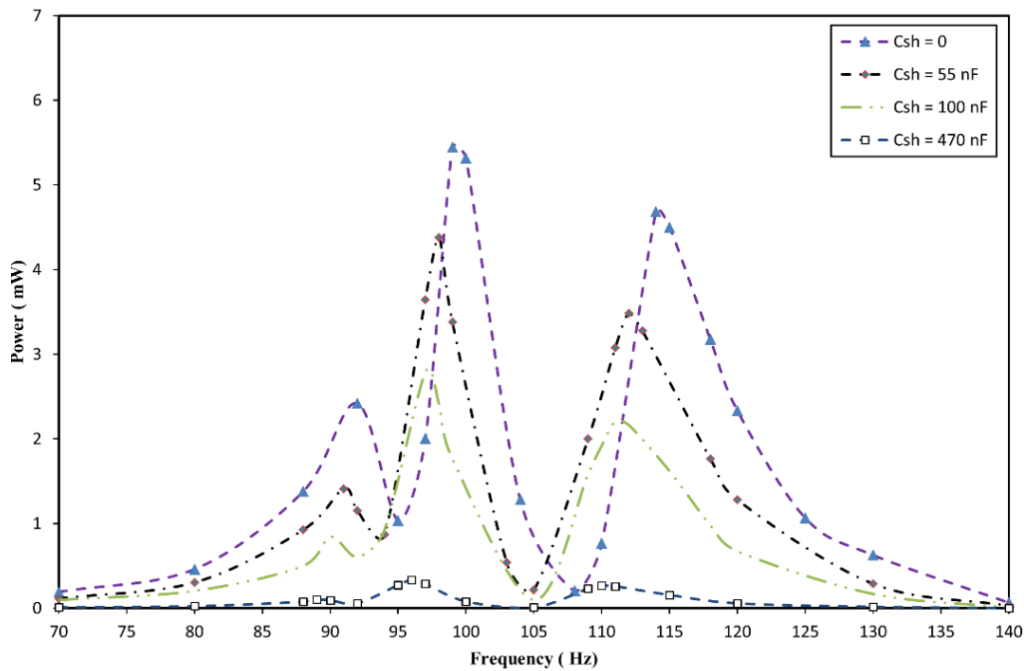


Figure 4.13. The 12 average power peaks for the series system with load resistance of 100 kΩ.

4.6 Enhanced Piezoelectric Energy Harvesting and Hybrid Frequency Tuning

The maximum electrical power can be extracted from a piezoelectric scavenger when the resonance frequency equals that of the ambient vibration which can be satisfied using tuning strategies. In this section, an experimental enhanced power harvester with hybrid tuning using multiple piezoelectric unimorphs is developed. This approach sought to enhance piezoelectric power and frequency spectrum using mechanical tuning, electrical tuning, and bandwidth widening techniques simultaneously with shunt inductance method.

First, an improved adjusting capacitor method for electrical tuning has been established to have an enhanced power output and to match piezoelectric resonance frequency to the ambient vibration frequency simultaneously. The influence of a shunt capacitor C_{sh} on the output power of a unimorph piezoelectric cantilever was validated by connecting four different shunt capacitors with values from C_p to $10C_p$. An inverse correlation between the two quantities was noticed. In other words, according to electrical tuning strategy the variable stiffness capabilities of piezoelectric layer can be utilized. By placing a shunt capacitance across the piezoelectric layer the effective elastic modulus of the layer and the stiffness of the beam change. Since the resonance frequency of the beam is dependent on its stiffness, by varying the shunt capacitance, this frequency can be tuned to a desired value. Also, the effect of a shunt capacitance is to reduce the effect of the electro-mechanical coupling on the system. There is a decrease in the output power of the piezoelectric cantilever when shunt capacitor C_{sh} is applied. An inductive reactance shunting was suggested as a remedy for this issue. The parallel inductive reactance would cancel a part of the capacitive reactance to have almost a pure resistive load with higher voltage and consequently higher output power. Also, as C_p is small and needs large L to cancel, adding C_{sh}

will make the effective capacitance C_p+C_{sh} larger and now a smaller inductance L_{sh} can be used to cancel the effect of C_p+C_{sh} .

Increases in power outputs were up to 93% and 88% for the shunt inductive impedances equal to 1 μ F and 1.16 μ F respectively. In addition, for the same unimorph cantilever tuned to resonance frequency of 205 Hz, two shunt capacitors of 0.6 μ F and 0.87 μ F were connected to shift resonance frequency to 200 Hz and 200.5 Hz respectively. Generally, to choose the suitable shunt inductance value Equation 4.3 should be used (A J Fleming et al., 2003):

$$L_1 = \frac{1}{\omega_1^2 C_p} \quad \text{Equation 4.3}$$

Where: ω_1 is the first vibrational mode frequency

An inductive shunt reactance with inductor L_{sh} of 2 H was connected to the system to improve the generated power. Increases in power outputs were up to 117% and 47% for shunt capacitors C_{sh} equal to 0.6 μ F and 0.87 μ F respectively.

Secondly, an enhanced power hybrid tuning technique using multiple piezoelectric unimorphs has been presented. Mechanical tuning, electrical tuning, and band-pass filtering methods were used simultaneously to develop an increase in frequency range for the piezoelectric harvester with enhanced power using inductive impedance. A small toroid inductor of 700 mH was connected in parallel to the load resistance and shunt capacitance. An extended frequency range of 12 resonance frequencies with 300% improvement was obtained experimentally with enhanced power density improvements of 19.7% to 197%. Future work

might include an ultra-low power microcontroller to develop an actively hybrid tuned energy harvester with power enhancement.

4.7 Experimental Set up

A new enhanced power piezoelectric energy harvesting system using several piezoelectric bimorph cantilevers with hybrid frequency tuning and conjugate impedance matching is developed. The equivalent circuit of the suggested scheme is shown in Figure 4.15. This improved method does not need a large inductance value, because of the high value of the capacitance. This high capacitance results from adding the shunted and inherent capacitances in parallel. The experimental setup consists of two parts: the improved adjusting capacitor method and the hybrid frequency tuning method.

4.7.1 Improved Adjusted Capacitor Method

An experimental scheme for electrical tuning and power maximization has been proposed. Several shunt capacitors with values between C_p and $10 C_p$ have been individually connected to a unimorph piezoelectric layer to shift the resonance frequency. It was shown that the harvested power and matching impedance are both inversely correlated to the capacitor value. An inductive reactance of 700 mH was connected in parallel to the system to address this issue and causes a substantial increase in the harvested power. An Arbitrary Function Generator (Tektronix AFG 2021, 20 MHz) was used to provide a sinusoidal 100 mV peak-to-peak voltage to a Power Amplifier (Brüel & Kjær Type 2718), which amplifies the small signal to have enough power to drive a Shaker (Brüel & Kjær Type 4809).

The shaker can provide vibrations with different levels of accelerations, which can be measured using an accelerometer (PCB PIEZOTRONICS Model # 352C33 with 102.9mV/g, and 0.5-10 kHz).

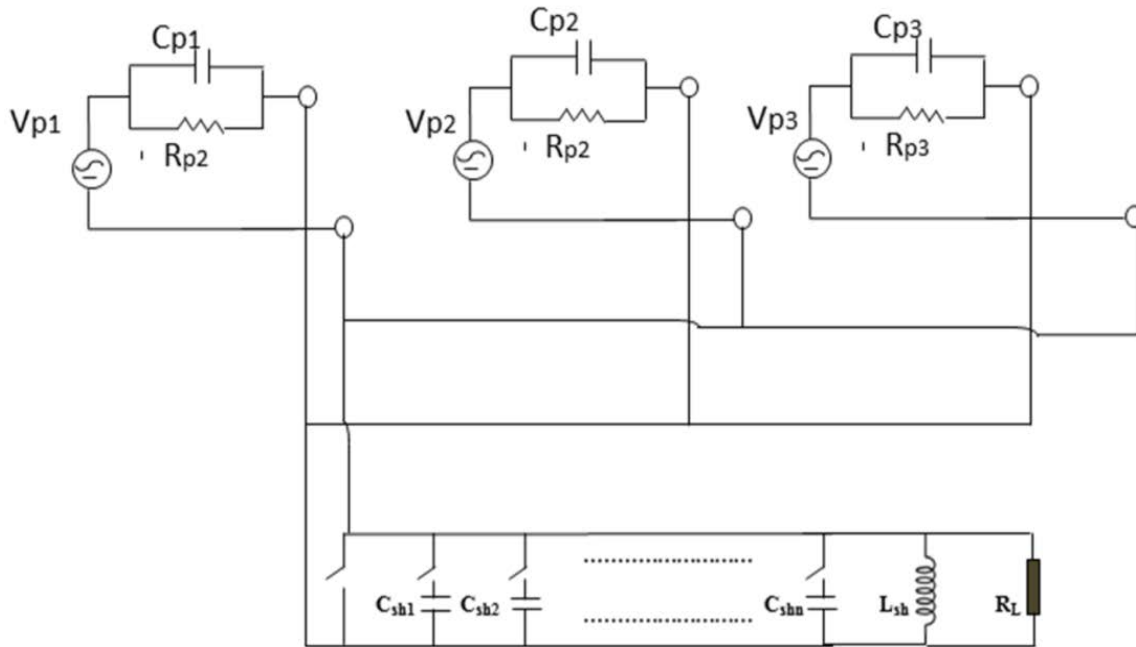


Figure 4.14 Equivalent circuits for enhanced power hybrid energy harvester

A piezoelectric unimorph cantilever (Type TH-7R, 18 g, 95.25 mm × 73.41 mm, 0.25 mm thickness piezo layer, 166 nF internal capacitance) was placed properly to a thick plastic piece on the top of a bar fastened to the shaker. This device was used to give a 208 Hz resonance frequency at its full length with no adjusting shunt capacitor connected. This cantilever was tuned mechanically by changing its length by 2 mm to work at 205 Hz to be utilized in a similar experiment as will be explained in the next section. Ceramic capacitors in a range of 0.2-1.6 μF were used to adjust the load impedance and verify the required electrical tuning. Two toroid inductors (Type TE-4Q3TA) with 700 mH and 2 H values were used for the cases of 208 Hz and 205 Hz resonance frequencies respectively. The mentioned inductor values were chosen such

that the inductive reactance almost cancels the capacitive reactance according to the conjugate impedance matching principle. A resistance decade box (TENMA 72-7270) was used to obtain load resistances in a range of 1 Ω -11 M Ω . The load resistance was connected in parallel with the unimorphs, the shunted capacitors, and inductors via serial switches to have different collections of R_L-C_p , $R_L-C_p-C_{sh}$, and $R_L-C_p-C_{sh}-L_{sh}$, as shown in Figure 4.16. A Digital Storage Oscilloscope (Type TDS2012B, 100 MHz, 1 GS/s) was used to measure the output peak-to-peak voltage across the load resistor, and then the measured voltage was used to calculate the output power.

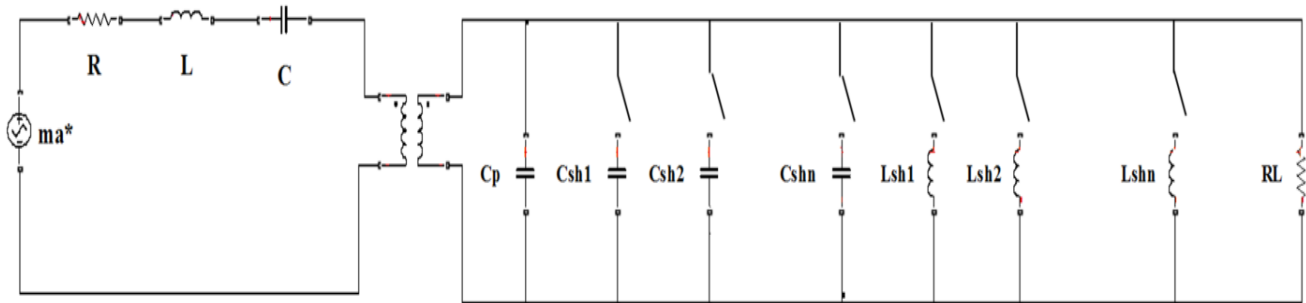


Figure 4.15 Equivalent circuit for improved adjusting capacitor method

4.7.1 Enhanced power Hybrid Frequency Tuning Method

To augment maximum power and widen the operating frequency range, an enhanced hybrid technique using three piezoelectric unimorph cantilevers has been presented. Mechanical tuning, electrical tuning, and band-pass filtering methods were used simultaneously with inductive impedance. Those three techniques were used to develop a broadband frequency range for the piezoelectric harvester. The inductive reactance has been used to cancel a significant portion of capacitive reactance, which is used for electrical tuning. To satisfy power enhancement, a small toroid inductor of 700 mH was connected in parallel to the load resistance and shunt capacitance.

Three similar unimorphs, by Face International Corporation with 166 nF inherent capacitance and dimensions shown in Table 4.1, have been placed properly to a thick plastic piece on the top of a bar fastened to the shaker. The load resistance was connected in parallel with the bimorph cantilevers' output and the shunted capacitors and inductor through serial switches to have different collections of RLC parallel circuits. The measured voltage was used to calculate the output power.

Table 4.1 Physical properties of TH-7R Cell

Mass	18 g
Footprint (domed)	95.25 mm × 73.41 mm
Footprint (flat)	97.66 mm × 73.41 mm
Piezo thickness	0.25 mm
Total thickness	0.53 mm
Dome height	9.55 mm

4.8 Results and discussion of enhanced power hybrid system

4.8.1 Improved Adjusting Capacitor

To demonstrate the electrical tuning for the piezoelectric unimorph cantilever, several shunt capacitors were connected individually in parallel to have different operating resonance frequencies. The voltage was measured using the digital storage oscilloscope at different load resistance values up to 20 kΩ, and the output power was calculated from the square of the measured voltage divided by the load resistance value.

These experimental results were used to validate the influence of shunt capacitance on the resonance frequency and power delivered to the load resistance as shown in Figure 4.17.

Resonance frequency was shifted from 208 Hz at no shunt capacitance to 204 Hz at a 1.5 μF shunt capacitor, which is equal to 1.9% of resonance frequency for the no capacitor case. It should be considered that the load resistance has a minor influence on the shifted frequency. Although a good resonance frequency range has been obtained, the power decreases when shunt capacitance increases, which is a main constraint and to be addressed. The maximum extracted power values were 14.38 mW and 6 mW with a shunt capacitor C_{sh} of zero and 1.5 μF respectively. It can be seen that for each case there is an optimal load resistance that depends mainly on the capacitive reactance, and it has a direct correlation with the shunt capacitor value.

The issue of output power decrement needs to be resolved and hence an inductive reactance of 700 mH was connected in parallel to the system for two different shunt capacitors. By considering Figure 4.18 it can be noticed that there is a significant improvement in power output with the shunt inductor. Increases in power outputs were up to 93% and 88% for the shunt capacitors equal to 1 μF and 1.16 μF respectively. In addition, the unimorph cantilever was tuned mechanically by changing its length by 2 mm to achieve a resonance frequency of 205 Hz, and then two shunt capacitors of 0.6 μF and 0.87 μF were connected individually with the load resistor R_L to shift the resonance frequency to 200 Hz and 200.5 Hz respectively. An inductive shunt reactance with inductor L_{sh} of 2 H was connected to the system to improve generated power. The results demonstrated in Figure 4.19 show that increases in power outputs were up to 117% and 47% for shunt capacitors C_{sh} equal to 0.6 μF and 0.87 μF respectively. Finally, the relation between the shunt capacitor and the resonance frequency has been studied. The results shown in Figure 4.20 demonstrate that the resonance frequency decreases when the shunt capacitor increases. The shunt capacitance change causes a change in the stiffness of the beam and consequently the natural frequency changes. For the unimorph cantilever with a natural

frequency of 208 Hz, the shunt capacitor value was changed from 0 to 1.5 μF . accordingly; the operating frequency was changed to 207-204 Hz and 208-204.2 Hz for load resistance values of 0.3-3 $\text{k}\Omega$ and 3-20 $\text{k}\Omega$ respectively.

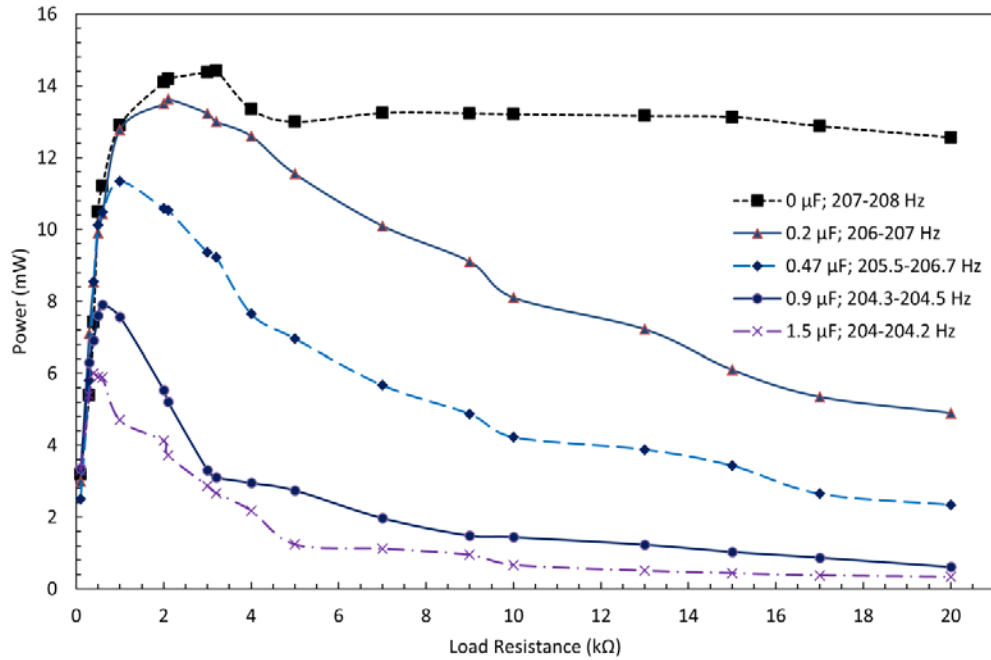


Figure 4.16. Power outputs for various load resistances R_L and several shunt capacitors C_{sh}

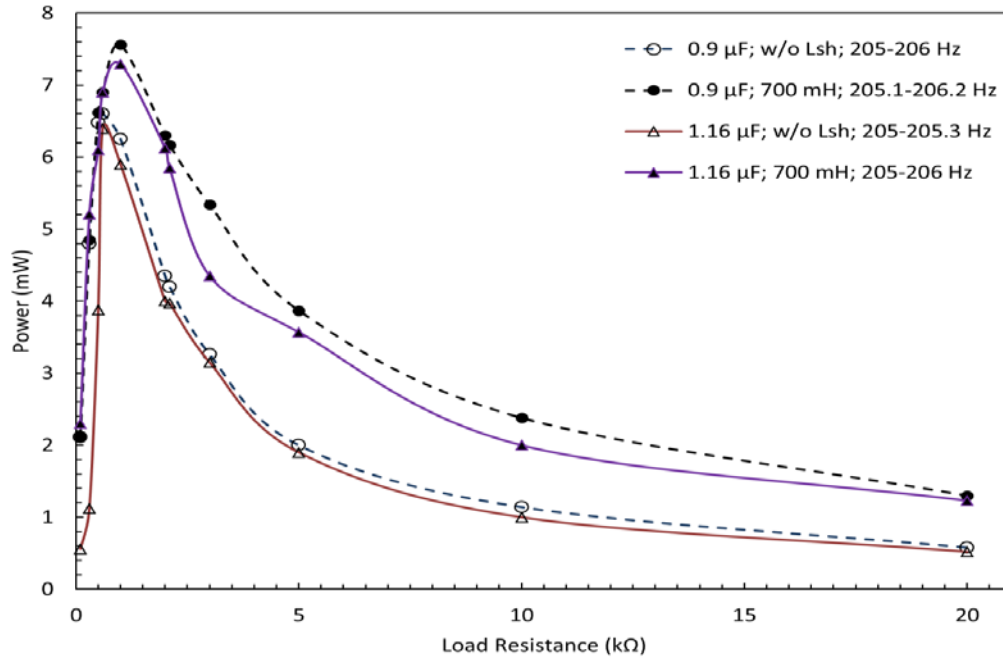


Figure 4.17. Power outputs using a shunt inductor L_{sh} of 700 mH and two different shunt capacitors.

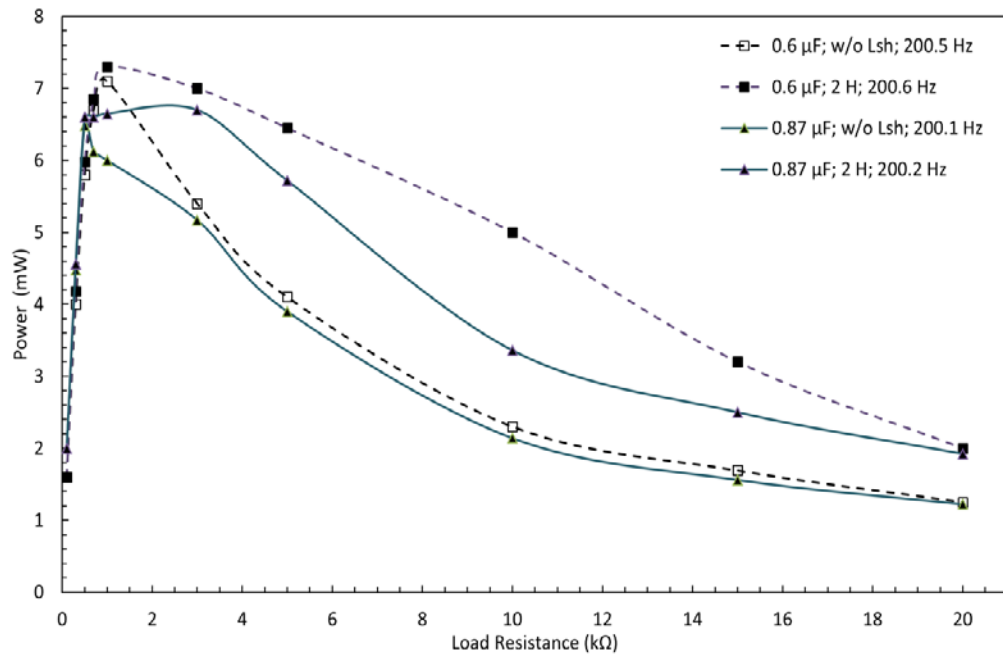


Figure 4.18. Power outputs using a shunt inductor L_{sh} of 2 H and two different shunt capacitors.

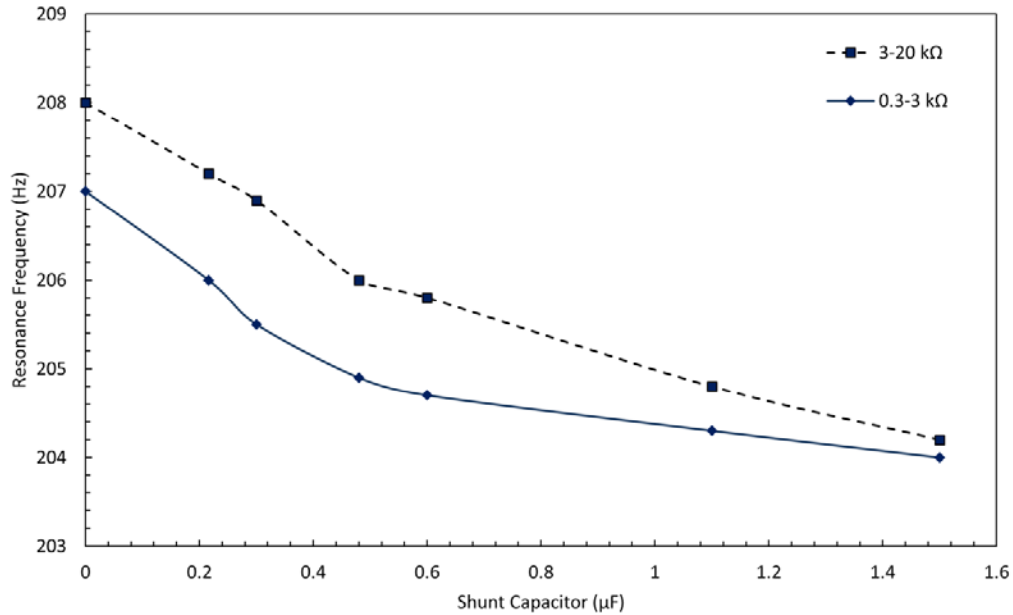


Figure 4.19. Resonance frequencies f_r versus shunt capacitors C_{sh} for various load resistances R_L .

4.8.2 Enhanced power hybrid tuning method

An enhanced hybrid technique to boost maximum piezoelectric power and widen the operating frequency range has been proposed. This new technique uses three piezoelectric unimorph cantilevers to achieve mechanical and electrical tuning, and band-pass filtering methods simultaneously with conjugate impedance matching. Those three tuning approaches have been used all together to develop a broadband frequency spectrum for the piezoelectric energy harvester. The inductive reactance has been used to reduce capacitive reactance which is used for electrical tuning. For electrical tuning (with shunted capacitors) without shunting an inductive load, it is clear that when the piezoelectric system is excited under random frequencies from 90 Hz to 115 Hz, the average harvesting output power of the energy scavenger with tuning will be higher than that without tuning. That shows a significant improvement of the average harvested power output by using an electrical tuning method. For example in another work (Wu W-J et al 2006), it was found experimentally that, when the piezoelectric beam cantilever was

excited under random frequencies from 80 Hz to 115 Hz, the average harvesting output power of the generator with electrical tuning was about 27.4% higher than that without tuning. When inductive impedance is shunted, the average harvested power is even more than that in the first case which shows the significance of the new method of shunt inductor.

Mechanical tuning was performed by setting different dimensions and tip masses, as shown in Table 4.2, and utilizing the experimental setup shown in Figure 4.21 for the three unimorphs. In the case of the open circuit, obtained resonance frequencies were 240 Hz, 277 Hz, and 294 Hz for the first, second, and third cantilever respectively. The three output voltages and the vibration acceleration signal for the case of a 10 k Ω load resistance are demonstrated in Figure 4.22 and Figure 4.23 respectively. When the three unimorphs are connected in parallel, a band pass filter with bandwidth widening is obtained with three new resonance frequencies of 237 Hz, 274 Hz, and 290 Hz for the three unimorphs respectively. Each cantilever now has a total parallel capacitance of $3C_p$ which is equal to 498 nF according to the parallel capacitors rule. This can be considered electrical tuning for each individual beam using C_{sh} of 332 nF. By adding two different shunt capacitors C_{sh} , other resonance frequency groups were 236 Hz, 271 Hz, and 289.5 Hz for C_{sh} of 1 μ F; and 235 Hz, 270 Hz, and 289 Hz for C_{sh} of 1.41 μ F.

During this hybrid tuning method, it was noticed that there is a power loss due to the shunt capacitor C_{sh} . To overcome this problem, an enhanced power method was developed by shunting a 700 mH inductor in parallel to the load resistor. The output voltage and power density versus frequency for this enhanced power hybrid energy harvester with and without the shunt inductor L_{sh} are shown in Figure 4.24 and Figure 4.25 respectively. It can be seen that there are 9 different additional resonance frequencies. The total number of resonance frequencies now is 12 with a 300% improvement. Significant increases in voltage and power outputs, varied from 19.7% to

197%, were also obtained. Voltages for three resonance frequencies of the bimorph cantilevers are presented in Figure 4.26.

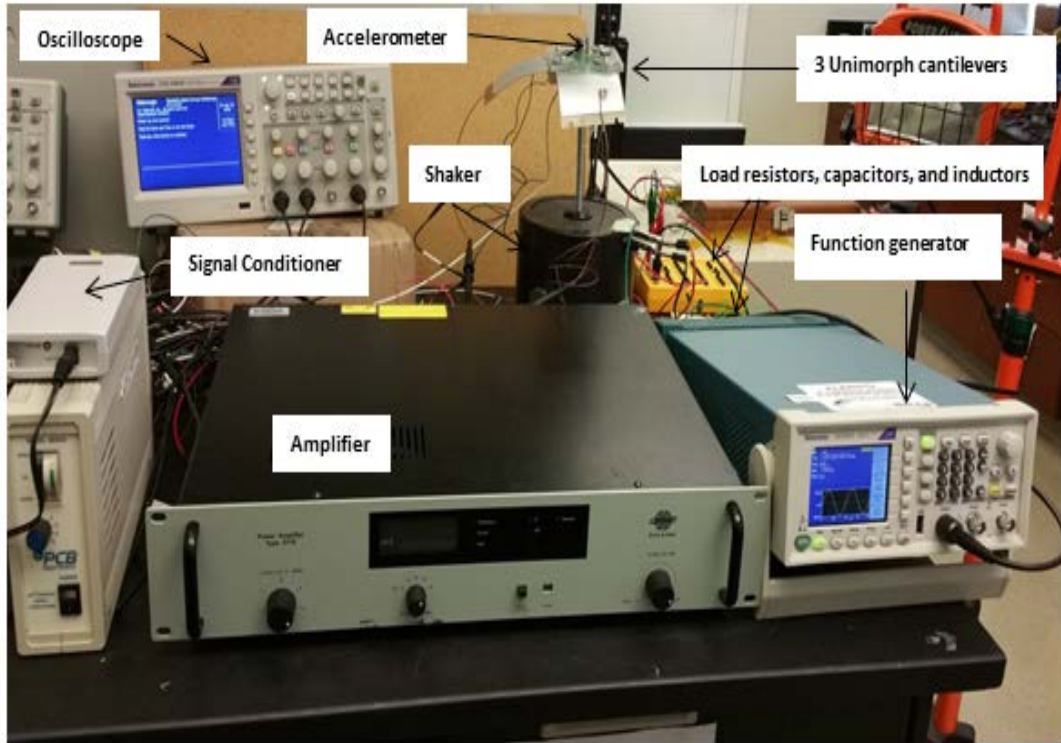


Figure 4.20. Experimental setup for enhanced power hybrid tuning method

Table 4.2 Properties of the three different unimorphs

Unimorph	Length (mm)	Width (mm)	Tip mass (g)	Frequency (Hz)
1	82	73	0.6	240
2	84	73	0	277
3	81.5	73	0	294

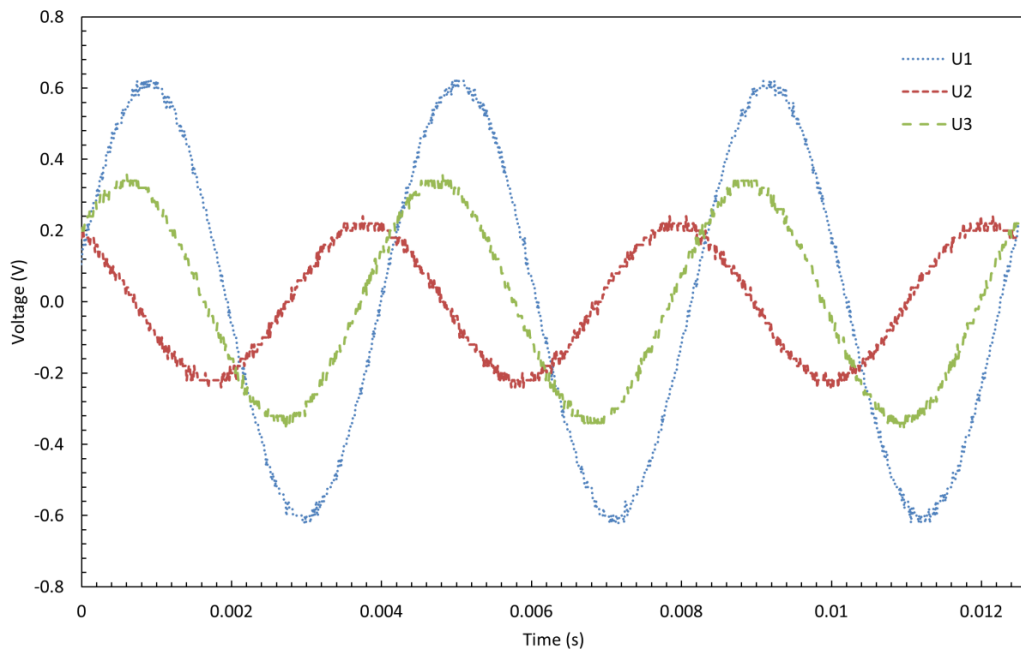


Figure 4.21 AC voltage outputs of three different unimorphs with 10 kΩ load resistance

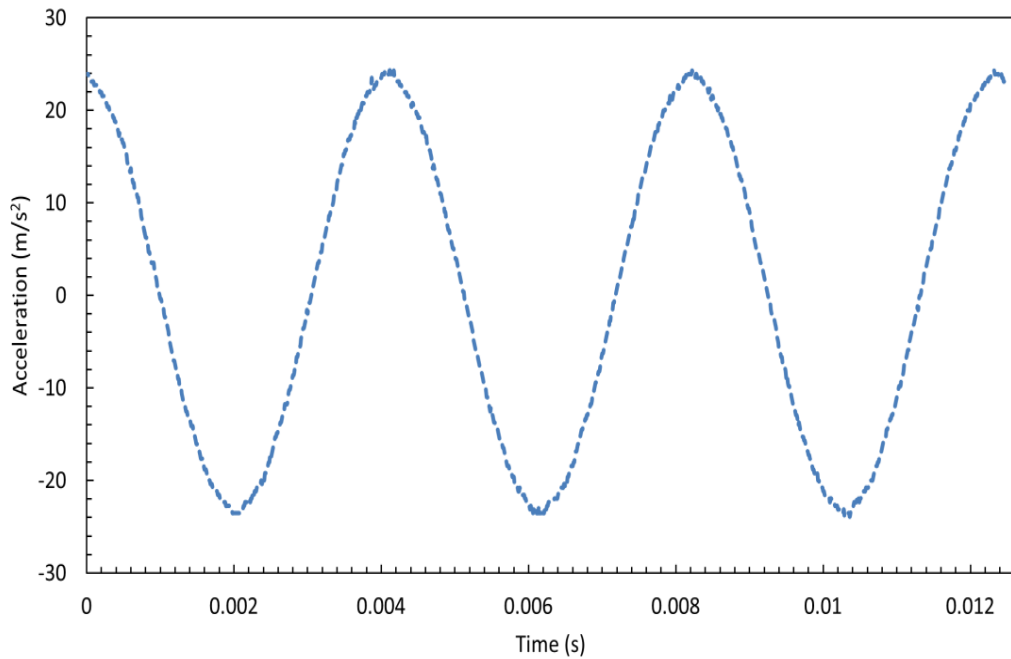


Figure 4.22 Vibration acceleration signal with 10 kΩ load resistance

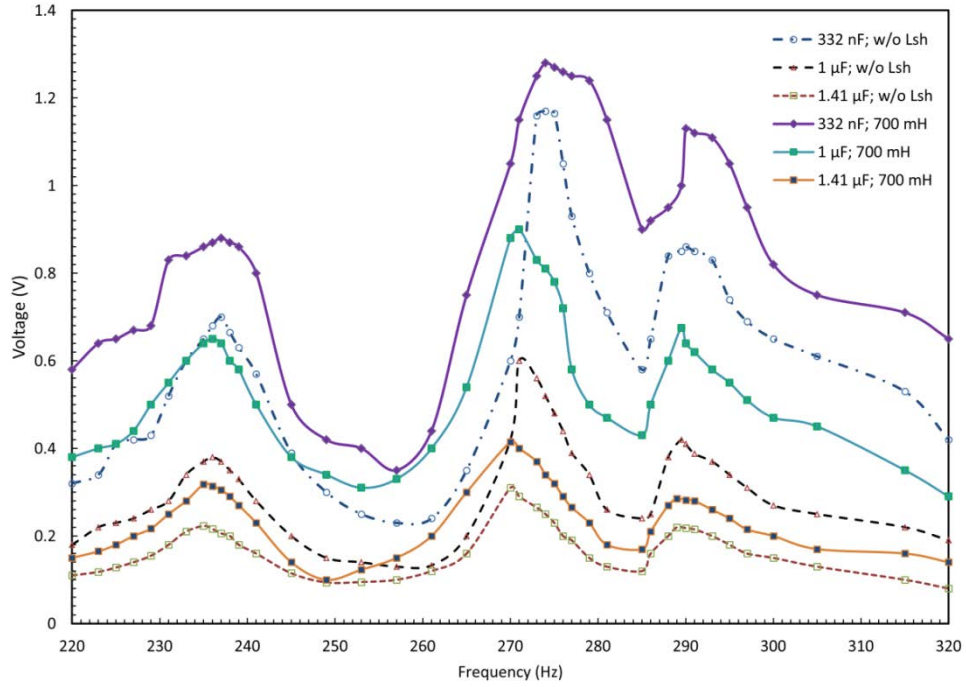


Figure 4.23 Output voltages versus frequency for enhanced power hybrid energy harvester

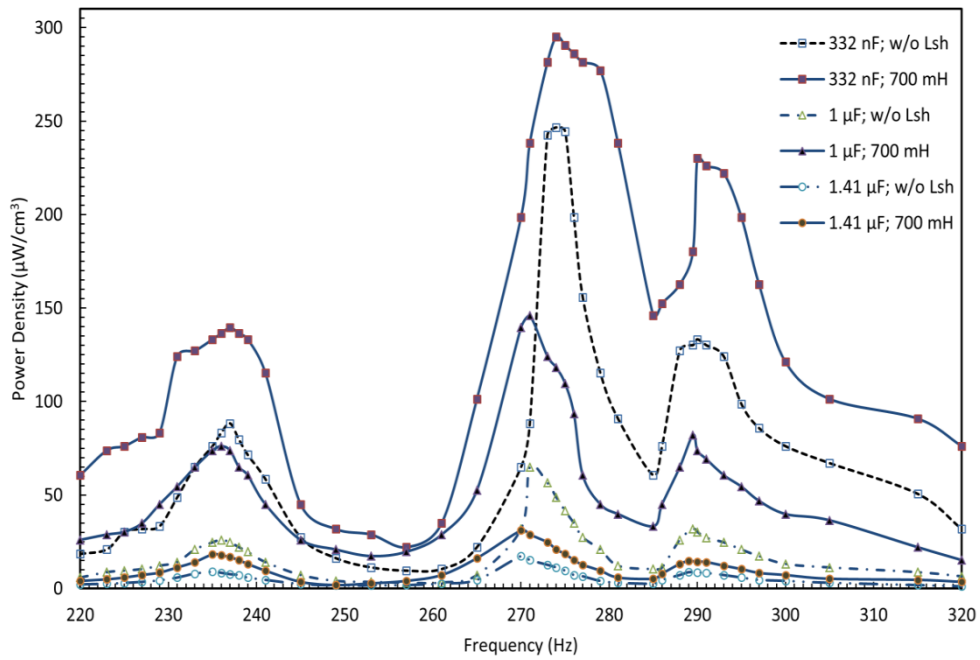


Figure 4.24 Power densities versus frequency for enhanced power hybrid energy harvester

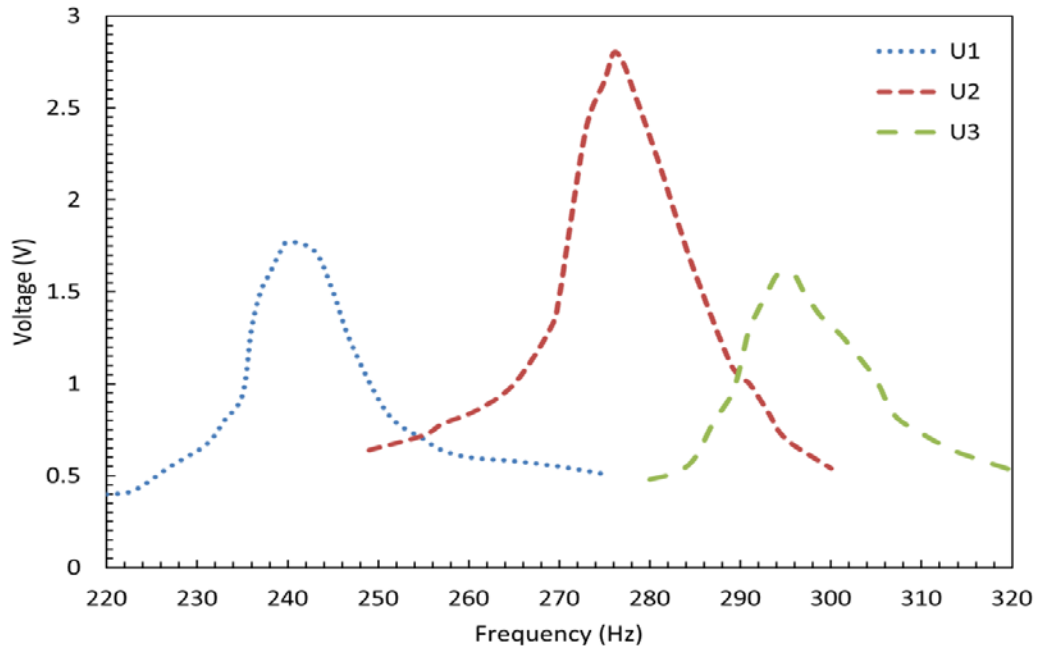


Figure 4.25 Voltages for three resonance frequencies of the bimorph cantilevers

Chapter 5. Hybrid Pyro-Piezo Energy Harvester

5.1 Introduction

The ultimate goal in the research field of energy harvesting is to enable self-powered electronic devices so that the maintenance costs resulting from the use and replacement of batteries can be reduced. (Xiao-biao Shan et al 2013). Heat, light, wind and vibration can be transformed to usable electrical energy for running such remote electronic devices independently.

Those energy sources are not always obtainable. In order to scavenge energy uninterruptedly, it is critical to design and produce a hybrid energy scavenger that combines light, heat, and piezoelectric vibration generators, enabling energy harvesting from several energy sources simultaneously (Wischke, M 2010, A. Collado et al 2013, J. Gummeson et al 2010, B. J. Hansen 2010, and Hua Yu et al 2014, Chulsung, P. 2006, and MacCurdy, B 2008). However, the main goal behind those researches was to integrate these sources to develop a new multi-source energy scavenger with improved power.

In this study an investigation for impedance matching and power maximization for hybrid piezoelectric and pyroelectric energy harvesting system is proposed. For maximum hybrid power, impedance matching between load impedance and internal impedance of the hybrid energy harvester must be satisfied. The total internal impedance dependence on the average temperature and the heating rate are both key parameters when characterizing a material used for hybrid energy harvesting. This indicates clearly that to optimize impedance when utilizing the pyroelectric and piezoelectric effects simultaneously, both operating average working temperature and the rate of temperature change need to be considered when designing energy

harvesting applications. Neglecting those parameters will result in inefficient and unpredictable hybrid energy harvesting systems.

Hybrid energy harvesting using a new voltage doubler circuit for rectifying and collecting pyroelectric and piezoelectric voltages individually is proposed and tested. The investigation showed that the hybrid energy is possible using the voltage doubler circuit from two independent sources for pyroelectricity and piezoelectricity due to marked differences of optimal performance. The obtained results were significantly higher than harvested energy simultaneously from the same material.

5.2 Pyroelectric, piezoelectric, and hybrid energy harvesting

A maximum hybrid energy harvesting extraction from piezoelectric materials requires load impedance matching. To verify impedance matching, the internal impedance Z_p for this material needs to be measured.

5.3 Study of heat effect on the impedance

The total impedance has two components, the inherent capacitive reactance C_p and the resistance R_p . In reality, the resistance R_p decreases as the applied electric field and temperature increase (A. Navid and L. Pilon 2011). On the other hand, the capacitance C_p has direct correlation with temperature. The total impedance is affected by heating as both parameters C_p and R_p do, so it is really necessary to consider the effect of heat on the total impedance Z_p to have accurate impedance matching and maximum power. The same SPLPF circuit and LCR precision meter were used to characterize bimorph T226-A4-503X at a piezoelectric frequency of 115 Hz when a light heating is applied. The expected optimal load impedance for maximum

hybrid power is equal to the total inherent impedance at the piezoelectric frequency and particular temperature range.

A 1 kW electric lamp is used for heating purposes and a thermometer (OMEGA HH506R) is used to measure the constant temperature by attaching its thermocouple properly to the bimorph as shown in Figure 5.1. The results are shown in Figure 5.2 and Figure 5.3 respectively. The internal capacitance was correlated directly to the temperature as in Figure 5.2; hence the capacitive reactance correlates reversely.

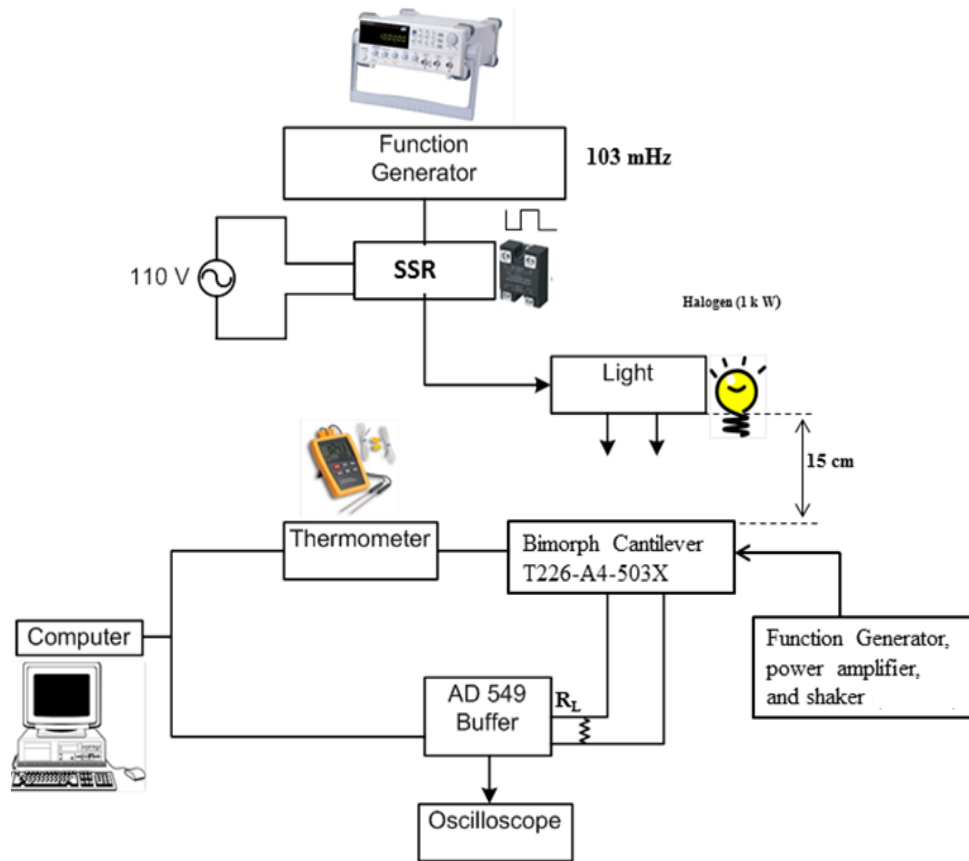


Figure 5.1. The Experimental set up for the hybrid energy harvesting.

The capacitance increases from 55 nF at 24°C to 107.8 nF at 80 °C. The resistance decreases from 148 kΩ at 24°C to 21 kΩ at 80 °C. The optimal load impedance should be equal to the total inherent impedance which can be obtained from Equation 2.14. The relationship between the total impedance Z_p and temperature is presented in Figure 5.3 which shows that Z_p decreases from 24.8 kΩ at 24°C to 11.4 kΩ at 80 °C.

The resistive impedance required for maximum hybrid energy harvesting should be equal to the average value of the total impedance Z_p in the particular temperature range resulted from the cyclic heating.

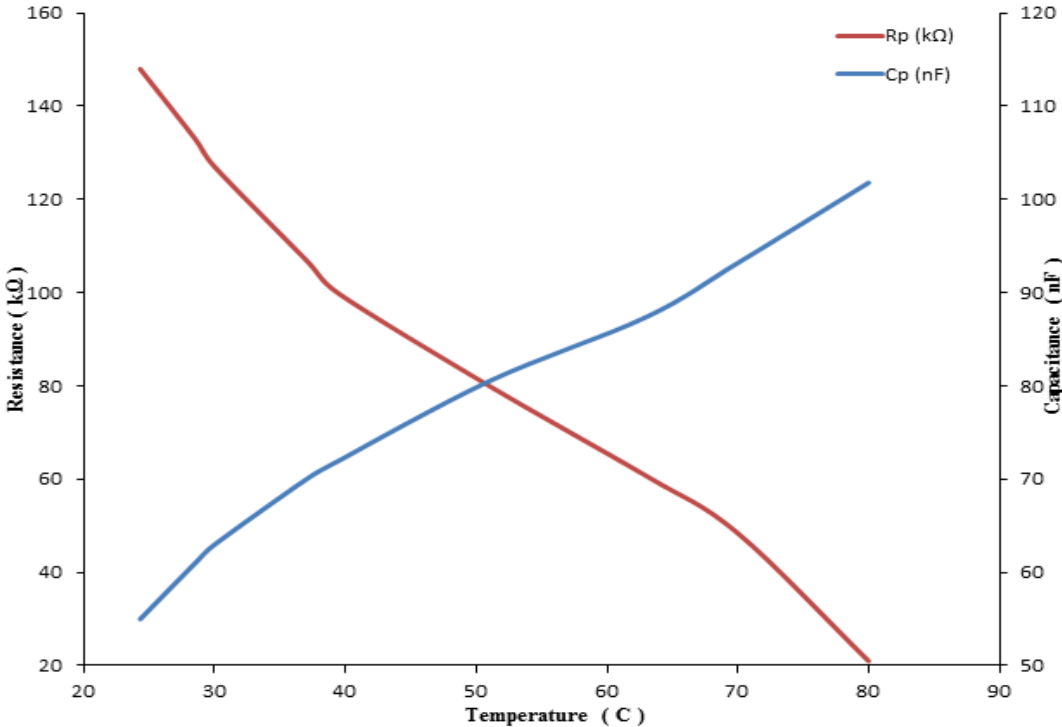


Figure 5.2. Inherent resistance and capacitance of the piezoelectric cell versus temperature at 115 Hz

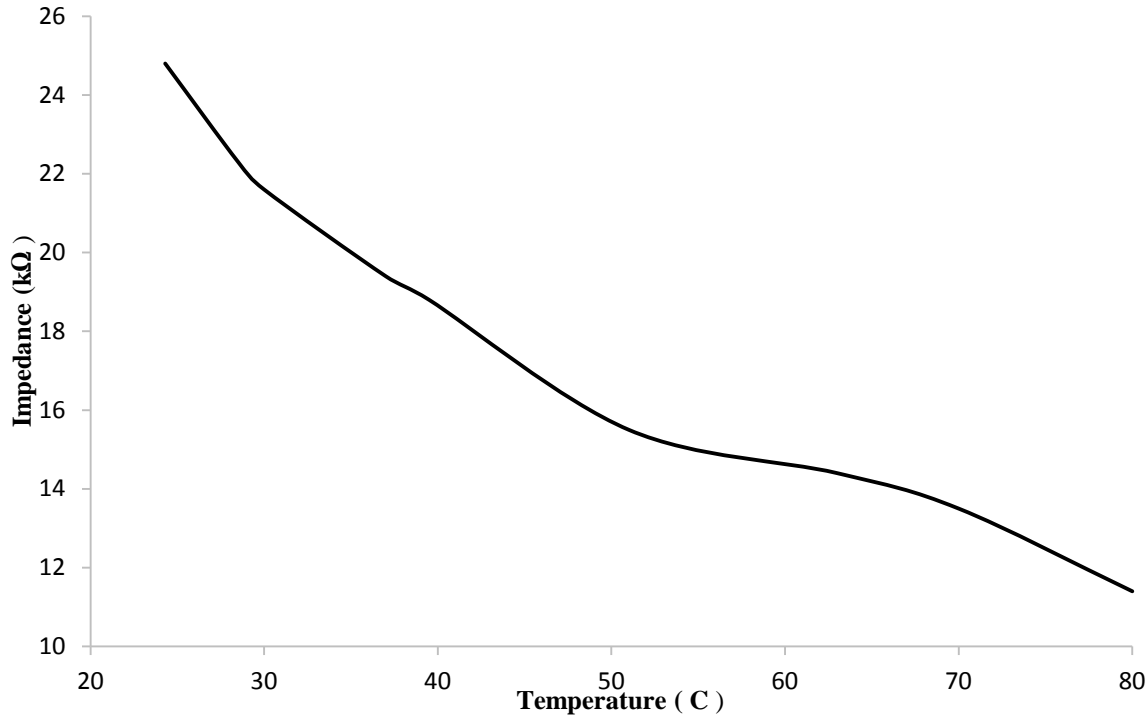


Figure 5.3. Impedance of the piezoelectric material versus temperature at 115 Hz

5.4 Experimental set up for hybrid energy harvesting

The prototype used for investigation of piezoelectric, pyroelectric, and hybrid energy harvesting is presented in Figure 5.1.

For the piezoelectric energy harvesting part, an arbitrary Function Generator (Tektronix AFG 2021, 20 MHz) has been used to supply a sinusoidal 50 mV peak-to-peak voltage to a power amplifier (Type 2718), which provides enough power to drive a shaker (Type 4809). The shaker provides vibration, whose acceleration can be measured using an accelerometer, Model # 352C33. A bimorph (manufactured by Piezo Systems, Inc. with model number T226-A4-503X) has been placed properly to a thick plastic piece on top of a bar fastened to the shaker. A resistance decade box with resistance values of 1Ω to 11 MΩ, (TENMA 72-7270) was used to have different load resistance values. The load resistance has been connected in parallel with the

bimorph cantilever. A Digital Storage Oscilloscope (Type TDS2012B, 100 MHz, 1 GS/s) was used to measure the output voltage across the load resistor, and then the measured voltage was used to calculate the output power.

For pyroelectric and hybrid energy harvesting some other equipment needed to be set up. The complete set up is shown in Figure 5.1. Another Function Generator (Hewlett Packard 15 MHz), a Solid State Relay (OMEGA SSR330 DC25) with 3-15 V_{dc} biasing voltage, a halogen lamp (110 V_{ac} and 1 kW), a thermometer (OMEGA HH506R), a Multimeter (Fluke 189-True RMS), and a personal computer are used for measurements. The function generator provides a square voltage wave with different frequencies for the SSR which has two normally opened contacts used to supply a 110 V_{ac} voltage to the light bulb to get cyclic heating with 100 mHz frequency. The load resistance is connected in parallel to the pyroelectric cell. The thermometer and voltmeter with DAQ system are connected to the pyroelectric cell to record the periodic temperature and voltage values respectively.

5.5 Results and Discussion

A cyclic heat with frequency of 100 mHz and rate of 0.44 degrees per second (between 61.1 and 65.5 °C) was applied to the bimorph simultaneously with a vibration of 0.21 g and a piezoelectric frequency of 115 Hz and at load resistance of 25 k. The instantaneous generated piezoelectric, pyroelectric, and hybrid voltages are shown in Figure 5.4, Figure 5.5, and Figure 5.6 respectively. The hybrid voltage shape was almost similar to a modulated signal which is mixed of a carrier signal with high frequency of 115 Hz and a modulating signal with low frequency of 100 mHz. The peak value of hybrid voltage (0.69 V) was less than the sum of pyroelectric (0.16 V) and piezoelectric (0.72 V) voltages. Considering Figure 5.7, it can be noticed that the maximum piezoelectric and hybrid powers of 22.9 μW and 16.5 μW were

extracted at a load resistances of 22 k Ω and 19 k Ω respectively. Based on the capacitance in Figure 5.2 the expected piezoelectric optimal load impedance at 24 °C and 115 Hz was 25.1 k Ω with which the experimental optimal piezoelectric shown in Figure 5.7 was in 12.3 % difference. Considering Figure 5.3, the expected hybrid optimal load impedance at 63.3 °C was 14.4 k Ω . The experimental hybrid optimal load impedance in Figure 5.7 was 19 k Ω which is within a 24 % difference with the predicted value. The PSLPF method has been utilized to measure the pyroelectric impedance at low frequency of 100 mHz. The measured optimal pyroelectric impedance at temperature of 63.3 °C was equal to 0.45 M Ω . There is an 11.1 % difference between the predicted value and the experimental value of optimal pyroelectric impedance shown in Figure 5.8 which was equal to 0.4 M Ω .

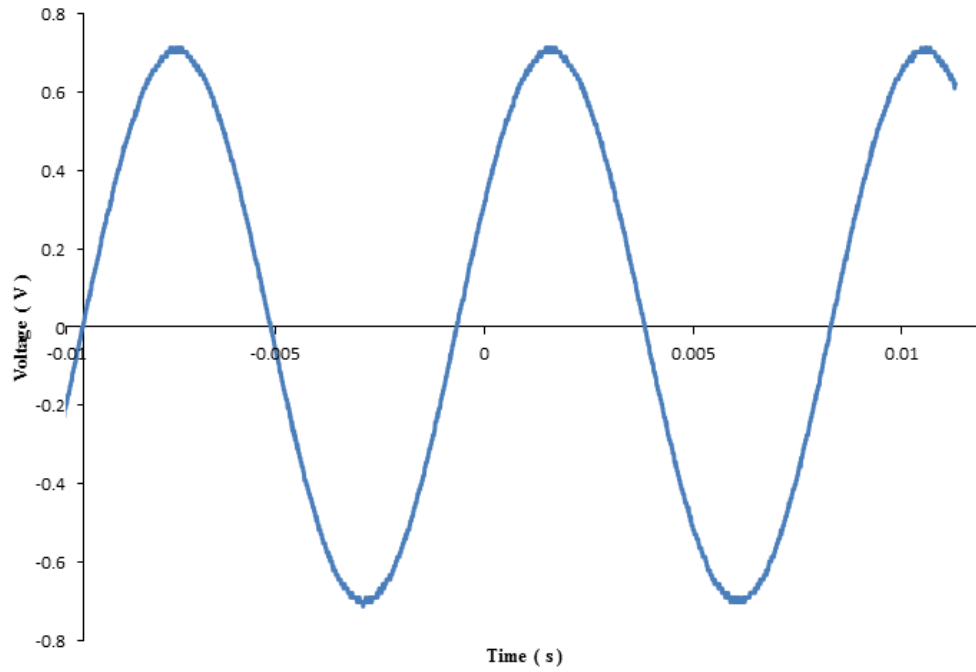


Figure 5.4. Piezo Voltage for the bimorph T226-A4-503X at 0.21 g and 115 Hz vibration, and R_L of 25 k Ω .

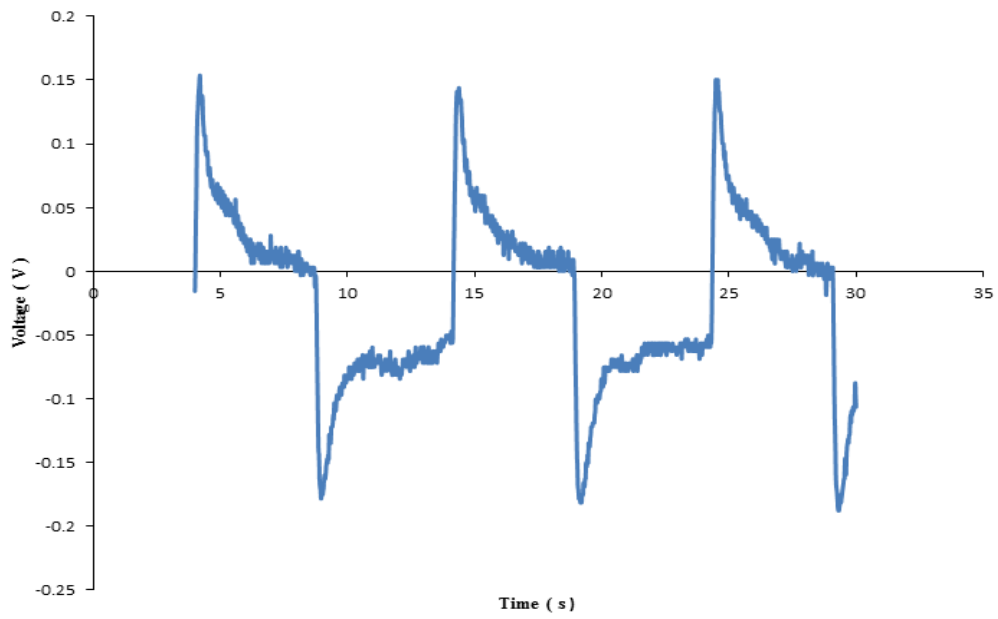


Figure 5.5. Pyro. voltage for bimorph T226-A4-503X at 100 mHz, and 0.44 degree/s heating, and R_L of 25 k Ω .

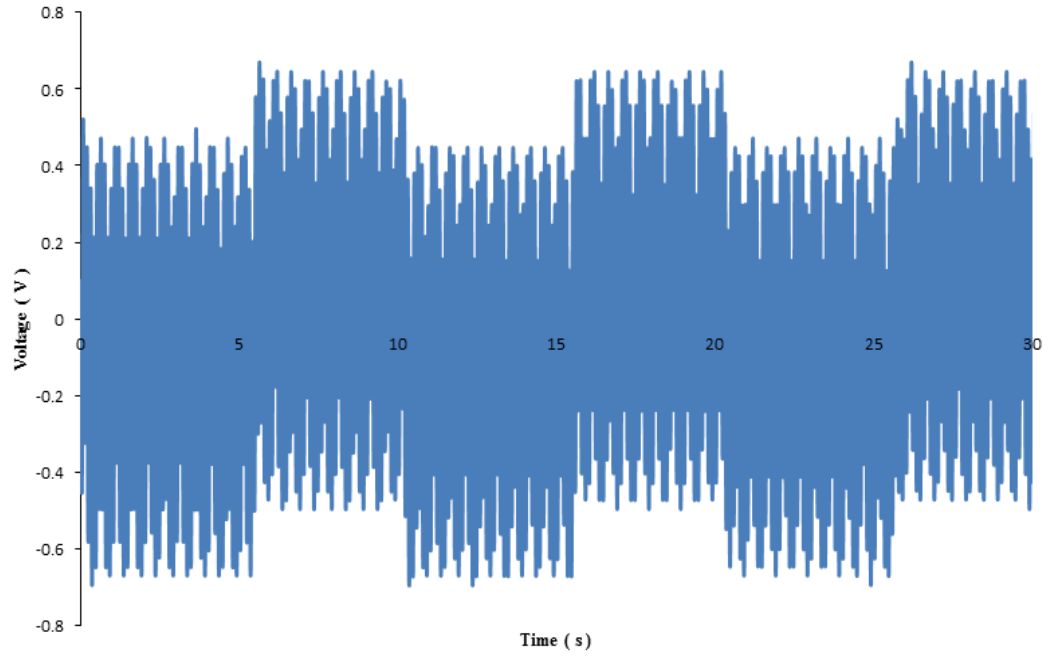


Figure 5.6. Hybrid voltage for bimorph T226-A4-503X at 100 mHz, 0.44 degree /s heating and at 0.21 g and 115 Hz vibration, and R_L of 25 k Ω

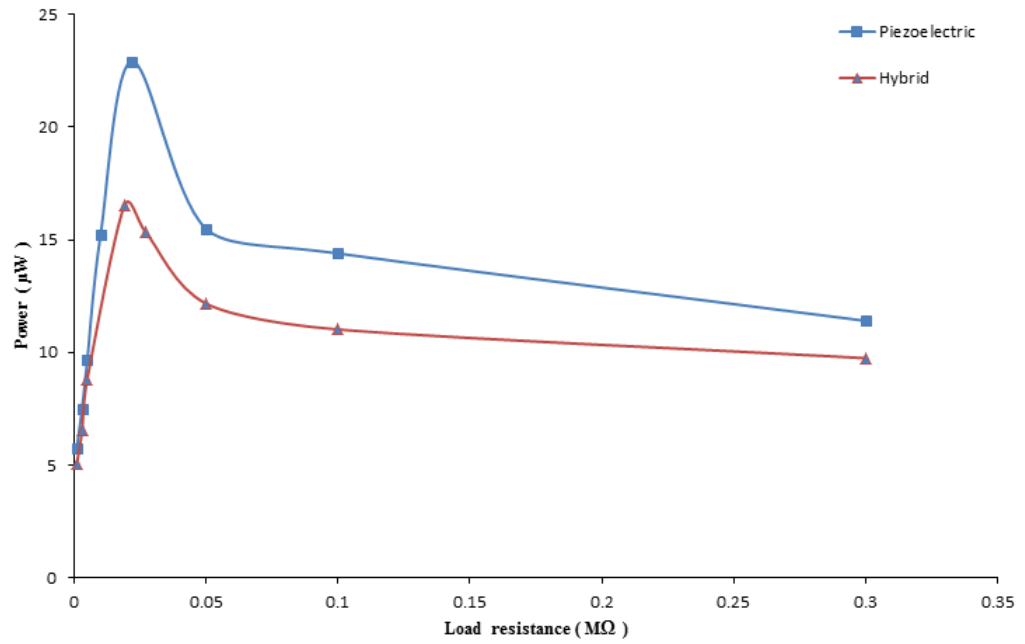


Figure 5.7. Piezoelectric and hybrid peak power versus load impedance

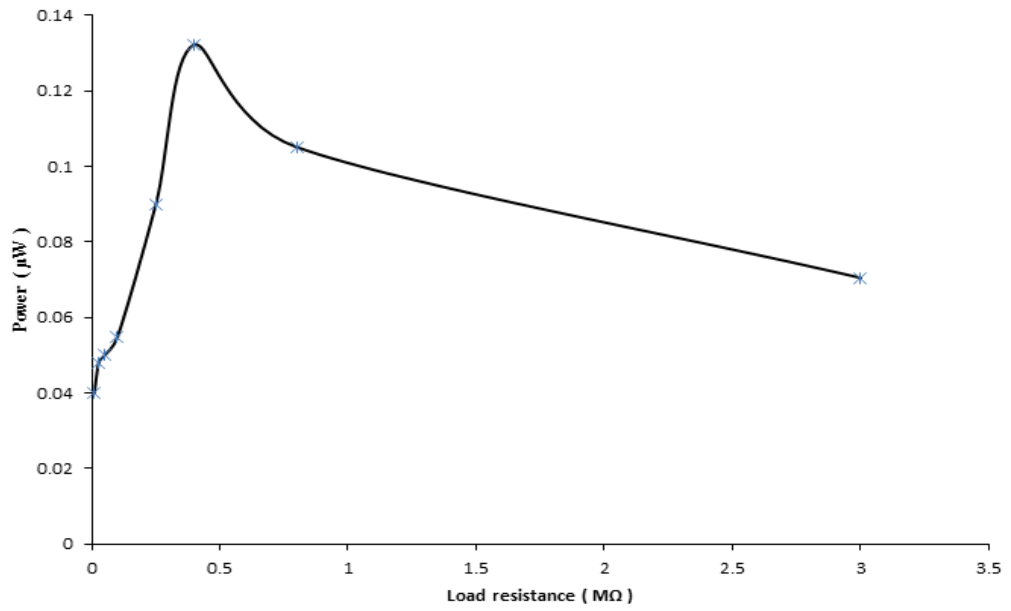


Figure 5.8. Pyroelectric peak power versus load impedance

5.6 Voltage doubler circuit for hybrid energy harvesting

In this section a suggested voltage doubler electronic scheme to combine pyroelectric and piezoelectric energy harvesting in one device has been demonstrated. The experimental study is carried out using two similar PZT bimorph piezoelectric cantilevers of the model number T226-A4-503X. Results show that the output voltage is equal to the sum of the doubled individual voltage outputs minus diodes' losses as shown in Equation 5.1. When choosing the optimal load impedances, the fact that piezoelectric matching impedance is different than that in pyroelectric energy harvesting needs to be considered. The total optimal load resistor was found to be equal to the sum of individual voltage sources since they are connected in series as shown in Figure 5.8.

$$V_o = 2 V_{pz} + 2 V_{pr} - 4V_f \quad \text{Equation 5.1}$$

Where:

V_o , V_{pz} , V_{pr} , and V_f : Are the output voltage, input piezoelectric voltage, input pyroelectric voltage, and voltage drop across diode respectively.

The equivalent circuit and experimental set up for Hybrid Pyro- Piezo Energy Harvester Using Voltage Doubler are shown in Figures 5.9 and 5.10 respectively. Four capacitors of 100 μ F each, and six diodes (two were used as freewheeling diodes) with V_f of 0.5 V have been used in the voltage doubler circuit.

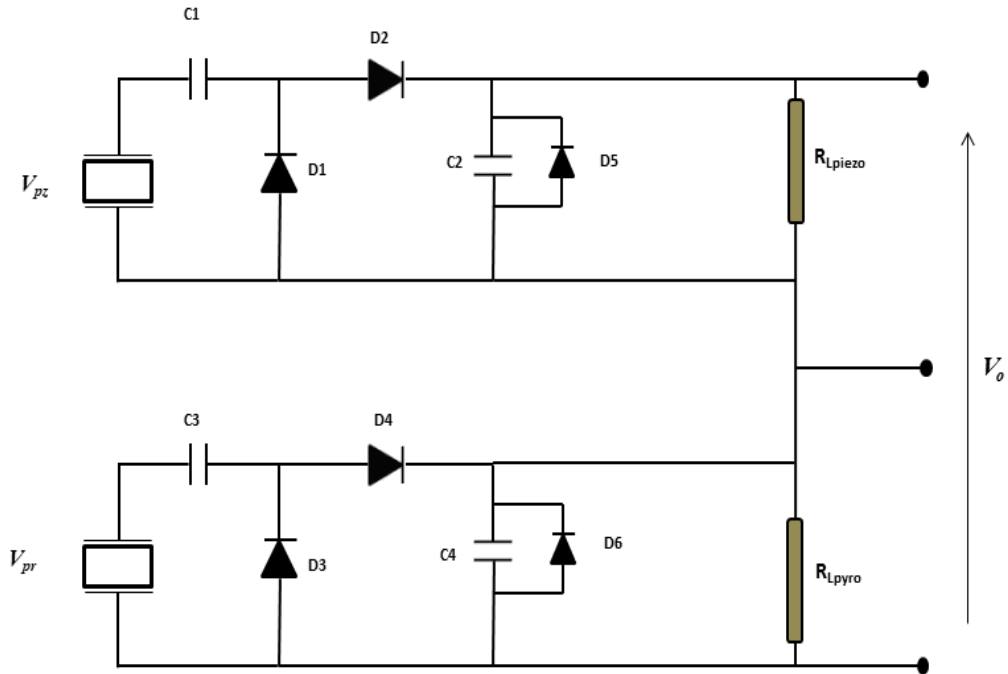


Figure 5.9 Hybrid Pyro- Piezo Energy Harvester Using Voltage Doubler scheme

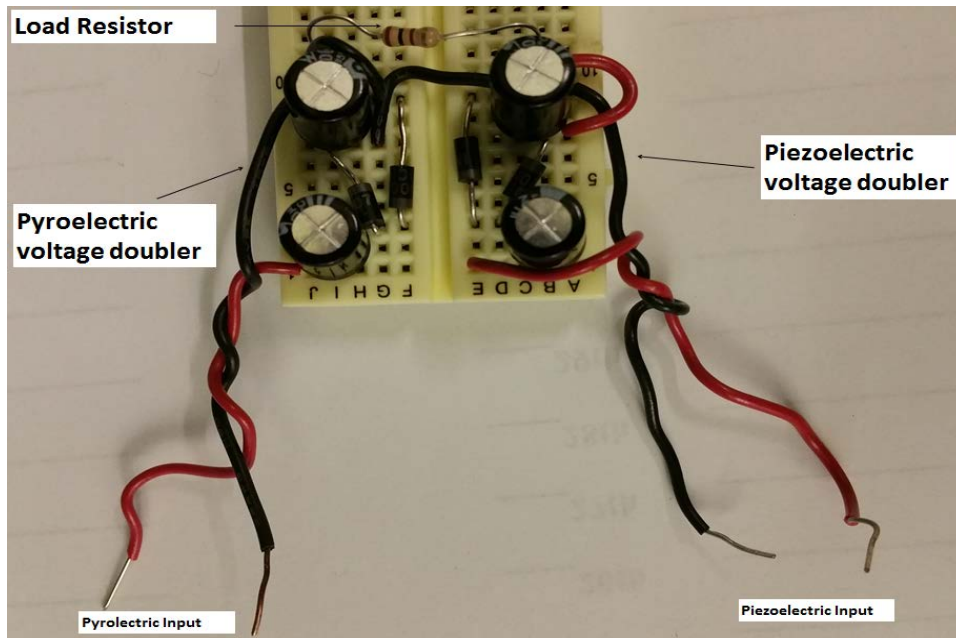


Figure 5.10 Experimental set up for Hybrid Energy Harvester Using Voltage Doubler

Experimental set up for the hybrid energy harvester using a voltage doubler has been implemented using the same equipment set up presented in Figure 5.1. The two bimorph cantilevers were connected in series and one of them was fastened to the shaker under a vibration level of 0.5 g and piezoelectric frequency of 115Hz. A cyclic heat with frequency of 100 mHz and rate of 0.85 degrees per second (between 59.2 and 68.7 °C) was applied to the second cantilever with no vibration.

The regular hybrid energy harvesting experiment without doubler under a similar condition of 0.5 g vibration acceleration and 115 Hz and cyclic heating rate of 0.85 degrees per second has been achieved. It can be noticed from table 5.1 that the average hybrid average voltage extracted at optimal resistance of 19 k Ω is equal to 3.93 V which is less than the sum of individual pyroelectric and piezoelectric peak voltages of 0.75V and 3.96 V respectively. This is an expected result because of drastic decrease in piezoelectric coefficient because of heating. However, the output hybrid power of (0.81 mW) is more than the sum of the individual pyro (1.4 μ W) and piezoelectric (0.71mW) powers, since the internal impedance of the piezoelectric decreases with the increasing of both the heat and the frequency.

By considering a hybrid energy harvesting with a voltage doubler, it can be seen that the DC output hybrid voltage at optimal resistances is equal to 7.96 V which is almost the same to the value obtained from Equation 5.1 considering the threshold voltage of diodes to be equal to 0.5 V. The optimal values for the load resistances in the case of the voltage doubler were equal to 22 k Ω and 0.4 M Ω for individual piezoelectric and pyroelectric sources respectively. The hybrid power resulted from voltage doubler method is significantly more than that extracted using the regular hybrid method. The hybrid power of (2.16 mW) is almost three times the sum of the individual pyro (1.369 μ W) and piezoelectric (0.71 mW) powers.

Table 5.1. Regular and voltage doubler hybrid energy harvesting at 115 Hz and 0.5 g vibration acceleration, and 0.85 deg / sec temperature rate

Regular Hybrid energy harvesting				Hybrid energy harvesting with voltage doubler			
Pyro. Voltage	Piezo. Voltage	Hybrid Voltage	Hybrid Power	Pyro. Voltage	Piezo. Voltage	Hybrid Voltage	Hybrid Power
0.75V	3.96 V	3.93 V	0.81 mW	0.74 V	3.94	7.96	2.15 mW

Chapter 6. Conclusions and Future work

6.1 Conclusions

Studies in the area of harvesting environmental energy to power small wireless electronic components and sensors have grown in the recent decades. Particularly, researching materials that exhibit a piezoelectric or a pyroelectric effect have been the subject of wide investigation for energy harvesting applications. However, these applications have encountered many technical challenges to maximize power efficiently. This work concentrates on improving the efficiency of energy harvesting using pyroelectric and piezoelectric materials in a system by the proper characterization of electrical parameters, widening operating frequency, and coupling of pyroelectric and piezoelectric effects to develop hybrid energy harvesting system.

6.1.1 Pyroelectric Energy harvesting

In this study, a simple method to characterize impedance for PVDF and PZT-5A cells at low frequencies has been invented such that the pyroelectric power harvested can be maximized. This method exploits a pyroelectric single pole low-pass filter (PSLPF) which consists of a pyroelectric cell instead of parallel R and C components in the feedback path of this common filter. By supplying a known input signal at low frequencies along with some simple computations, the inherent capacitance C_p and resistance R_p of the pyroelectric cell can be calculated. Once these parameters were calculated, the results were verified by measuring output pyroelectric energy at various values of load impedance. The maximum power corresponds to the predicted value of R_L using the PSLPF method within a 9.8 % difference for PVDF cell and a 1.4 % difference for PZT-5A cell.

The importance of the effect of ambient working temperature on the total pyroelectric impedance has been highlighted. When PVDF or PZT-5A is exposed to ambient working temperatures that are higher than 24 °C, the inherent capacitance and resistance change. For example, in the case of PVDF cell, impedance drops approximately 10 times from 24 °C to 90 °C. This order of magnitude change can have an adverse impact on application design especially on energy harvesting applications.

To stress the significance of impedance matching, energy harvesting experiments using pyroelectric cells are conducted. The results corroborate the impedance values computed by experimentation and the ones measured by the presented PLSPF method. Two pyroelectric cells, PVDF and PZT-5A, were characterized in a frequency range from 1 mHz to 100 Hz. For PVDF, it was shown that R_p were in 8 % and 1.2% differences as compared to LCR meter for 10 and 100 Hz, respectively, and in 3.1% difference as compared to IA at 100 Hz. The inherent capacitance C_p was measured to be in 1.9 %, 4.3%, and 6.4% differences with the LCR meter, IA, and manufacturer measurements, respectively. For PZT-5A, it was revealed that R_p were in 5.8 % and 1.4% differences as compared to LCR meter for 10 and 100 Hz, respectively, and in 6.1% difference as compared to IA at 100 Hz. The inherent capacitance C_p was measured to be in 0.5%, 7.5%, and 9.04% differences with the LCR meter, IA, and manufacturer measurements, respectively. The suggested method is used with a pyroelectric cyclic heating at a temperature rate of 0.6 degrees per second for PVDF. For PZT-5A, a temperature rate of 0.44 degrees per second has been proposed. The optimal load impedance for PVDF and PZT-5A samples was 55 and 7 M Ω at the mentioned temperature rates, respectively. The optimal load resistances for PVDF and PZT-5A were consistent with the measured pyroelectric impedance at the particular heat range with 10.9% and 1.4% differences, respectively. In addition, the dependence of

impedance on operating median temperature was also measured. In the case of PVDF, it was shown that the impedance values can decrease from 400 to 40 M Ω with temperatures between 25 °C and 95 °C. In the case of PZT-5A, the changes are smaller and are in the order of 3 M Ω at the same temperature ranges.

The PSLPF technique proposed here shows that impedance dependence on the average temperature and the heating rate are both key parameters when characterizing a pyroelectric material. This indicates obviously that to optimize impedance when exploiting the pyroelectric effect, both operating average working temperature and the rate of temperature change need to be considered when designing energy harvesting systems. Neglecting those parameters will result in inefficient and unpredictable systems.

6.1.2 State space modeling for piezoelectric bimorph harvester with RLC load

In this study, a state space dynamics model of the piezoelectric cantilever with RLC load has been developed. This model can be utilized to analyze the feasibility of shunting an inductance with small value to improve the output power of vibration based scavengers with passive electrical tuning. A general dynamics model of the piezoelectric cantilever with RLC load has been developed, and test results from this generator were presented and discussed.

There was good correspondence between experimental and simulated waveforms of the output voltages with 10 % difference.

It was shown analytically and experimentally that there is a significant improvement in the harvested power of the circuit with the shunt inductor. A shunted inductor of L_{sh} of 3 H has been connected to the system to improve the generated power when the shunt capacitance was equal to 1.47 μ F and 3 μ F. Generally, the gained power percentages were (10 % - 60 %). Experimental

and simulated data for output peak power P_p of the piezoelectric generator were in good correspondence with a maximum difference of 7.5 %.

6.1.3 Hybrid Piezoelectric Frequency Tuning

Piezoelectric energy harvesters deliver the maximum power when working at resonance, which means that the harvesters are not efficient in environment vibrations with random and unpredictable frequencies. In this study, some suggested approaches have been developed to increase the frequency bandwidth and maximize output power for piezoelectric energy harvesters.

At first, a hybrid frequency tuning methodology using multiple piezoelectric bimorph cantilevers is presented. This is done to accomplish mechanical tuning, electrical tuning, and bandwidth widening simultaneously to develop a significant growth in frequency spectrum for the piezoelectric energy scavenger. In this new work three bimorph cantilevers with the same characteristics have been utilized. Each one has the same natural frequency, but mechanically tuned by using two different tip masses and different lengths to have three different natural frequencies. These three bimorphs were connected electrically in series and mechanically in parallel. Using three diverse ceramic capacitors for each cantilever, each one has a stretched operating frequency range of several hertz around each individual resonance frequency. Hence rather than having three resonant frequencies the system has twelve natural frequencies and maximum power peaks.

A total of 12 resonance frequencies are achieved. It was concluded that this design which includes three cantilevers and four capacitors for each beam could deliver more power than the case if one bimorph cantilever is assumed to be used with 12 capacitors. It was shown

that the output power corresponding to the largest shunt capacitor of 470 nF is less than 0.5 mW. In order to have a broader frequency band, capacitors with values more than 470 nF should be used, and consequently the power achieved could be even less and less than 0.1 mW. Also, if 12 beams are used to get 12 resonance frequencies by mechanical tuning, the size limitation would be a serious problem. The proposed hybrid tuning technique was feasible and optimal method for wide broadband piezoelectric energy harvesting.

Secondly, an experimental enhanced power harvester with hybrid tuning using multiple piezoelectric unimorphs is developed. This approach sought to enhance piezoelectric power and frequency spectrum using mechanical tuning, electrical tuning, and bandwidth widening techniques simultaneously with conjugate impedance matching. This approach aimed to enable piezoelectric energy harvesters to work efficiently in a variety of environments with random ambient vibration frequencies. First, an improved adjusting capacitor method for electrical tuning has been established to have an enhanced power output and to match piezoelectric resonance frequency to the ambient vibration frequency simultaneously. The influence of a shunt capacitor C_{sh} on the output power of a unimorph piezoelectric cantilever was validated by connecting four different shunt capacitors with values from C_p to $10C_p$. An inverse correlation between the two quantities was noticed. An inductive reactance connected in parallel to the system was suggested as a remedy for this issue. Increases in power outputs were up to 93% and 88% for the shunt inductive impedances equal to 1 μ F and 1.16 μ F respectively. In addition, for the same unimorph cantilever tuned to resonance frequency of 205 Hz, two shunt capacitors of 0.6 μ F and 0.87 μ F were connected to shift resonance frequency to 200 Hz and 200.5 Hz respectively. An inductive shunt reactance with inductor L_{sh} of 2 H was connected to the system

to improve the generated power. Increases in power outputs were up to 117% and 47% for shunt capacitors C_{sh} equal to 0.6 μF and 0.87 μF respectively.

Finally, an enhanced power hybrid tuning technique using multiple piezoelectric unimorphs has been presented. Mechanical tuning, electrical tuning, and band-pass filtering methods were used simultaneously to develop an increase in frequency range for the piezoelectric harvester with enhanced power using inductive impedance. A small toroid inductor of 700 mH was connected in parallel to the load resistance and shunt capacitance. An extended frequency range of 12 resonance frequencies with 300% improvement was obtained experimentally with enhanced power density improvements of 19.7% to 197%. Future work might include an ultra-low power microcontroller to develop an actively hybrid tuned energy harvester with power enhancement

6.1.4 Hybrid Energy Harvesting

For maximum hybrid power, impedance matching between load impedance and inherent impedance of the hybrid energy harvester must be fulfilled. The total internal impedance dependence on the average temperature and the heating rate are both key parameters when characterizing a material used for hybrid energy harvesting. In this study, it was shown that to optimize impedance when utilizing the pyroelectric and piezoelectric effects simultaneously, both operating average working temperature and the rate of temperature change need to be considered when designing energy harvesting applications. Neglecting those parameters will result in inefficient and unpredictable hybrid energy harvesting systems.

In addition, an impedance matching using a new voltage doubler circuit for rectifying and collecting pyroelectric and piezoelectric voltages individually is proposed and tested. The

investigation showed that the hybrid energy is possible using the voltage doubler circuit from two independent sources for pyroelectricity and piezoelectricity due to marked differences of optimal performance. The obtained results were significantly higher than harvested energy simultaneously from the same material.

A cyclic heat with frequency of 100 mHz and rate of 0.44 degree per second (between 61.1 and 65.5 °C) was applied to the bimorph simultaneously with a vibration of 0.21 g and piezoelectric frequency of 115 Hz. The hybrid voltage shape was almost similar to a modulated signal which is mixed of a carrier signal with high frequency of 115 Hz and a modulating signal with low frequency of 100 mHz.

It was seen that the hybrid one was less than the sum of pyroelectric and piezoelectric voltages. Also, it was noticed that the maximum piezoelectric and hybrid powers of 22.9 μW and 16.5 μW were extracted at a load resistance of 22 k Ω and 19 k Ω respectively. The predicted optimal piezoelectric impedance at 24 °C and 115 Hz was 25.1 k Ω with which the experimental optimal impedance was in 12.3 % difference.

The expected hybrid optimal load impedance at 63.3 °C was 14.4 k Ω . The experimental hybrid optimal load impedance was 19 k Ω which is within a 24 % difference with the expected value. The measured optimal pyroelectric impedance at temperature of 63.3 °C was equal to 0.45 M Ω . There is an 11.1 % difference between the expected value and the experimental value of optimal pyroelectric impedance which was equal to 0.4 M Ω .

The hybrid power resulted from voltage doubler (2.15 mW) method is significantly more than that extracted using the regular hybrid method (0.8 mW).

6.2 Future Work

6.2.1 Pyroelectric Cell characterization equipment:

The proposed PSLPF, a simple method for the measurement of inherent resistance and capacitance for pyroelectric materials and confirmed their results using pyroelectric energy harvesting set-up. This is useful for situations where the impedances were not measurable using the traditional instruments. For future work a new measurement instrument could be designed based on the mechanisms used for this technique. We would aim to optimize the reliability and functionality for such beneficial equipment.

6.2.2 Actively tuned hybrid piezoelectric frequency tuning system

It can be noticed that there is a significant increase in the operating frequencies bandwidth using the suggested hybrid technique for frequency tuning. Future work will consider designing and implementing an actively tuned hybrid frequency tuning system using an ultra-low power microcontroller chip.

6.2.3 Enhanced hybrid piezoelectric frequency tuning system

To optimize the efficiency of the new hybrid piezoelectric tuning technique, different series-parallel configurations of capacitance, inductance, and resistance can be considered to increase the power output with even a smaller shunt inductance.

References

- Ajitsaria, J., Choe, S. Y., Shen, D., and Kim, D. J., 2007, "Modeling and Analysis of a Bimorph Piezoelectric Cantilever Beam for Voltage Generation, "Smart Mater. Structure. 16, pp. 447-454.
- Amokrane, M., Baysse, A., Nogarede, B., 2012 Low-voltage active diode rectifier for pyroelectric harvesting cell. IECON 2012-38th Annual Conference on IEEE Industrial Electronics Society, IEEE, pp. 1055–1060.
- Amirtharjan and Chandrakasan, P., 1998 " Self-powered signal processing using Vibration-based power generation "IEEE Journal of Solid State Circuits (Volume : 33, Issue:5) P687-695
- An-Shen Siao, Ching-Kong Chao , and Chun-Ching Hsiao 2015 Study on Pyroelectric Harvesters with Various Geometry. Sensors 2015, 15, 19633-19648.
- Bauer, S., Lang, B., 1996, IEEE Trans. Dielectric. Electricity Insul.3, 647
- Beeby P., M J Tudor and N M White "Energy harvesting vibration sources for microsystems applications" a review Meas. Sci. Technol. **17** (2006) R175–R195
- Beer f., Elwood Russell Johnston, John T. DeWolf McGraw-Hill, 1992 , Technology & Eng.
- Blevins RD (1979) "Formulas for natural frequency and mode shape"
- Byeongil Kim, Gregory N Washington, and Hwan-Sik Yoon, 2014" Control and hysteresis reduction in pre-stressed curved unimorph actuators using model predictive control"

- Journal of Intelligent Material Systems and Structures 2014, Vol 25(3) 290–307
- Challa, R., Prasad, G., Fisher, T., 2009 "A coupled piezoelectric-electromagnetic energy harvesting technique for achieving increased power output through damping matching". *Smart Materials and Struct.*, **18**(9):095029. [doi:10.1088/0964-1726/18/9/095029]
- Chang HHS and Huang Z (2010) Laminate composites with enhanced pyroelectric effects for energy harvesting. *Smart Materials and Structures* 19(6): 065018.
- Charnegie D (2007) "Frequency tuning concepts for piezoelectric cantilever beams and plates for energy harvesting" Master thesis, University of Pittsburgh
- Choi, J., Y Jeon, J., H. Jeong, R. Sood ·S.G. Kim, 2006" Energy harvesting MEMS device based on thin film piezoelectric cantilevers" *Journal of Electroceram* (2006) 17:543–548
- Chulsung, P. and Chou P.H., 2006 Autonomous energy harvesting platform for multi-supply wireless sensor nodes. 3rd IEEE Annual Communications Society on Sensor and *Ad Hoc* Communications and Networks, Reston, VA, USA, September 2006; pp. 168–177.
- Collado A, and A Georgiadis A, 2013"Conformal Hybrid Solar and Electromagnetic (EM) Energy Harvesting Rectenna" *IEEE Transactions on Circuits and Systems: Regular papers*, Vol. 60, No. 8, August 2013. p2225-2234.
- Cuadras, A., 2006 Energy harvesting from PZT pyroelectric cells. In: *2006 IEEE Instrumentation and Measurement Technology Conference Proceedings*, pp. 1668–1672.
- Cuadras A, Gasulla M and Ferrari V (2010) Thermal energy harvesting through pyroelectricity. *Sensors and Actuators A: Physical* 158(1): 132–139.

- Dalola S, Ferrari V and Marioli D (2010) Pyroelectric effect in PZT thick films for thermal energy harvesting in low-power sensors. *Procedia Engineering* 5: 685–688.
- Dukhyun, C., Keun Y., Kang H. Lee, E., Kim, S., Young C., and Kim, J., 2010. Piezoelectric touch-sensitive flexible hybrid energy harvesting nano architectures" *Nanotechnology* 21 405503 doi:10.1088/0957-4484/21/40/405503
- Erturk A., and Inman, D., 2008 "A Distributed Parameter Electromechanical Model for Cantilevered Piezoelectric Energy Harvesters" *Journal of Vibration and Acoustics* August 2008, Vol. 130 / 041002-1
- Erturun U, Green C, Richeson ML, et al. (2014) Experimental analysis of radiation heat-based energy harvesting through pyroelectricity. *Journal of Intelligent Material Systems and Structures* 25(14): 1838–1849.
- Ferrari M, Ferrari V, Guizzetti M, (2008) "Piezoelectric multifrequency energy converter for power harvesting in autonomous microsystems" *Sensors and Actuators A: Physical*, 142(1), 329–335
- Fleming, A., Behrens, S., and Moheimani, R. 2003"Reducing the inductance requirements of piezoelectric shunt damping systems" *Smart Materials and Structures*. 12(2003) p57-64.
- Gambier P, Anton SR, Kong N, et al. (2012) Piezoelectric, solar and thermal energy harvesting for hybrid low-power generator systems with thin-film batteries. *Measurement Science and Technology* 23(1): 01510

Glynne-Jones, P., M. El-hami, N.M. White, M. Hill, S. Beeby, E. James, A.D. Brown, J.N.

Ross "Design and fabrication of a new vibration-based electromechanical power generator" *Sensors and Actuators A: Physical* Volume 92, Issues 1–3, 1 August 2001, Pages 335–342

Gonzalez, G., Franco, R., Brennan, J., Silva, S., Junior, L., 2010. Energy Harvesting Using Piezoelectric and Electromagnetic Transducers. 9th Brazilian Conference on Dynamics, Control and Their Applications, Serra Negra, Brazil, p.1166-1171.

Gummesson, J., Clark, S., K Fu, D Ganesan, 2010 " On the Limits of Effective Hybrid Micro-Energy Harvesting on Mobile CRFID Sensors" *MobiSys'10*, June 15–18, 2010, San Francisco, California, USA, p195-208

Guyomar D, Sebald G, Lefeuvre E, et al. (2008) "Toward heat energy harvesting using pyroelectric material" *Journal of Intelligent Material Systems and Structures* , July 11, 2008 doi:10.1177/1045389X08093564 <http://www.farmingdale.edu/faculty/peter-nolan/pdf/UPCh29.pdf>

Guyomar, D., Lallart, M. and Monnier, T. 2008 "Stiffness Tuning Using a Low-cost Semi-active Nonlinear Technique," *IEEE/ ASME Trans. Mech.*, 13:604–607

Hansen B J., Ying R Y, and Zhong L W, 2010 "Hybrid Nano generator for concurrently Harvesting Biomechanical and Biochemical Energy" *ACS Nano* VOL. 4. NO. 7 .3647–3652 . 2010

Heung Soo Kim, Joo-Hyong Kim and Jaehwan Kim, 2011 "A Review of Piezoelectric Energy Harvesting Based on Vibration International Journal of Precision Engineering and Manufacturing Vol. 12, No. 6, pp. 1129-1141"

Hill, L.; and D. E. Culler, 2002 "Mica: a wireless platform for deeply embedded networks" , 2002, Volume: 22, Issue: 6 , P12 - 24

Hsiao C-C, Siao A-S and Ciou J-C (2012) Improvement of pyroelectric cells for thermal energy harvesting. *Sensors* 12(1): 534–548

Hsu J-C, Tseng C-T and Chen Y-S (2014) "Analysis and experiment of self-frequency-tuning piezoelectric energy harvesters for rotational motion" *Smart Materials and Structures*, 23(7), 075013

<http://www.piezo.com/catalog8.pdf%20files/Cat8.31.pdf>

Hua Y, Qiuqin Y, Jieli Z., Wei W., "A Hybrid Indoor Ambient Light and Vibration Energy Harvester for Wireless Sensor Nodes " *Journal of Sensors* **2014**, 14, 8740-8755

Iqbal, M., 2003 "Simulation of a small wind fuel cell hybrid energy system *Renewable Energy*" Volume 28, Issue 4, April 2003, Pages 511–522

Kandilian R, Navid A and Pilon L (2011) The pyroelectric energy harvesting capabilities of PMN–PT near the morphotropic phase boundary. *Smart Materials and Structures* 20(5): 055020.

- Kong, N., Dong, S., Ha, Erturk, A., and Inman, D., (2010) "Resistive impedance matching circuit for piezoelectric energy harvesting" *Journal of Intelligent Material Systems and Structures*, Jan 2010, DOI: 10.1177/1045389X09357971
- Kouchachvili L and Ikura M (2007) Pyroelectric conversion—effects of P (VDF–TrFE) preconditioning on power conversion. *Journal of Electrostatics* 65(3): 182–188.
- Krishnan SH, Ezhilarasi D, Uma G, et al. (2014) Pyroelectric-based solar and wind energy harvesting system. *Sustainable Energy, IEEE Transactions on* 5(1): 73–81.
- Lang SB (2005) Pyroelectricity: from ancient curiosity to modern imaging tool. *Physics Today* 58(8): 31–36
- Lang, B., Sourcebook of Pyroelectricity, Gordon & Breach Science, London (1974)
- Lee, F., Goljahi S, McKinley IM, et al. (2012) Pyroelectric waste heat energy harvesting using relaxor ferroelectric 8/65/35 PLZT and the Olsen cycle. *Smart Materials and Structures* 21(2): 025021
- Leland, S., and Paul K Wright, 2006" Resonance tuning of piezoelectric vibration energy scavenging generators using compressive axial preload" *Smart Mater. Structure* 15 (2006) 1413–1420
- Lihua, T., Yaowen, Y., and Chee Kiong S., 2010" Toward Broadband Vibration-based Energy Harvesting" *Journal of Intelligent Material Systems and Structures* 2010 21: 1867-1897
- Lines, M., Glass, M., Glass, Principles and Applications of Ferroelectrics and Related Materials,

- Clarendon Press, Oxford (1977)
- MacCurdy, B., Reissman, T., Garcia, E., 2008. Energy Management of Multi-component Power Harvesting Systems. Proc. SPIE 6928, Active and Passive Smart Structures and Integrated Systems, San Diego, California, USA, p.692809. [doi:10.1117/12.776545.
- Mane P, Xie J, Leang KK, et al. (2011a) Cyclic energy harvesting from pyroelectric materials. Ultrasonics, Ferroelectrics, and Frequency Control, IEEE Transactions on 58(1): 10–17.
- Mane P, Xie J, Leang KK, et al. (2011b) Cyclic energy harvesting from pyroelectric materials Ultrasonics, Ferroelectrics and Frequency Control, IEEE Transactions on 58(1): 10–17.
- Mathew W. Hooker. (1998) “Properties of PZT-Based Piezoelectric Ceramics between -150 and 250 °C. NASA /CR-1998-208708.
- Mickael L., Steven, R., Anton and Inman, D., (2010) "Frequency Self-tuning Scheme for Broadband Vibration Energy Harvesting" Journal of Intelligent Material Systems and Structures, April 20, 2010 as doi:10.1177/1045389X10369716
- Navid A and Pilon L (2011) Pyroelectric energy harvesting using Olsen cycles in purified and porous poly (vinylidene fluoride-trifluoroethylene)[P (VDF-TrFE)] thin films. *Smart Materials and Structures* 20(2): 025012.
- Navid A, Lynch CS and Pilon L (2010) Purified and porous poly (vinylidene fluoride-trifluoroethylene) thin films for pyroelectric infrared sensing and energy harvesting.
- Nayar,S.J. Phillips, W., James, T.L. Pryor, D. Remmer,1993"Novel wind/diesel/battery hybrid

energy system" *Solar Energy* Volume 51, Issue 1, July 1993, Pages 65-78 *Smart Materials and Structures* 19(5): 055006.

Nesbitt, W., Walter H. and Andreas V., "Modeling of Piezoelectric Actuator Dynamics for Active Structural Control " *Journal of Intelligent Material Systems and Structures* July 1990 vol. 1 no. 3 327-354

Newnham, E., *Properties of Materials: Anisotropy, Symmetry, Structure*, Oxford U. Press, New York (2005)

Noel Eduard du Toit , 2005 Modeling and Design of a MEMS Piezoelectric Vibration Energy Harvester Submitted to the Department of Aeronautics and Astronautics in partial Fulfillment of the requirements for the degree of Master of Science in Aeronautics and Astronautics at the Massachusetts Institute of Technology May 2005

Olsen RB, Bruno DA, Briscoe JM, et al. (1985) High electric field resistivity and pyroelectric properties of vinylidene fluoride-trifluoroethylene copolymer. *Journal of applied physics* 58(8): 2854–2860.

Pierre Curie, 1859-1906) <http://www.ncbi.nlm.nih.gov/pmc/articles/PMC1891197>

Richards, D., Anderson, J., Bahr, F., and Richards, F., 2004 "Efficiency of energy conversion for devices containing a piezoelectric component" *J. Micromech.* 14 717–2

Roundy, S., and P K Wright, 2004 "A piezoelectric vibration based generator for wireless electronics *Smart Mater. Structure* 13 (2004) 1131–1142

- Roundy, S., Yang Zhang , 2005 "Toward self-tuning adaptive vibration-based micro generators", *Proc. SPIE* 5649, Smart Structures, Devices, and Systems II, 373 (March 09, 2005); doi:10.1117/12.581887; <http://dx.doi.org/10.1117/12.581887>
- Salem Saadon and Othman Sidek, 2015 " Micro-Electro-Mechanical System (MEMS)-Based Piezoelectric Energy Harvester for Ambient Vibrations" *Procedia - Social and Behavioral Sciences* 195 (2015) 2353 – 2362
- Sebald G, Lefeuvre E and Guyomar D (2008) Pyroelectric energy conversion: optimization principles. *Ultrasonics, Ferroelectrics, and Frequency Control, IEEE Transactions on* 55(3): 538–551.
- Shaheen, M., Erturun, U., Campbell, B., and Mossi. M., 2016" A simple method to characterize the impedance of pyroelectric materials at ultra-low frequencies" *Journal of Intelligent Material Systems and Structures*, May 5, 2016, doi: 10.1177/1045389X16645865.
- Shahruz, M., (2006a)" Design of mechanical band-pass filters for energy scavenging" *Journal of Sound and Vibration*, 292(3), 987–998
- Shahruz SM (2006b) "Limits of performance of mechanical band-pass filters used in energy Scavenging" *Journal of sound and vibration*, 293(1), 449–461
- Shahruz, M., 2005"Elimination of vibration localization in mistuned periodic structures" *Journal of Sound and Vibration* 281 (2005) 452–462

- Sodano HA, Inman DJ and Park G (2004) A review of power harvesting from vibration using piezoelectric materials. *Shock and Vibration Digest* 36(3): 197–206.
- Sohn, W., Choi, B., and Lee, Y., 2005 "An investigation on piezoelectric energy harvesting for MEMS power sources" *Journal of Mech. Eng. Sci.* **219** 429–36
- Stephen, N., 2006, " On energy Harvesting from Ambient Vibration" *Journal of Sound and Vibration* Vol. 293, Issues1-2, 30 May 2006, pp409-425
- Sterken T, Baert, K., Hoof C, Puers R. , Borghs G. and Fiorini p. 2004 "Comparative modeling for vibration scavengers *Proc. IEEE Sensors Conf. (Vienna, Oct.)* pp 1249–52
- Steven R Anton¹ and Henry A Sodano "A review of power harvesting using piezoelectric Materials"(2003–2006) *Smart Mater. Struct.* 16 (2007) R1–R21)
- Swee-Leong, K., Mohd F., David Fook Weng, Yap, Yih Hwa, Ho 2011 "Bandwidth widening strategies for piezoelectric based energy harvesting from ambient vibration sources" In: *Computer Applications and Industrial Electronics (ICCAIE), 2011 IEEE International Conference on, IEEE, pp. 492–496*
- Swee-Leong, K., Norizan, M., David, F., Weng, Y., Soo Kien, C., Chang F., Dee, 2011 "Multi-Frequency Energy Harvesting Using Thick-Film Piezoelectric Cantilever" *international Conference on Electrical, Control and Computer Engineering Pahang, Malaysia, June 21-22, 2011*,p420-423
- Tayahi M B, Johnson B, Holtzman M and Cadet G 2005 Piezoelectric materials for powering remote sensors *Proc. IEEE 24th Int. Performance, Computing, and Communications Conf.(Phoenix, AZ, April)* pp 383–6

- Taylor, G. , Burns J , Kammann S. , Powers W and Welsh T R 2001 The energy harvesting EEL: a small subsurface ocean/ river power generator *IEEE J. Oceanic Eng.* 26 539–47
- Texas Instrument (2002) Texas Instrument incorporated 2002 Data sheet. Available from:
<http://www.ti.com/lit/ds/symlink/lm348.pdf>.
- Torah, R., Glynn-J P., Tudor M., O'Donnell T., Roy S., Beeby, S., 2008. Self-powered autonomous wireless sensor node using vibration energy harvesting. *Measurement Science and Technology*, **19**(12):125202.
- Weiquan Liu et al. (2014) " A wideband integrated piezoelectric bi-stable generator: Experimental performance evaluation and potential for real environmental vibrations" *Journal of Intelligent Material Systems and Structures* DOI: 10.1177/1045389X14546660.
- Wickenheiser M. and Garcia E. 2010. “Broadband Vibration-based Energy Harvesting Improvement through Frequency Up-Conversion by Magnetic Excitation,” *Smart Materials. Structure*, 19:065020.
- Wilkie , K., Bryant G., High W., Fox L., Hellbaum F., Jalink A., Little, D., and Mirick H. 2000 "Low-cost piezocomposite actuator for structural control applications" *Proc. 7th Int. Symp. Smart Structures and Materials; Proc. SPIE 3991 323–34*
- Williams C B and R Yates R 1995 Analysis of a micro-electric generator for microsystems *Transducers 95/Eurosensors IX vol 1 pp 369–72*
- Wischke, M., Masur, M., Goldschmidtboeing, F. and Woias, P. 2010. “Electromagnetic Vibration Harvester with Piezoelectrically Tunable Resonance Frequency,” *J. Micromech. Microeng.*, 20:035025

- Wisegar J, Pereira C and Nguyen H L 2006 Piezoelectric-based power sources for harvesting energy from platforms with low frequency vibration *Proc. Smart Structures and Materials Conf.; Proc. SPIE* 6171 6171011
- Wu W., Chen Y., Lee, S., Yu-Yin, C., and Yen-Tun, P., (2006) "Tunable resonant frequency power harvesting devices" *Proceedings of SPIE - The International Society for Optical Engineering* March 2006 DOI: 10.1117/12.658546
- Wu X, Lin J, Kato S, et al. (2008) "A frequency adjustable vibration energy harvester" *Proceedings of Power MEMS*, 245–248
- Xie J, Mane PP, Green CW, et al. (2008) Energy harvesting by pyroelectric effect using PZT. In: *ASME 2008 Conference on Smart Materials, Adaptive Structures and Intelligent Systems*, American Society of Mechanical Engineers, pp. 273–277.
- Xie J, Mane XP, Green CW, et al. (2010) Performance of thin piezoelectric materials for pyroelectric energy harvesting. *Journal of Intelligent Material Systems and Structures* 21(3): 243–249.
- Xiao-biao S., Shi-wei g., Zhang-shi L., Zhen-long X., Tao X. , 2013 "A new energy harvester using a piezoelectric and suspension electromagnetic mechanism" *Journal of Zhejiang University-SCIENCE A (Applied Physics & Engineering)* 2013 14(12):890-897
- Xue, H., Hu, Y., and Wang, M., (2008) "Broadband piezoelectric energy harvesting devices using multiple bimorphs with different operating frequencies" *Ultrasonic, Ferroelectrics, and Frequency Control*, *IEEE Transactions on*, 55(9), 2104–2108

Yang Y, Zhang H, Zhu G, et al. (2012) Flexible hybrid energy cell for simultaneously harvesting thermal, mechanical, and solar energies. *ACS nano* 7(1): 785–790.

Yang Y, Wang S, Zhang Y, et al. (2012) Pyroelectric nanogenerators for driving wireless sensors. *Nano letters* 12(12): 6408–6413.

Yang Y, Zhou Y, Wu JM, (2012) Single micro/nanowire pyroelectric nanogenerators as self-powered temperature sensors. *ACS nano* 6(9): 8456–8461

Yang, Y., Hulin Zhang, Guang Zhu, Sangmin Lee, Zong-Hong Lin, and Zhong Lin Wang , 2013 "Flexible Hybrid Energy Cell for Simultaneously Harvesting Thermal, Mechanical, and Solar Energies" *ASC Nano* Vol. 7' NO. 1' 785–790 '

Yonas T., Shujun Z., and Shashank P., 2009 "Multimodal Energy Harvesting System: Piezoelectric and Electromagnetic " *Journal of Intelligent Material Systems and Structures March 2009 vol. 20 no. 5* 625-632.

Yu-Jen Wang et al. (2012) "Natural frequency self-tuning energy harvester using a circular Halbach array magnetic disk" *Journal of Intelligent Material Systems and Structures*
DOI: 10.1177/1045389X12441510

Zengtao Yang et al. (2009) "Connected Vibrating Piezoelectric Bimorph Beams as a Wide-band Piezoelectric Power Harvester" *Journal of Intelligent Material Systems and Structures*, Vol. 20- DOI: 10.1177/1045389X08100042

Zhu D, Tudor MJ and Beeby SP (2010) "Strategies for increasing the operating frequency range of vibration energy harvesters: a review" *Measurement Science and Technology*, 21(2), 022001

Appendices

Appendix A1.1 Effect of temperature on Dielectric constant for some piezo ceramics

The effect of temperature on some piezo ceramic materials was achieved by some researchers. All of the these materials evaluated in this work exhibited their lowest dielectric constant values at -150°C , and the dielectric constant of each material increased as the temperature was increased as shown in Figure A.1.

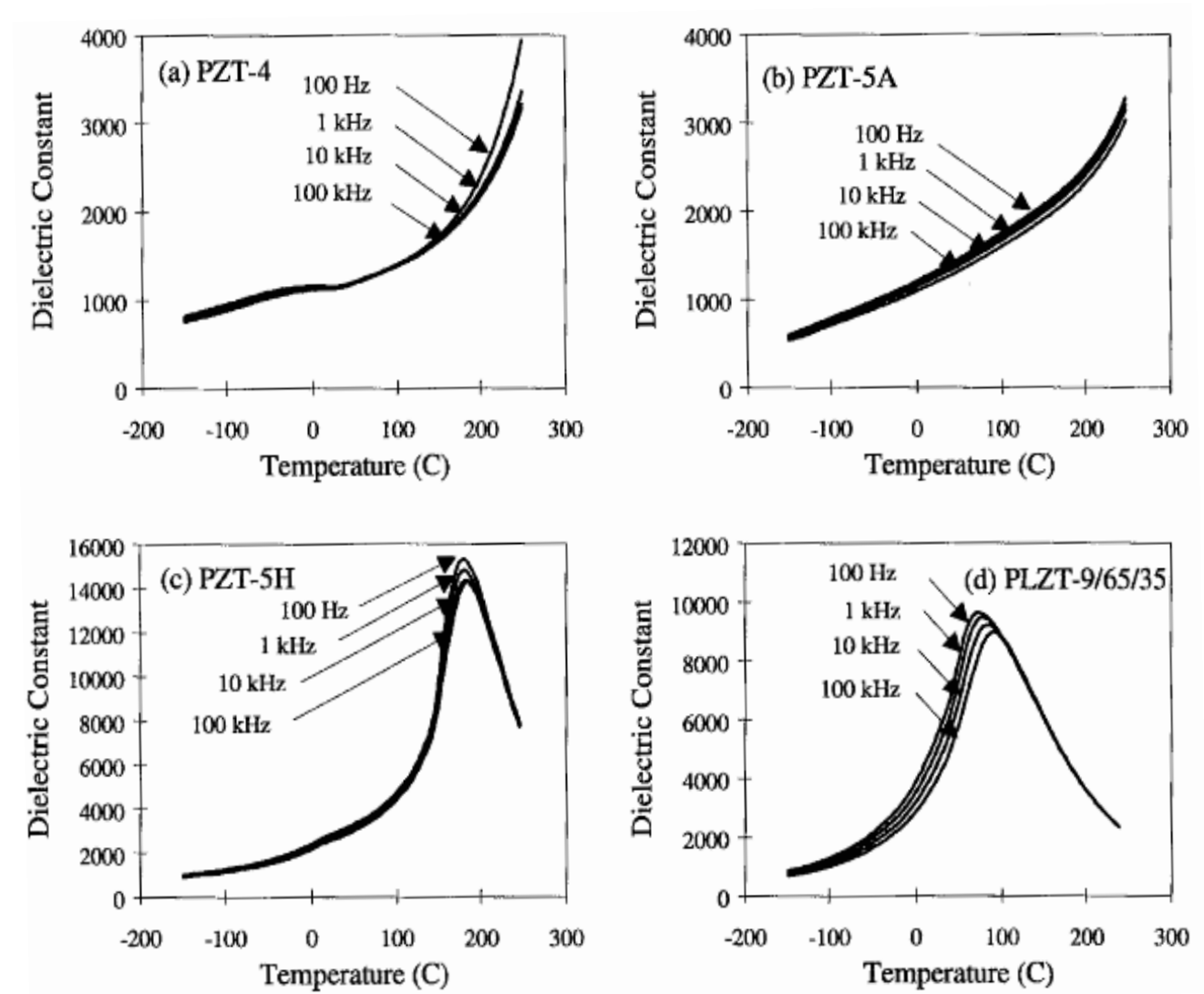


Figure A.1 Dielectric constant versus temperature data for (a) PZT-4, (b) PZT-5A, PZT-5H, and (d) PLZT-9/65/35 (Mathew W. Hooker, 1998).

The dielectric constants of the PZT-4 and PZT-5A ceramics correlated directly to the temperature. The other two materials evaluated, PZT-5H and PLZT-9/65/35, exhibited Curie points within the -150 to 250°C range. The PZT-5H ceramics possessed a T_c value of 180°C at each frequency, whereas the PLZT-9/65/35 materials exhibited T_c properties typical of a relaxer ferroelectric (i.e., varying with frequency). In this instance, the temperature at which the maximum dielectric constant was observed increased from 72 to 91°C as the measurement frequency increased from 100 Hz to 100 kHz (Mathew W. Hooker 1998).

Appendix A1.2 Effect of temperature and frequency on resistivity for some piezo ceramics

The effect of temperature on resistivity for several piezo ceramic materials was studied by M. W. Hooker too. As shown in Figure A.2, when the temperature was increased more than 50°C, resistivity was found to decrease significantly. The resistivity of the PZT-5A specimens was found to decrease with increasing temperature, but the change was not a sharp decrease as that exhibited by the PZT-4 beyond 50°C. The resistivity of the PZT-5H materials was correlated inversely with temperature and reached a minimum value at the T_c and increased as the test specimen was heated to 250°C. A resistance minimum corresponding to the Curie temperature was also observed for the PLZT-9/65/35 ceramics. As previously noted, this material is a relaxer ferroelectric and therefore the temperature of minimum resistance was found to increase from 72 to 91°C as the measurement frequency increased from 100 Hz to 100 kHz (Mathew W. Hooker 1998). It can be noticed that the resistivity is correlated inversely with the frequency in the range from 100 Hz to 100 kHz for all the piezo ceramic materials in this study.

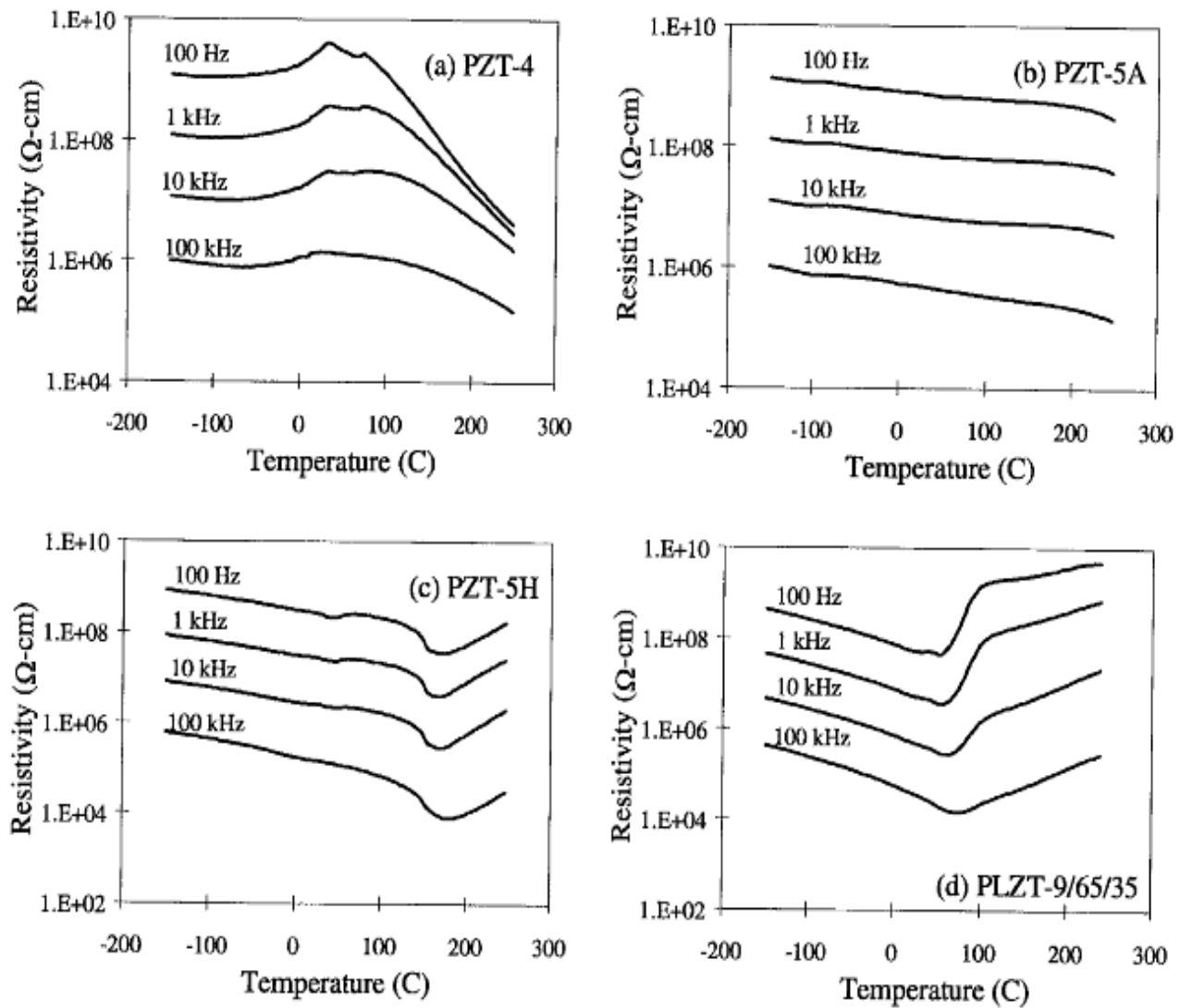


Figure A.2 Resistivity versus temperature data for (a) PZT-4, (b) PZT-5A, PZT-5H, and (d) PLZT-9/65/35 (Mathew W. Hooker, 1998).